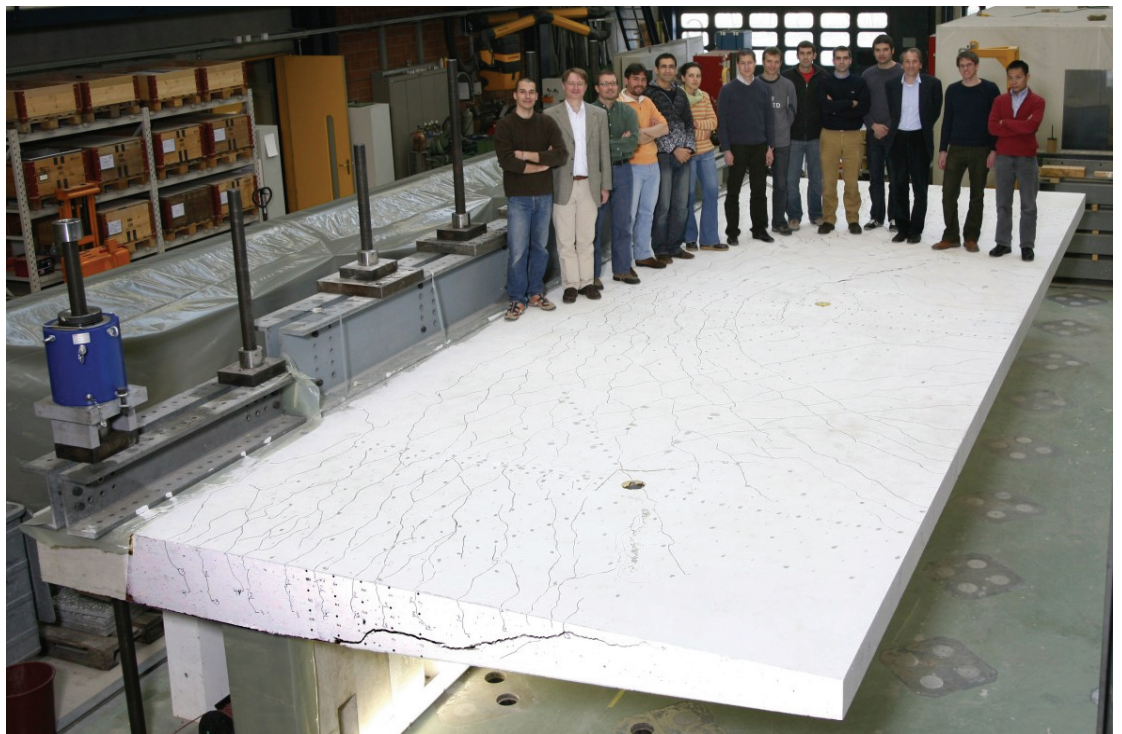


# Large Scale Tests on Reinforced Concrete Bridge Deck Slabs

## Essais à grande échelle sur des Dalles de Roulement des Ponts en Béton Armé



Ecole Polytechnique Fédérale de Lausanne  
Institut de Structures  
Laboratoire de Construction en Béton (IS-BETON)

Rui Vaz Rodrigues  
Prof. Dr Aurelio Muttoni

9 mai 2006

This research is funded by the Swiss Federal Roads Authority (OFROU)



and by the Portuguese Foundation for Science and Technology (FCT)

**FCT** Fundação para a Ciência e a Tecnologia  
MINISTÉRIO DA CIÊNCIA, TECNOLOGIA E ENSINO SUPERIOR Portugal

## Table of contents

<b>A-1 Introductory remarks</b> .....	<b>1</b>
A-1.1 Aim .....	1
A-1.2 Acknowledgements.....	1
<b>A-2 Description of the slabs</b> .....	<b>3</b>
A-2.1 Test concept and overview .....	3
A-2.2 Geometry and reinforcement .....	4
A-2.3 Construction of specimens.....	7
A-2.4 Material properties.....	8
Concrete .....	8
Reinforcement .....	11
<b>A-3 Experimental set-up and procedure</b> .....	<b>13</b>
A-3.1 Reaction frames and load application.....	13
A-3.2 Preparation of slabs.....	18
A-3.3 Continuous measurements .....	19
A-3.4 Demountable deformer measurements .....	23
A-3.5 Test procedure .....	24
<b>A-4 Results</b> .....	<b>27</b>
A-4.1 Analysis and presentation of data .....	27
A-4.2 Test DR1-a.....	29
A-4.3 Test DR1-b.....	37
A-4.4 Test DR1-c.....	40
A-4.5 Test DR2-a.....	43
A-4.6 Test DR2-b.....	51
A-4.7 Test DR2-c.....	56
A-4.8 Test PR1.....	61
<b>A-5 Conclusions</b> .....	<b>63</b>
A-5.1 Tests on bridge deck cantilevers.....	63
A-5.2 Punching shear test with simulation of vehicle wheel.....	66
<b>Bibliography</b> .....	<b>67</b>



## **A-1 Introductory remarks**

### **A-1.1 Aim**

The main objective of the tests on bridge cantilevers is to study the actual behavior of bridge deck cantilevers without shear reinforcement, under concentrated loads. The application of failure criteria for shear and punching shear (Muttoni 2003, and others) is investigated for the obtained test results.

From the obtained results of cantilevers failing in shear or punching shear, practical rules such as the location of control perimeters should be proposed. This could contribute to a more accurate assessment of bridge deck slabs failing in shear or punching shear.

Measurements of the surface strains, rotations, deflections, variation of slab thickness and geometry of the critical crack were made. These measurements can be used to compare with results from non linear finite element analysis or other models.

The tests were performed at full scale, without size-effect.

The objective of the punching shear test is to compare the case of punching shear with a vehicle wheel with the case of punching shear with a concrete column.

### **A-1.2 Acknowledgements**

This research was performed at the Structural Concrete Laboratory (IS-BETON) of the Ecole Polytechnique Fédérale de Lausanne, under the supervision of Prof. Dr. Aurelio Muttoni, to whom I would like to express my gratitude for his advice and encouragement provided.

The financial support granted by the Swiss Federal Roads Authority (FEDRO) and by the Portuguese Foundation for Science and Technology (FCT / BD 13259 / 2003) is gratefully acknowledged.

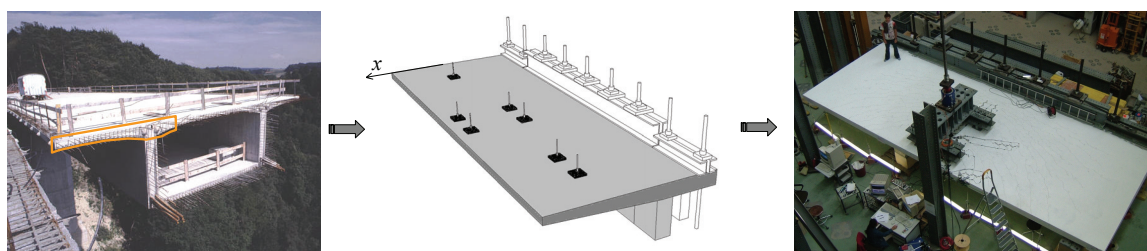
I wish to thank to all the field staff of the Structures Laboratory of the Ecole Polytechnique Fédérale de Lausanne for their support provided to the experimental activities.



## A-2 Description of the slabs

### A-2.1 Test concept and overview

The cantilevers are full scale models of part of a reinforced concrete bridge box girder, as shown in figure A-2.1. Two slabs (DR1 and DR2) were tested under loading patterns of one, two and four concentrated loads. Table A-2.1 shows the main parameters for the tests on cantilevers. The reinforcement ratio is calculated at the clamped edge, for the top bars at the transversal direction (bars along  $x$  axis).



a) Bridge girder with cantilever

b) Full scale model under loading patterns

c) Test DR1a, under four concentrated loads

Figure A-2.1: Test concept and load arrangement for the bridge cantilevers

Table A-2.1: Parameters for tests on cantilevers

Slab	Test	Number of concentrated loads	Reinforcement ratio for top bars along $x$ at the clamped edge
DR1	DR1-a	4	0.78%
	DR1-b	2	
	DR1-c	1	
DR2	DR2-a	2	0.60%
	DR2-b	2	
	DR2-c	1	

The reinforcement ratio of slab DR1 is representative of an elastically dimensioned reinforced concrete cantilever using the traffic loads prescribed by the Eurocode 1 (2003). The reinforcement ratio of the slab DR2 was reduced to validate the models described by (Muttoni 2003) for lower reinforcement ratios. None of the slabs has an edge beam.

The applied loads for test DR1-a are the twin axle loads prescribed by the Eurocode 1 (2003) with all dimensions reduced by 3/4. The subsequent tests were performed using only two or one concentrated loads to better focus on shear and punching shear failure modes.

Concerning the punching shear test, figure A-2.2 compares two types of punching shear tests. Both slabs have the same reinforcement layout and similar concrete properties. The central support for case a) at figure A-2.2 is a flat jack. The flat jack is made of a copper sheet envelope with water inside. The schematic distribution of the contact

pressure is indicated. For case a) the contact pressures at the interface  $a-b$  are approximately constant up to the failure of the slab. For case b) the central support is a concrete column. The contact pressures are not uniform and tend to increase near the column edge as the deflection of the slab increases. Guandalini (Guandalini 2005) tested a reinforced concrete slab with a concrete column as a central support (PG-10). This report presents only the results of the punching shear test with a flat jack (test PR1).

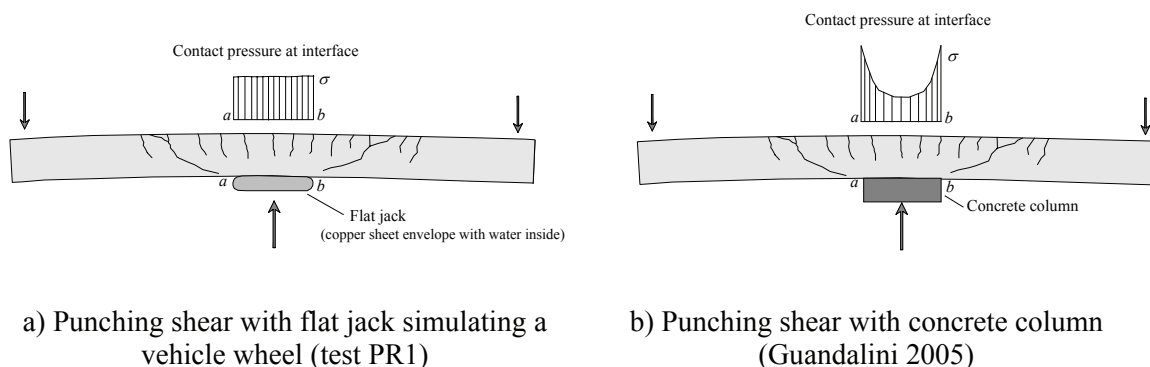


Figure A-2.2: Two punching shear experiments

The reinforcement ratio at the top layer in both directions for slab PR1 and PG-10 is equal to 0.33%. This value is representative of the bottom reinforcement at both directions for cantilevers, at the region near the cantilever edge.

## A-2.2 Geometry and reinforcement

The figures A-2.3 and A-2.4 illustrate the dimensions, the reinforcement layout and the applied loads for slabs DR1 and DR2. The cantilevers have a span of 2.78 meters (distance from the fixed end to the tip of the cantilever) and a total length of 10.00 meters. The thickness of the cantilevers is 0.19 meters at the free edge and 0.38 meters at the fixed end. For slab DR1, the transversal reinforcement of the top layer at the fixed end consists of 16 mm diameter bars at 75 mm spacing (reinforcement ratio  $\rho = 0.78\%$ ). The top transversal reinforcement is reduced to 16 mm diameter bars at 150 mm spacing at halfway of the span. For slab DR2, the transversal reinforcement of the top layer at the fixed end consists of 14 mm diameter bars at 75 mm spacing (reinforcement ratio  $\rho = 0.6\%$ ). The top transversal reinforcement is reduced to 14 mm diameter bars at 150 mm spacing at halfway of the span. No vertical shear reinforcement was provided between the free edge and the fixed end. The bottom reinforcement in both directions and the top longitudinal reinforcement consists of 12 mm diameter bars at 150 mm spacing for both slabs DR1 and DR2. An edge reinforcement consisting of 12 mm diameter bars at 150 mm spacing was added along the side edges ( $y = 0$  and  $y = 10.0$  m). The concrete cover is 30 mm.



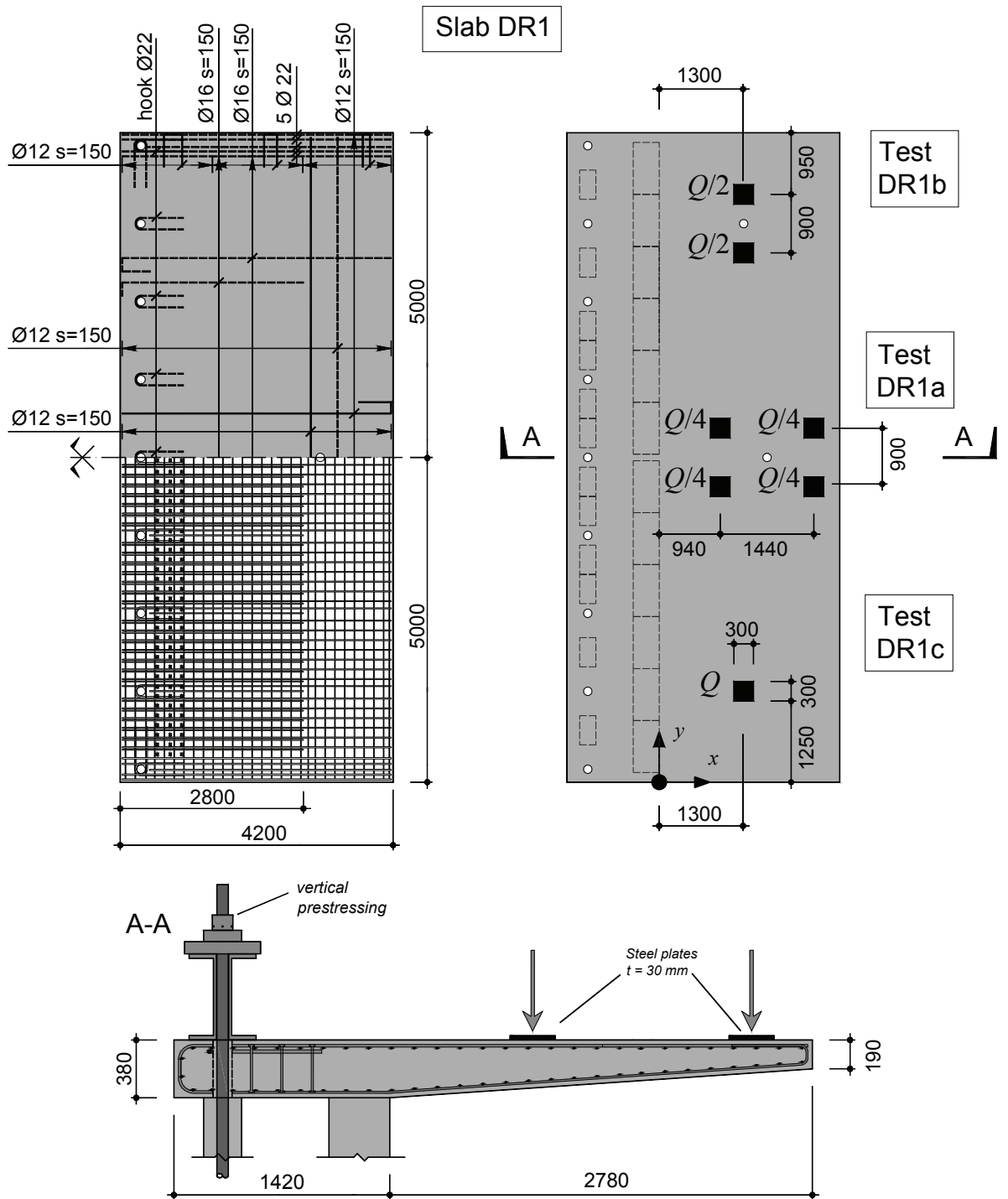


Figure A-2.3: Slab DR1. Dimensions, reinforcement layout and applied loads [mm]

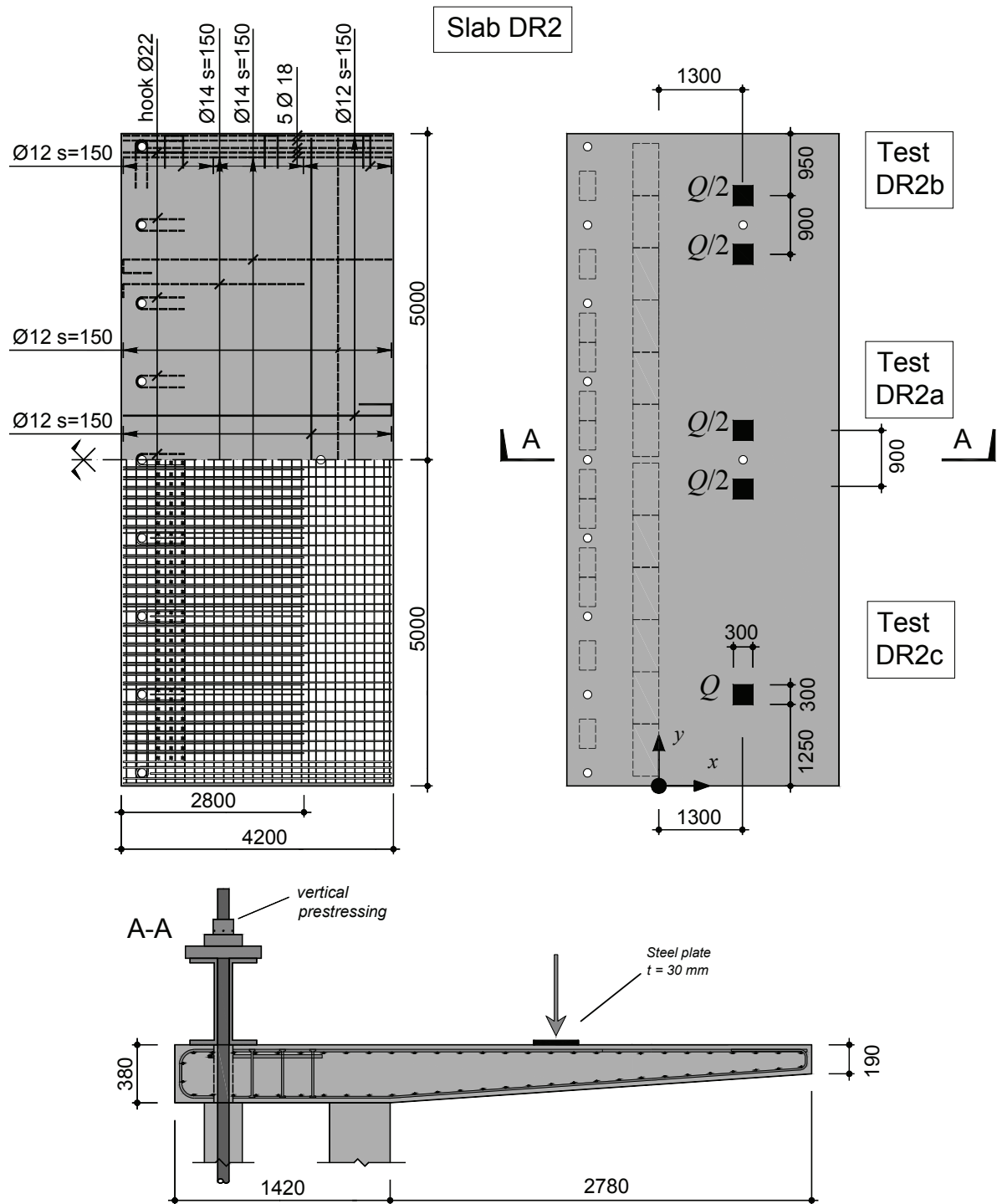


Figure A-2.4: Slab DR2. Dimensions, reinforcement layout and applied loads [mm]

Figure A-2.5 shows the reinforcement layout and geometry of slab PR1. The reinforcement at the top layer consists of 10 mm diameter bars at 115 mm spacing for both directions (reinforcement ratio  $\rho = 0.33\%$ ). The average effective depth between both directions at the top layer is 210 mm. The reinforcement at the bottom layer

consists of 8 mm diameter bars at 115 mm spacing for both directions. The concrete cover is 30 mm. The central support consists of a circular flat jack with a nominal surface of  $0.156 \text{ m}^2$ . No vertical shear reinforcement was provided.

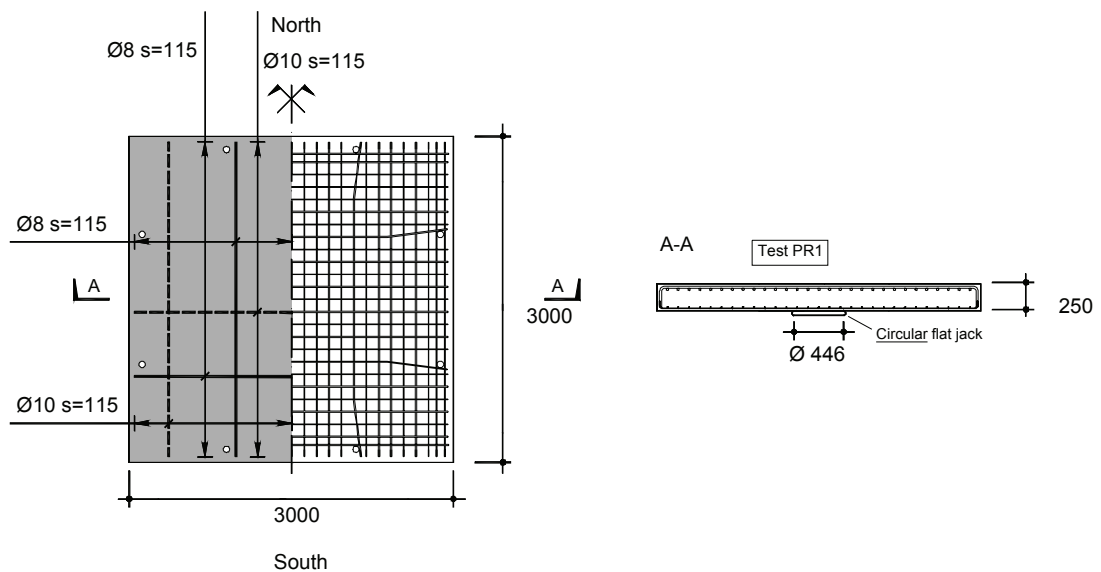


Figure A-2.5: Slab PR1. Dimension and reinforcement layout [mm]

### A-2.3 Construction of specimens

Figure A-2.6 shows some steps of the construction of slabs DR1 and DR2. Both slabs were cast at the Laboratory of Structures of the Ecole Polytechnique Fédérale de Lausanne. The plywood formwork surface in contact with concrete was impregnated with mould oil prior to the setting of reinforcement. Metallic hollow cylinders were fixed to the bottom of the formwork to create the holes required to apply loads on the cantilever. The casting of each slab required approximately 14 square meters of concrete. The concrete was made at a factory outside of the Structures Laboratory and was transported by a concrete mixer truck. Three shuttle trips were required to cast each slab. A conveyor belt was used to efficiently dispose the concrete in the formwork (fig. A-2.6 c). Two concrete vibrators were used to correctly place the concrete. The slump and flow table tests were performed before the casting of the slab. The table A-2.2 shows the results of the slump and flow table tests. About thirty concrete cylinders were cast for each slab using the same batch of concrete. The surface of the slab was leveled and smoothed with the help of a ruler and a mason's mortar board. After casting, the slab was covered with a plastic sheet to maintain a moist environment. Water was sprayed onto the slab during the period of curing.

Slab DR1 was cast on the 27<sup>th</sup> of April of 2005 and slab DR2 was cast on the 4<sup>th</sup> of October of 2005. The formwork was partially removed two weeks after casting to allow the vertical prestressing of the fixed end (figs. A-2.3 and A-2.4). A total prestress force of 7 MN ensured that the fixed end was well clamped. Three weeks after casting the entire formwork was removed.

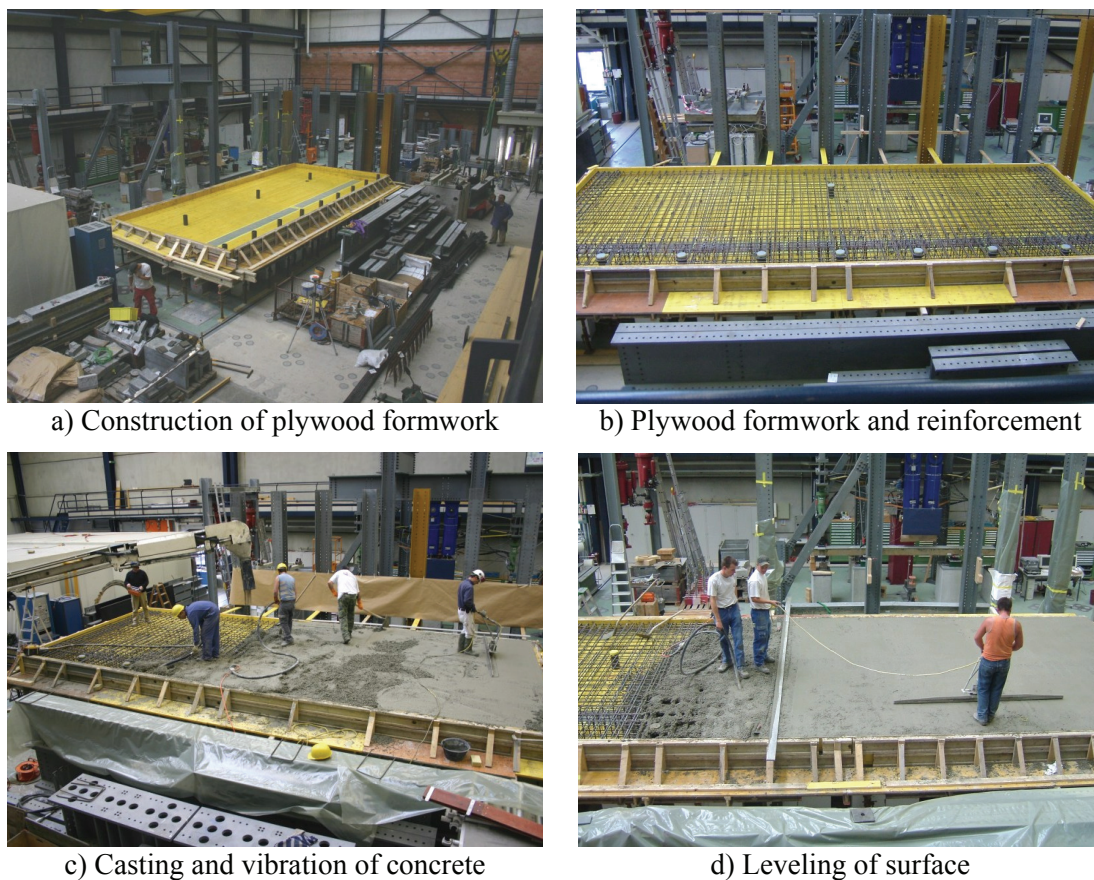


Figure A-2.6: Construction of slabs DR1 and DR2

## A-2.4 Material properties

### Concrete

The composition of concrete used for slabs DR1 and DR2 is indicated in table A-2.2. The water-cement ratio is 0.54 for both slabs. The maximum size of the aggregate is 16 mm. Concrete cylinders were cast for each slab using the same batch of concrete. Each concrete cylinder had a diameter  $\varnothing = 159$  mm and height of  $h = 320$  mm. The mechanical properties were measured with tests on concrete cylinders. The tests were performed at the Laboratory of Construction Materials (LMC) of the Ecole Polytechnique Fédérale de Lausanne. The measured properties are the concrete compressive strength, the tensile strength, the Young's modulus and the apparent density. Tables A-2.4, A-2.5 and A-2.6 show the results of tests on concrete cylinders for slabs DR1, DR2 and PR1, respectively. The mechanical properties at the time of testing are calculated using fitted equations of form  $a \cdot \text{days}^b + c$ . Figure A-2.7 (1) shows the time evolution of the concrete compressive strength ( $f_c$ ), the concrete tensile strength ( $f_{ct}$ ) and the Young's modulus ( $E_c$ ). Figure A-2.7 (2) shows the measured stress-strain curve in compression for concrete of slab DR1, after (Fernández Ruiz 2005). The table A-2.3 indicates the average value and the coefficient of variation of the mechanical properties at the time of failure.

Table A-2.2: Composition of 1 cubic meter of concrete and results of tests on fresh concrete

Slab	Sand 0-4	Gravel 4-8	Gravel 8-16	Cement	Water	Slump test [mm]	Flow table test [mm]
	[kg]	[kg]	[kg]	[kg]	[kg]		
DR1	753	604	661	325	174	20	360
	37%	30%	33%		W/C = 0.54		
DR2	753	604	661	325	174	15	320
	37%	30%	33%		W/C = 0.54		

Table A-2.3: Concrete properties at the time of failure (average value and coefficient of variation)

Test	Date	Number of days	Compressive strength	Tensile strength	Young's modulus
			( $f_c$ ) [MPa]	( $f_{ct}$ ) [MPa]	( $E_c$ ) [GPa]
DR1-a	12.07.2005	76	39.11	2.94	36.03
			3.3%	8.3%	4.2%
DR1-b	28.07.2005	92	39.91	3.02	36.09
			5.1%	8.3%	4.3%
DR1-c	19.08.2005	114	40.82	3.11	36.16
			7.6%	8.3%	4.6%
DR2-a	09.12.2005	66	38.92	3.13	36.26
			4.8%	4.9%	0.8%
DR2-b	17.01.2006	105	41.98	3.14	37.39
			15.5%	0.0%	4.0%
DR2-c	24.01.2006	112	42.42	3.14	37.54
			4.3%	0.0%	3.8%
PR1	24.05.2004	47	35.17	2.23	31.84
			4.3%	5.2%	4.0%

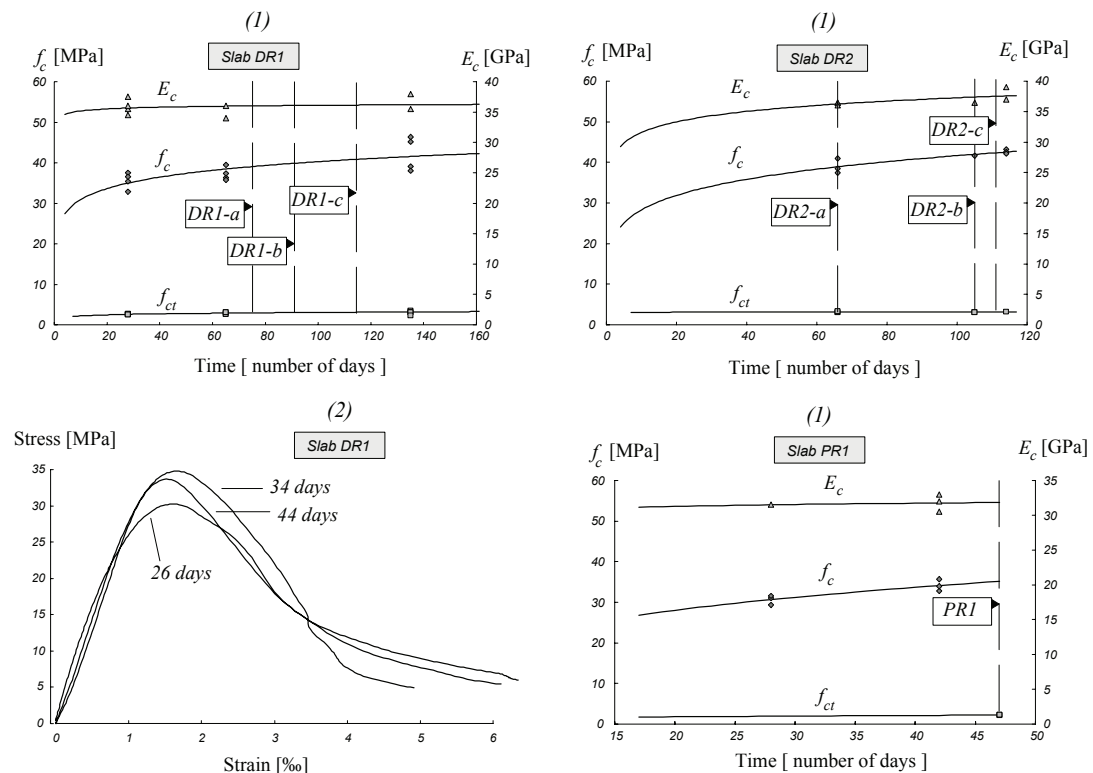


Figure A-2.7: (1) Evolution of mechanical properties of concrete with time for slabs DR1, DR2 and PR1; (2) Stress-strain curve of concrete in compression after tests performed by (Fernández Ruiz 2005)

## Chapter A-2

Table A-2.4: Results of tests on concrete cylinders (slab DR1)

Report	Date	Number of days	Compressive strength ( $f_c$ ) [MPa]	Tensile strength ( $f_{ct}$ ) [MPa]	Young's modulus ( $E_c$ ) [GPa]	Apparent density [t/m <sup>3</sup> ]
Casting	27.04.2005	0	0.00	0.00	0.00	-
124/05/LMC	25.05.2005	28	35.40		35.50	2.43
124/05/LMC	25.05.2005	28	37.50		36.00	2.45
124/05/LMC	25.05.2005	28	36.60		34.50	2.44
124/05/LMC	25.05.2005	28	32.90		37.50	2.45
125/05/LMC	25.05.2005	28		2.60		2.44
125/05/LMC	25.05.2005	28		2.70		2.44
125/05/LMC	25.05.2005	28		2.50		2.45
125/05/LMC	25.05.2005	28		2.50		2.45
171/05/LMC	01.07.2005	65	36.30		34.00	2.44
171/05/LMC	01.07.2005	65	37.40		36.00	2.44
172/05/LMC	01.07.2005	65		2.70		2.45
172/05/LMC	01.07.2005	65		3.00		2.43
172/05/LMC	01.07.2005	65		2.60		2.44
172/05/LMC	01.07.2005	65		3.10		2.45
170/05/LMC	01.07.2005	65	39.50			2.44
170/05/LMC	01.07.2005	65	35.70			2.42
227/05/LMC	09.09.2005	135		3.50		2.44
227/05/LMC	09.09.2005	135		3.00		2.44
227/05/LMC	09.09.2005	135		3.10		2.43
227/05/LMC	09.09.2005	135		2.20		2.43
226/05/LMC	09.09.2005	135	46.30			2.44
226/05/LMC	09.09.2005	135	39.10			2.45
224/05/LMC	09.09.2005	135	45.10		38.00	2.44
224/05/LMC	09.09.2005	135	38.00		35.50	2.42

Table A-2.5: Results of tests on concrete cylinders (slab DR2)

Report	Date	Number of days	Compressive strength ( $f_c$ ) [MPa]	Tensile strength ( $f_{ct}$ ) [MPa]	Young's modulus ( $E_c$ ) [GPa]	Apparent density [t/m <sup>3</sup> ]
Casting	04.10.2005	0	0.00	0.00	0.00	-
299/05/LMC	09.12.2005	66		3.10		2.44
299/05/LMC	09.12.2005	66		3.00		2.45
299/05/LMC	09.12.2005	66		3.30		2.44
298/05/LMC	09.12.2005	66	38.40		36.50	2.44
298/05/LMC	09.12.2005	66	41.00		36.50	2.44
298/05/LMC	09.12.2005	66	37.40		36.00	2.44
004/06/LMC	17.01.2006	105	41.60		36.50	2.44
005/06/LMC	17.01.2006	105		3.1		2.45
005/06/LMC	17.01.2006	105		3.1		2.44
006/06/LMC	26.01.2006	114	43.20		39.00	2.44
006/06/LMC	26.01.2006	114	42.50		37.00	2.43
007/06/LMC	26.01.2006	114		3.20		2.43
008/06/LMC	26.01.2006	114	42.20			2.43

Table A-2.6: Results of tests on concrete cylinders (slab PR1)

Report	Date	Number of days	Compressive strength ( $f_c$ ) [MPa]	Tensile strength ( $f_{ct}$ ) [MPa]	Young's modulus ( $E_c$ ) [GPa]	Apparent density [t/m <sup>3</sup> ]
Casting	07.04.2004	0	0.00	0.00	0.00	-
099/04/LMC	05.05.2004	28	31.00		31.50	2.43
098/04/LMC	05.05.2004	28	31.60			2.43
098/04/LMC	05.05.2004	28	29.40			2.43
112/04/LMC	19.05.2004	42	32.80		33.00	2.43
112/04/LMC	19.05.2004	42	33.90		30.50	2.42
112/04/LMC	19.05.2004	42	35.70		32.00	2.44
115/04/LMC	24.05.2004	47		2.30		2.43
115/04/LMC	24.05.2004	47		2.10		2.43
115/04/LMC	24.05.2004	47		2.30		2.43

## Reinforcement

The reinforcement bars were tested in tension at the Laboratory of Mechanical Metallurgy of the Ecole Polytechnique Fédérale de Lausanne. The stress-strain curves are shown in figure A-2.8, along with the surface of the reinforcement bars and the dimension of the ribs. All the bars are of type B500B accordingly with the Swiss code SIA 262 (2003). The mechanical properties are indicated in table A-2.7. All the bars are hot-rolled except for bars with 12 mm of diameter for slab DR2. Table A-2.8 indicates the detailed results for each tensile test. The strains were measured using extensometers with a measurement length of 150 mm. The loading speed was 10 MPa/s.

Table A-2.7: Mechanical properties of reinforcement

Slab	Diameter (Ø) [mm]	Yield Strength ( $f_y$ ) [MPa]	Tensile strength ( $f_t$ ) [MPa]	Deformation under maximum load ( $\epsilon_u$ ) [%]	$f_t/f_y$	Steel type
DR1	16	499 4.2%	600 2.0%	10.73 6.0%	1.20 2.2%	hot-rolled
	12	541 0.4%	629 0.2%	9.05 6.1%	1.16 0.5%	hot-rolled
	22	534 0.2%	644 0.3%	10.91 12.8%	1.21 0.5%	hot-rolled
DR2	14	505 3.1%	591 4.1%	11.11 28.4%	1.17 1.5%	hot-rolled
	12	469* 6.0%	580 1.2%	5.19 15.2%	1.24 4.8%	cold formed
	18	541 -	639 -	11.54 -	1.18 -	hot-rolled
PR1	10	566 -	648 -	9.66 -	1.15 -	hot-rolled
	12	566 0.3%	622 0.4%	8.80 8.6%	1.10 0.1%	hot-rolled

\* Offset yield-point at 0.2% strain

Table A-2.8: Results of tests on reinforcement

Test	Nominal Diameter (Ø) [mm]	Yield Strength ( $f_y$ ) [MPa]	Tensile strength ( $f_t$ ) [MPa]	Deformation under maximum load ( $\epsilon_u$ ) [%]	$f_t/f_y$	Distance between anchorages [mm]	Measurement length with extensometer [mm]
DR1_16_1	16	519	612	10.53	1.18	670	150
DR1_16_2	16	516	610	9.92	1.18	670	150
DR1_16_3	16	480	590	11.39	1.23	670	150
DR1_16_4	16	482	590	11.09	1.22	670	150
DR1_12_1	12	542	628	9.04	1.16	790	150
DR1_12_2	12	539	630	8.51	1.17	790	150
DR1_12_4	12	543	630	9.61	1.16	790	150
DR1_22_1	22	536	644	10.33	1.20	660	150
DR1_22_2	22	533	646	12.50	1.21	660	150
DR1_22_3	22	534	642	9.90	1.20	660	150
DR2_14_1	14	517	600	16.30	1.16	500	150
DR2_14_2	14	502	592	10.10	1.18	470	150
DR2_14_3	14	501	588	9.45	1.17	470	150
DR2_14_4	14	500	585	8.59	1.17	470	150
DR2_12_1	12	500*	588	5.95	1.18	525	150
DR2_12_3	12	461*	576	5.25	1.25		150
DR2_12_4	12	445*	575	4.38	1.29		150
DR2_18_1	18	541	639	11.54	1.18	660	150
PR1_10_2	10	566	648	10.53	1.15	595	150
PR1_12_1	12	565	621	9.92	1.10	625	150
PR1_12_2	12	568	624	11.39	1.10	810	150

\* Offset yield-point at 0.2% strain

## Chapter A-2

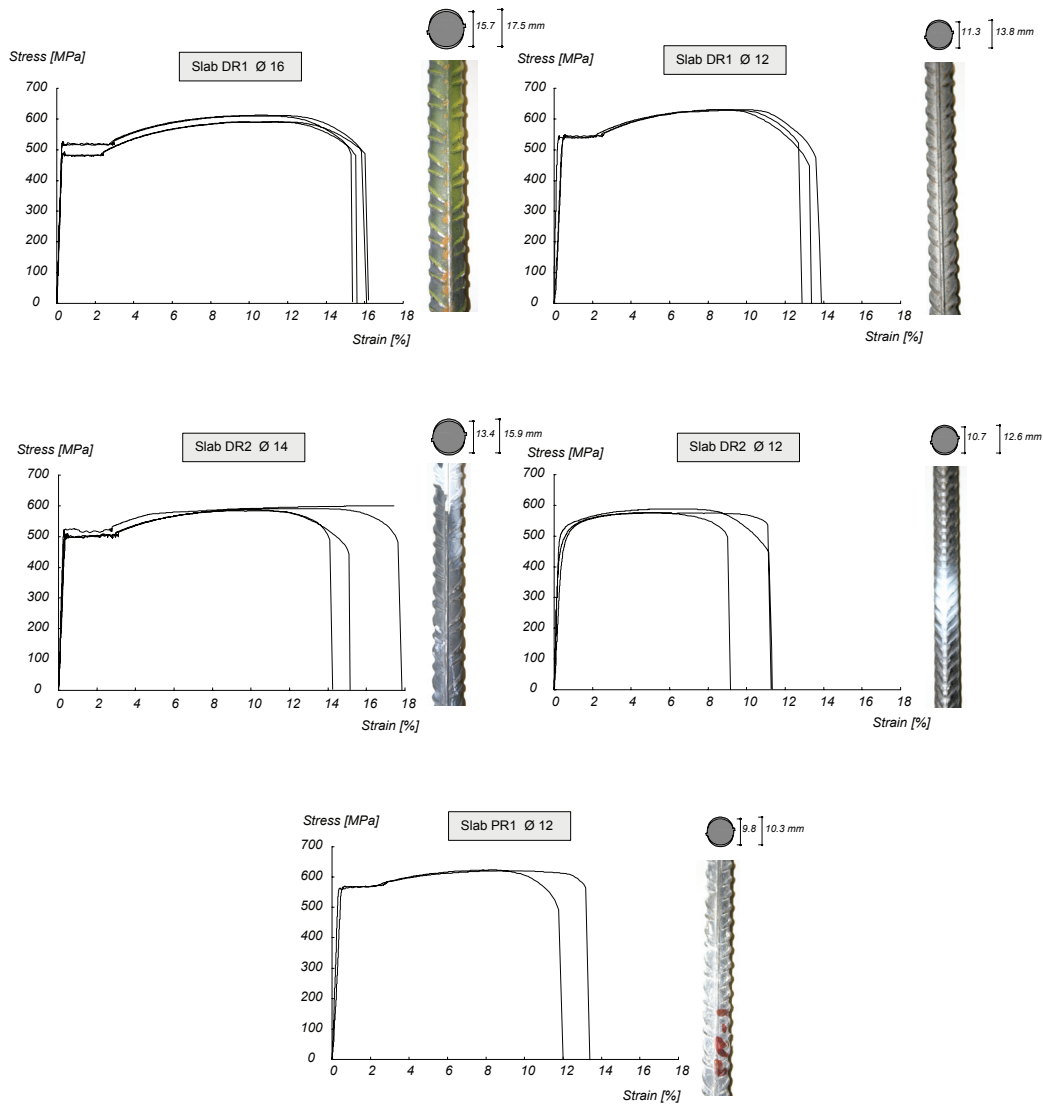


Figure A-2.8: Stress-strain curves for steel bars



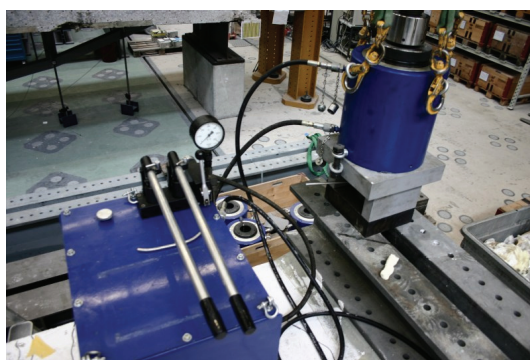
### A-3 Experimental set-up and procedure

All tests have been performed at the Structural Laboratory of the Ecole Polytechnique Fédérale de Lausanne.

#### A-3.1 Reaction frames and load application

Figure A-3.2 shows the test set-up for test DR1-a. Four concentrated loads were applied using square steel plates of 300 x 300 x 30 mm. The distance between the center points of the loads is of 1440 mm in the transversal direction and 900 mm in the longitudinal direction. These dimensions correspond to 3/4 of the dimensions of the twin axle loads prescribed by Eurocode 1 (2003). A hollow hydraulic jack introduced a self-equilibrated stress state in the system. The load was transmitted to the concentrated loads by one steel beam in the transversal direction and four channels in the longitudinal direction. Steel bars of 75 mm of diameter were anchored below the strong floor and above the hydraulic jack. A cylindrical opening of 120 mm of diameter was created in the center of the slab. Spherical nuts and washers were used to accommodate rotation at the anchorage point of the steel bars. The forces were measured at the four applied loads and at the bar above the hydraulic jack. This allowed for redundancy in the system and to know the effective force at each of the four concentrated loads. A hand pump was used in all tests.

A total prestress force of 7 MN was applied at the nine bars behind the fixed end to ensure that the slab was properly clamped. The prestress was applied three weeks after casting. Figure A-3.1 shows the prestressing set-up used to clamp the fixed end of the cantilever.



a) Prestressing set-up



b) Detail of bench and nut

Figure A-3.1: Prestressing of the fixed end of cantilevers DR1 and DR2

Figure A-3.3 illustrates the test set-up for test DR1-b. Only two concentrated loads were applied. The distance between the concentrated loads is of 900 mm in the longitudinal direction. This loading pattern corresponds to half of the loading pattern prescribed by the Eurocode 1 (2003), with dimensions reduced by 3/4.

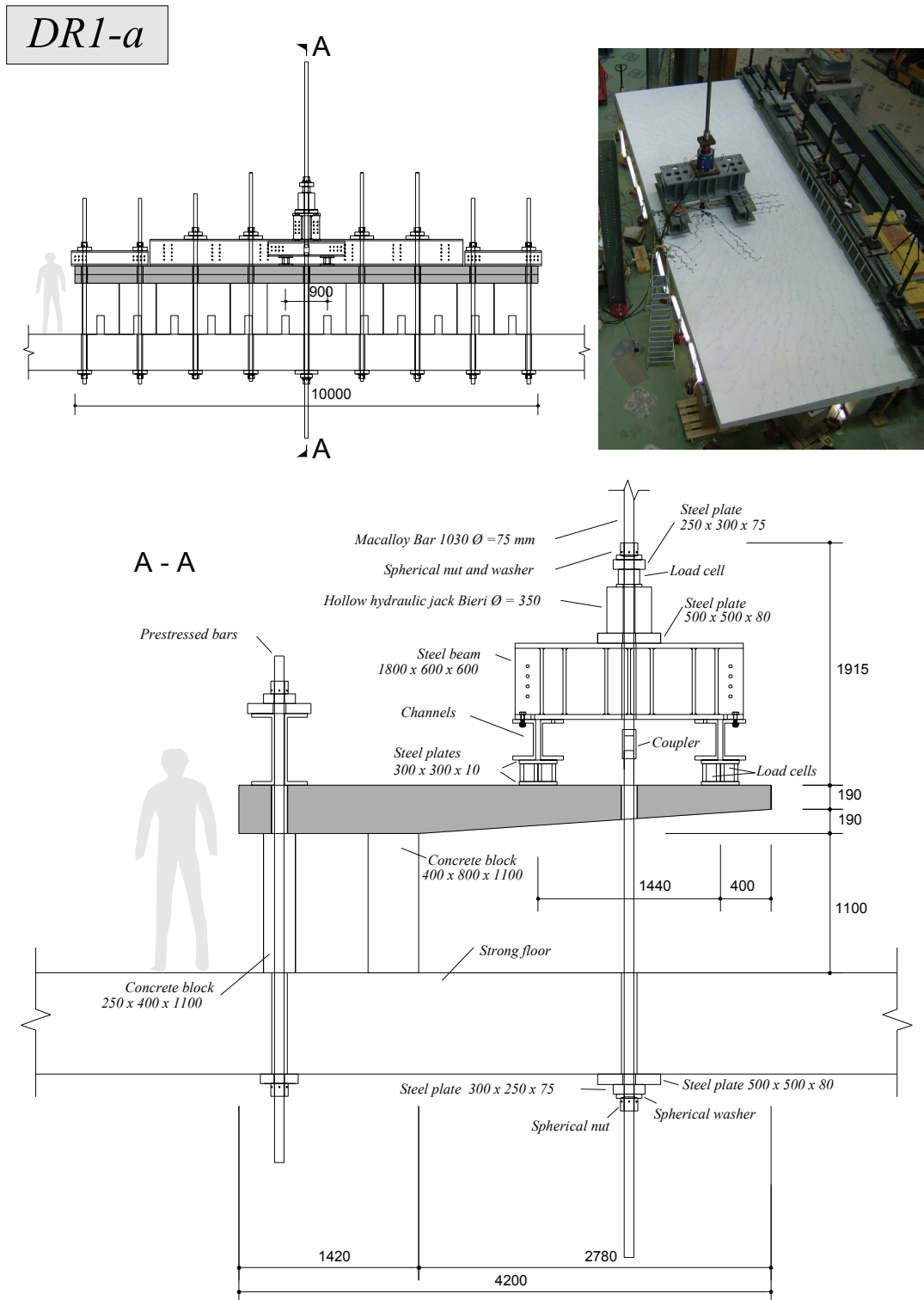


Figure A-3.2: Test set-up for test DR1-a [mm]

DR2-a

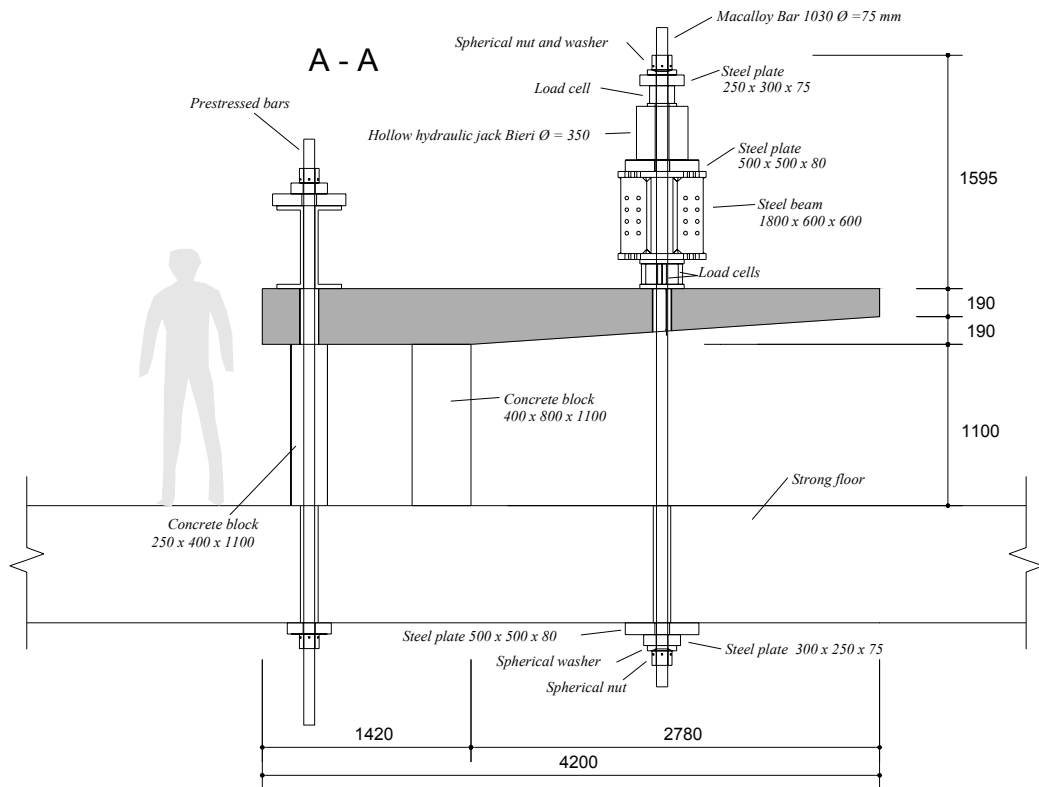
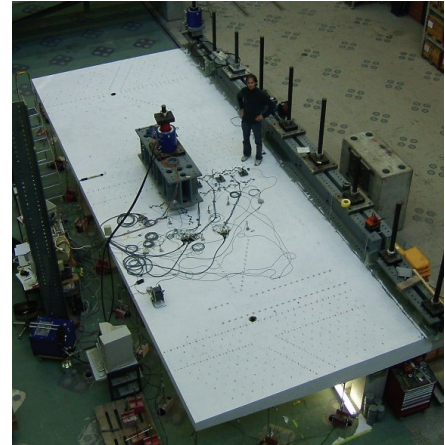
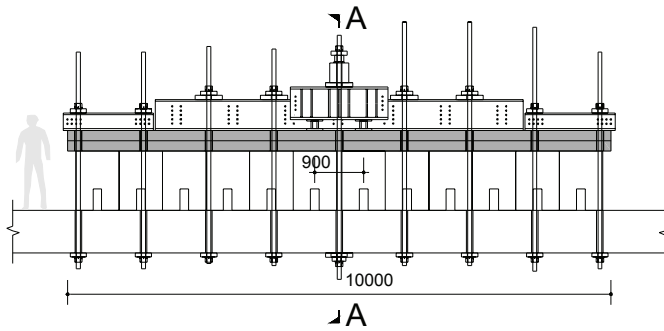


Figure A-3.3: Test set-up for test DR2-a [mm]

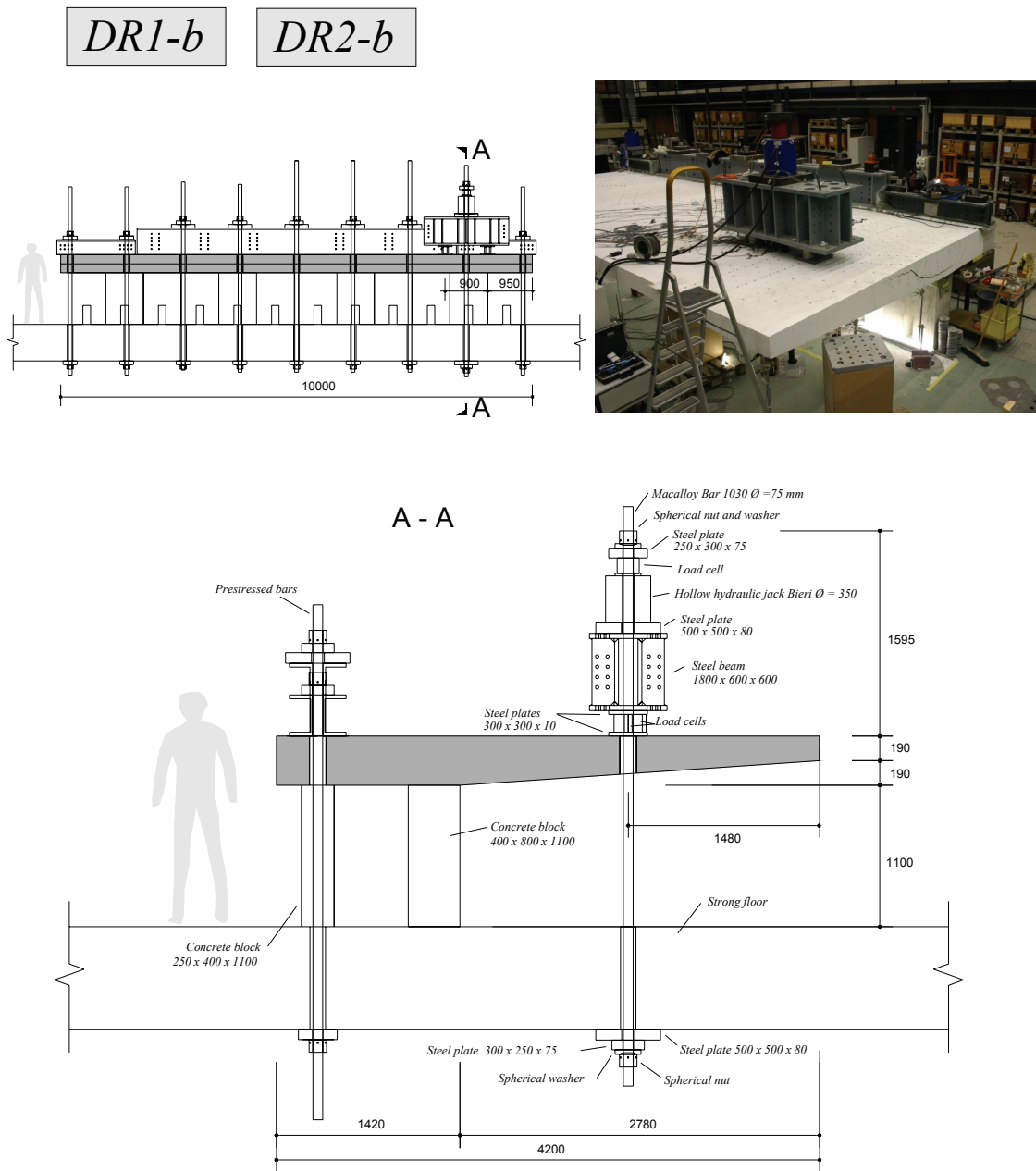


Figure A-3.4: Test set-up for tests DR1-b and DR2-b [mm]

Figure A-3.4 illustrates the test set-up for test DR1-b and DR2-b. Only two concentrated loads were applied, as in the case of test DR2-a. The loads were applied near the short free edge of the cantilever.

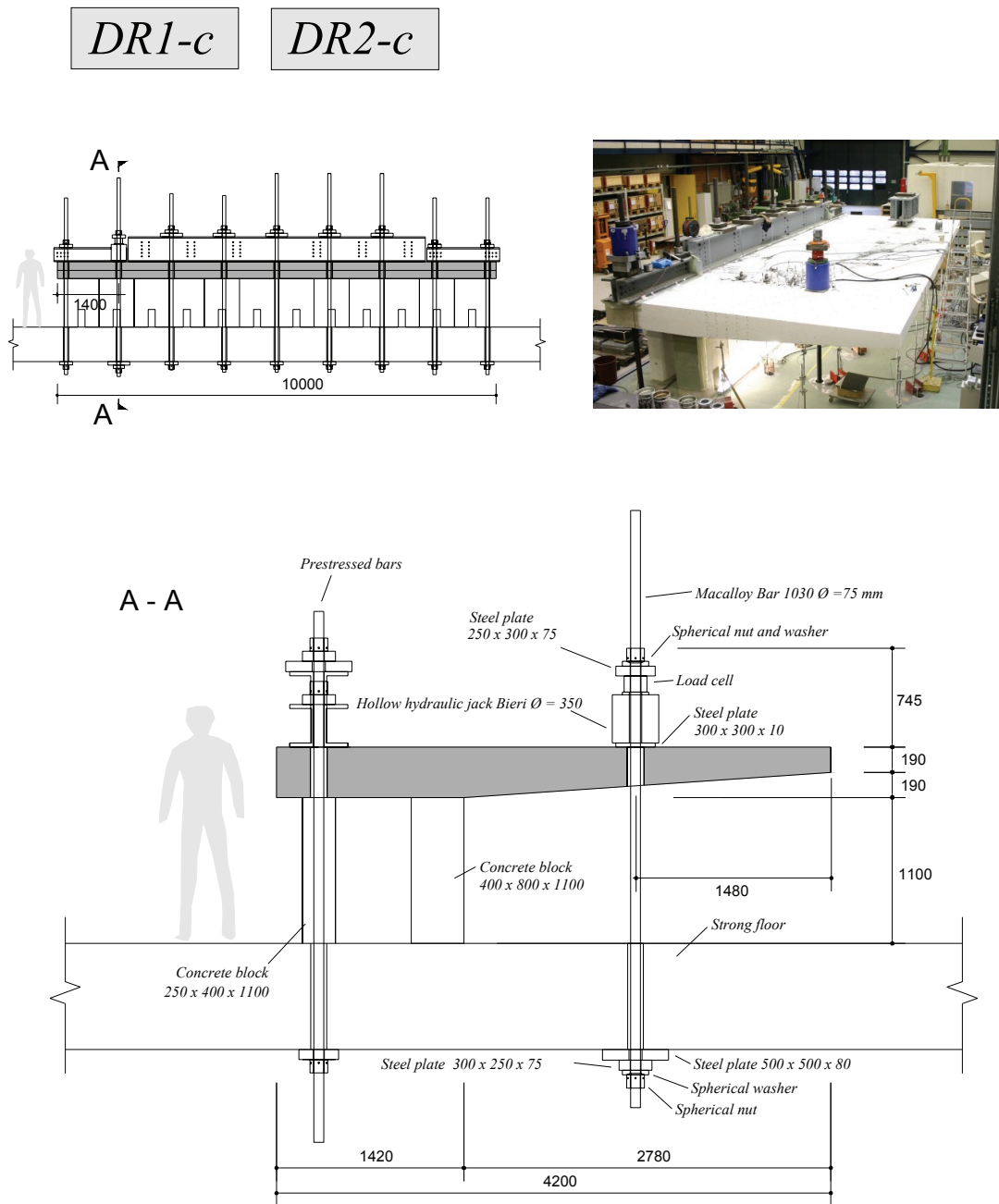


Figure A-3.5: Test set-up for tests DR1-c and DR2-c [mm]

Figure A-3.5 illustrates the test set-up for test DR1-c and DR2-c. Only one concentrated load was applied near the short free edge of the cantilever.

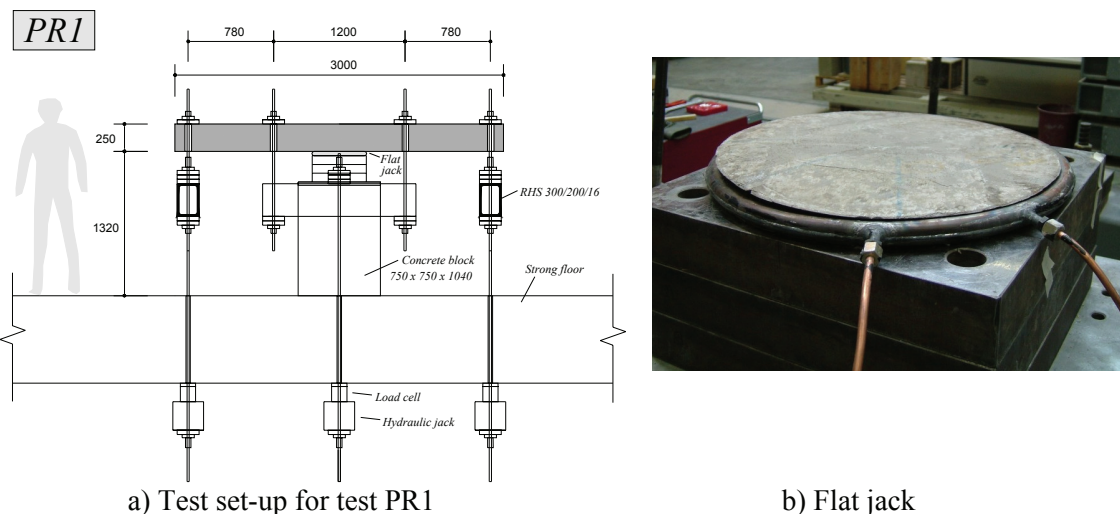


Figure A-3.6: Test set-up for test PR1 [mm]

Figure A-3.6 shows the test set-up for test PR1. The loads were applied using four hydraulic jacks below the strong floor. The force was measured using four load cells between the jacks and the strong floor. At each of the four sides of the slab, two openings were created to allow the introduction of the forces. The central support was a flat jack. The flat jack is made of a copper sheet envelope with water inside. The nominal surface is 0.156 m<sup>2</sup> and the nominal diameter 446 mm. Before the test the flat jack was completely filled with water. During the test the water volume was kept constant.

The self-weight of the steel elements of the test rig is indicated in table A-3.1. For the tests on cantilevers, only the elements in the cantilever part are considered.

Table A-3.1: Self-weight of the test rig

Test	Self-weight [kN]
DR1-a	32.2
DR1-b, DR2-b, DR2-a	22.1
DR1-c, DR2-c	6.7
PR1	16.8

### A-3.2 Preparation of slabs

After the introduction of the prestressing behind the fixed end to ensure that the slabs DR1 and DR2 were properly clamped, the sensors were installed for each test. The following procedure was used to install the sensors:

- The entire cantilever was painted using dispersion white paint.
- The measuring grids (fig. A-3.13) and the position of all sensors were printed on full scale paper of the size of the slab and marked on the bottom and top surfaces.
- The surface was cleaned with compressed air and smoothed with a sanding block at the locations of the sensors.
- The aluminum measuring targets of the demountable deformer grid were glued to the concrete surface using synthetic rapid hardening glue.

- The aluminum supports of the omega-shaped extensometers were glued to the concrete surface using a two component glue, X60.
- The slab was perforated along the cantilever thickness with a 8 mm drill at the measuring locations (only for slab DR2, fig. A-3.9).
- The positions of the demountable deformer were numbered.
- The omega-shaped extensometers, the LVDTs and the inclinometers were installed along with their cables.
- Three computers were installed, one for the omega-shape extensometers, LVDTs and load cells, one for the measurements of the demountable deformer and one for the inclinometers.
- All measuring devices were tested by individually moving them and controlling the response on the computer.
- All measuring devices were zeroed.
- A light load of about 50% of cracking was applied to ensure that all measures were properly saved in the results file.

### A-3.3 Continuous measurements

The following values were continuously measured during the tests:

- The forces were measured using load cells (figs. A-3.2 to A-3.6).
- The deflections were measured using LVDTs (figs. A-3.7 and A-3.11).
- The strains on the concrete surface were measured using omega-shaped extensometers (figs. A-3.8, A-3.9 and A-3.11).
- The rotations of slab were measured using inclinometers (figs. A-3.8, A-3.9 and A-3.11).
- The variation of the thickness of the slab was measured using LVDTs (fig. A-3.9).
- The time was measured with the clock of the computers.

The minimum time interval between two measures is of 10 seconds. The oil pressure was measured for all tests as a redundant value. The figure A-3.10 illustrates the top surface of slab DR2 during test DR2-c.

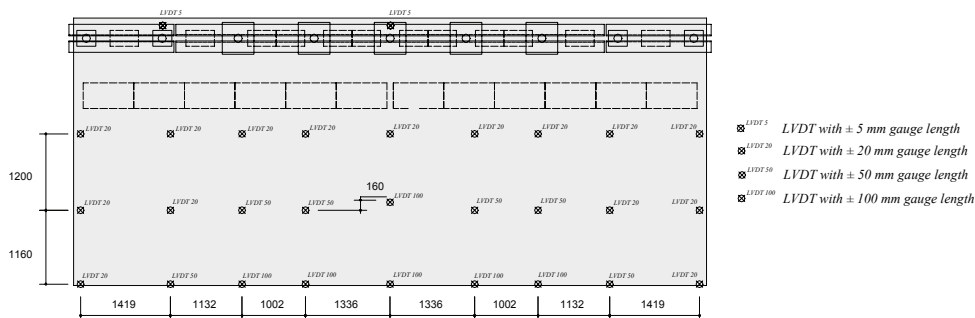


Figure A-3.7: Deflection measurements for all tests on cantilevers (DR1-a, DR1-b, DR1-c, DR2-a, DR2-b and DR2-c) [mm]

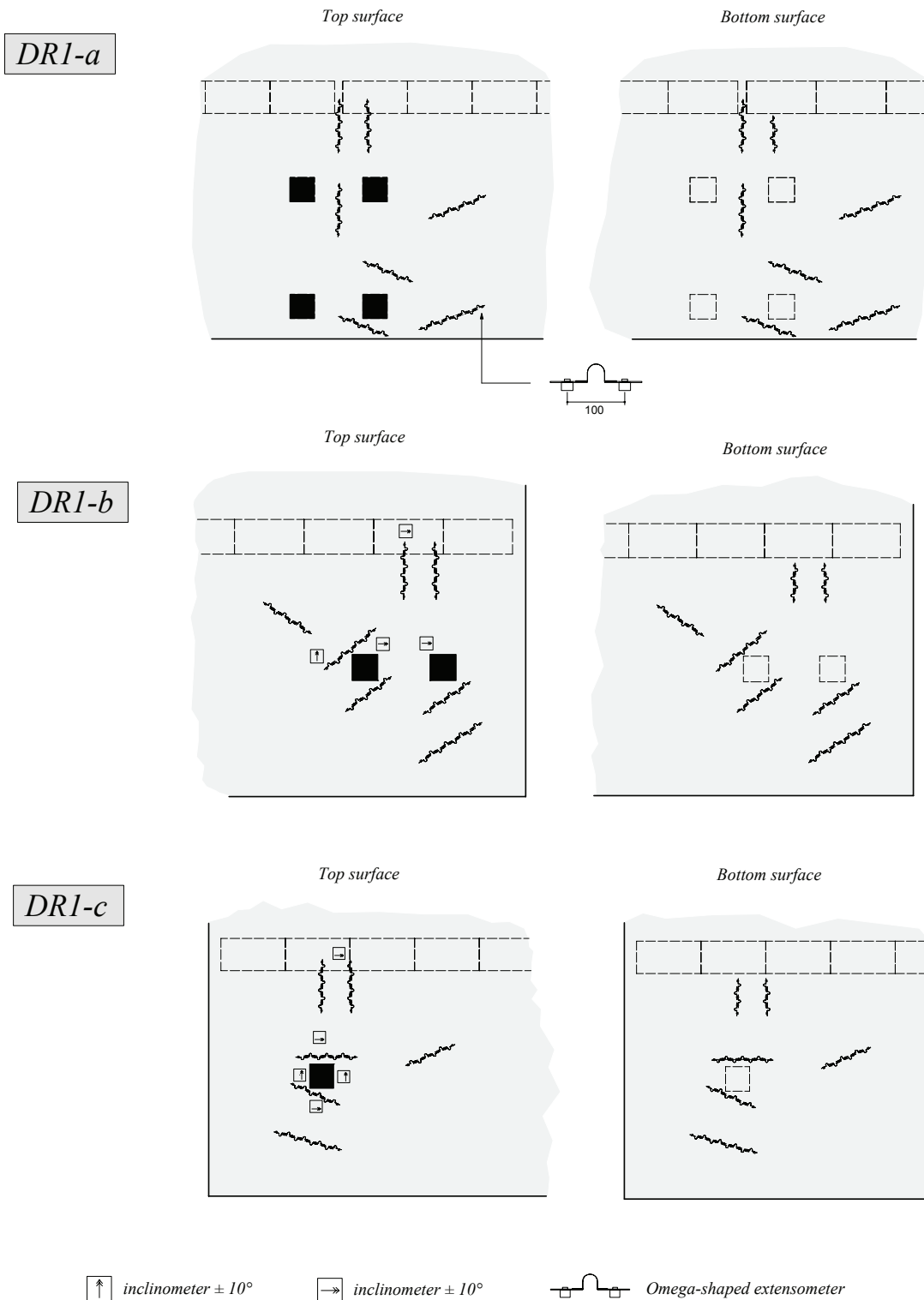


Figure A-3.8: Inclinometers and omega-shaped extensometers for tests DR1-a, DR1-b and DR1-c [mm]



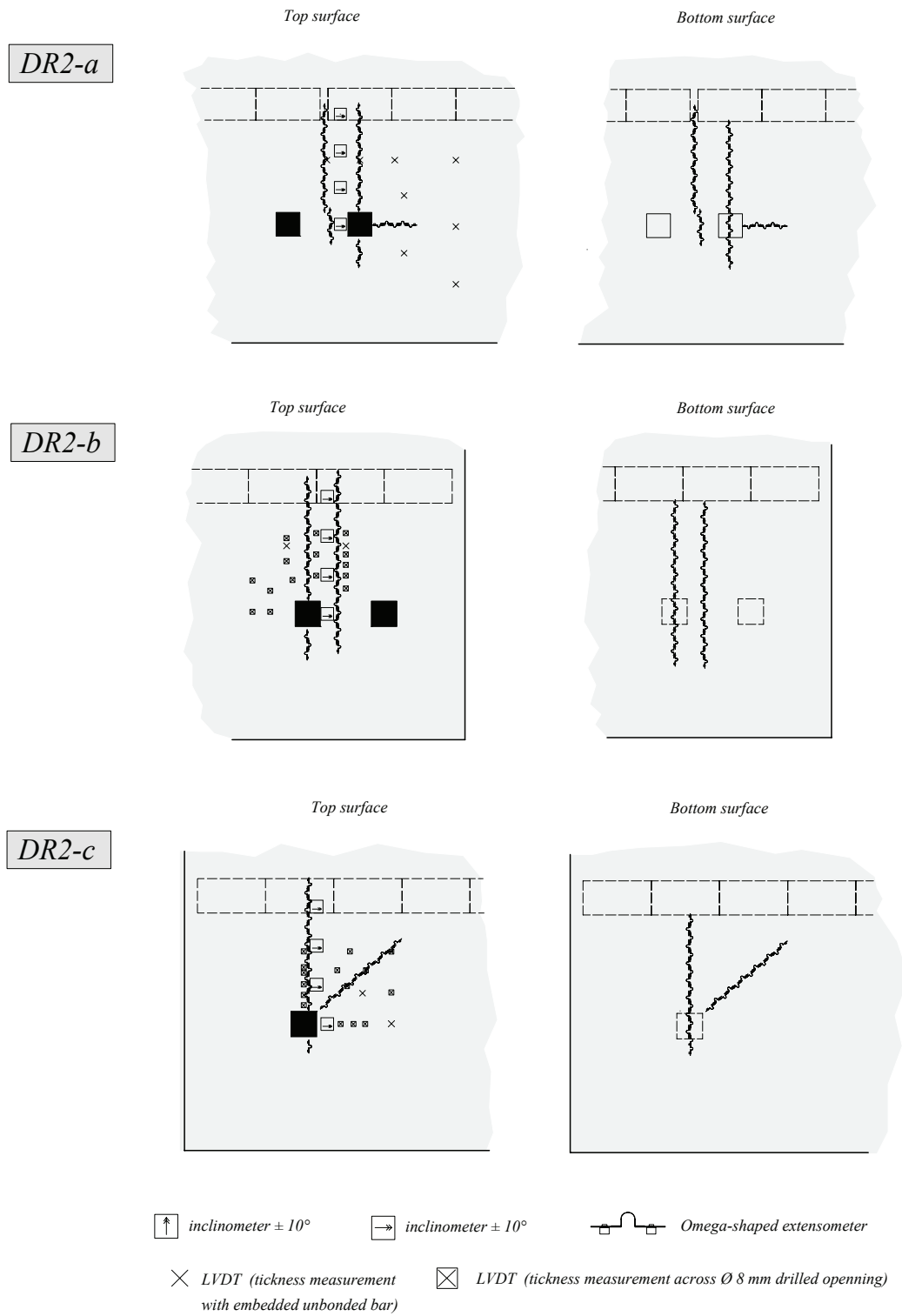


Figure A-3.9: Inclinometers, omega-shaped extensometers and LVDTs used to measure the variation of the tickness of the cantilever (tests DR2-a, DR2-b and DR2-c)

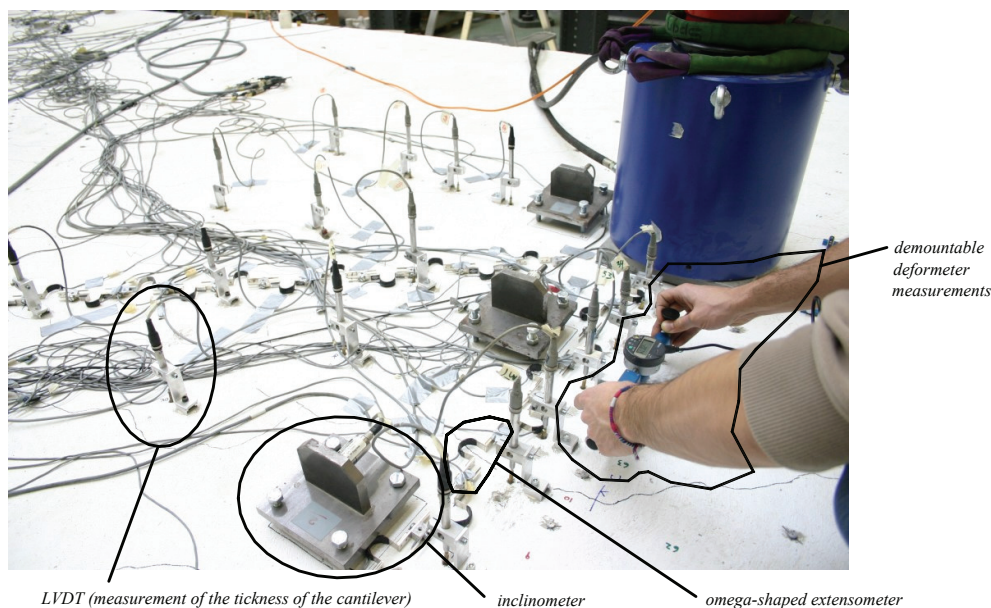


Figure A-3.10: Top surface of slab DR2 during test DR2-c

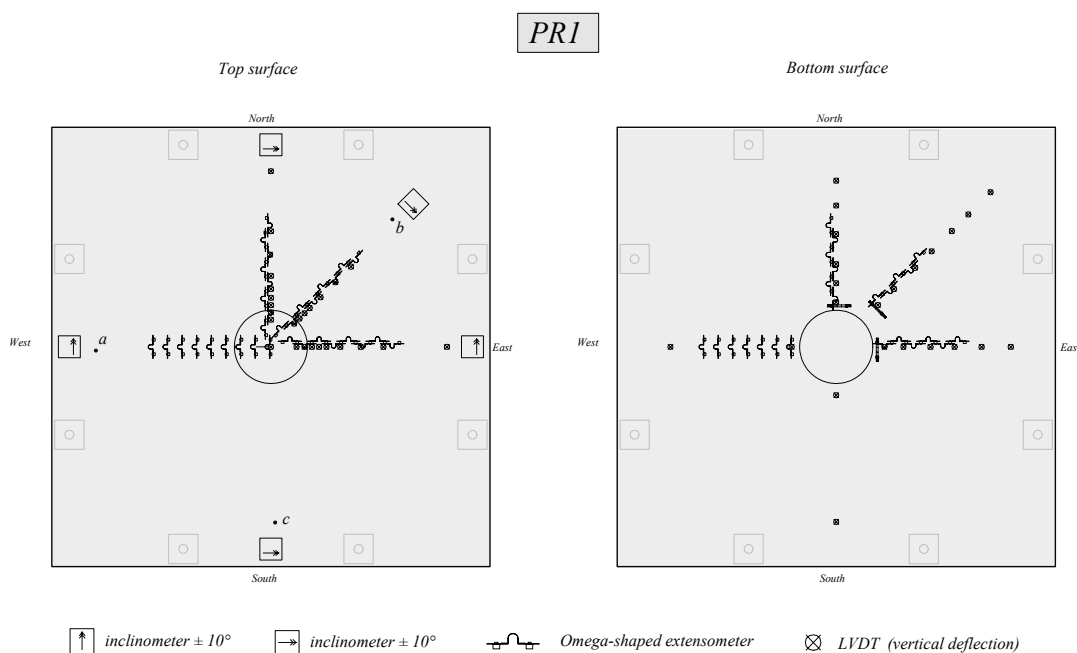


Figure A-3.11: Inclinometers, omega-shaped extensometers and LVDTs for test PR1

For the tests performed on slab DR1, the omega-shaped extensometers were placed in the zones where the largest flexural strains were expected. For tests performed on slab DR2, the omega-shaped extensometers were placed almost exclusively in the region between the concentrated loads and the clamped edge. For slab PR1, the omega-shaped extensometers were placed in the radial direction along three lines and in the tangential direction along one line (fig. A-3.11).

The LVDTs for tests on slabs DR1 and DR2 were arranged in a grid and measured the deflection from the strong floor (fig. A-3.7). Each LVDT was fixed to a structure that was prestressed to the strong floor. This prevented the LVDT to be accidentally

displaced during the tests. Two LVDTs were placed behind the clamped edge. The maximum deflection measured at these locations was of 0.17 mm for test DR1-a at the failure load. This value represents only 0.3% when compared with the measured deflection at the tip of the cantilever. For slab PR1, the LVDTs measured the deflection of the slab at both top and bottom surfaces (fig. A-3.11). The LVDTs on the top surface were fixed to a rigid aluminum structure. The points *a*, *b*, and *c* in figure A-3.11 are the bearing points of the aluminum structure.

The LVDTs were also used to measure the variation of the thickness of the slab for the tests on slab DR2 (fig. A-3.9). Two systems were used. The idea of the first system consists of using a vertical metallic bar of small diameter that is not bonded to concrete (fig. A-3.12a). There is a plastic duct around the metallic bar. A small circular plate is welded in the bottom end of the bar. This point is where the bar is anchored to concrete. The displacements between the top end of the bar and the top surface of the concrete slab are measured using LVDTs. If a shear crack forms, the top end of the bar will be vertically displaced. The value of this displacement is equal to the variation of the thickness of the slab. The metallic bars have to be fixed to the formwork before casting. The second system (fig. A-3.12b) is simpler and consists of using a LVDT that directly measures the displacements across small cylindrical openings, between the top and bottom surfaces of the slab. A drill of 8 mm of diameter and a length of about 450 mm was used to perform the cylindrical openings. The measurements using the first system (fig. A-3.12a) are sensible to the friction between the metallic bar and the plastic duct.

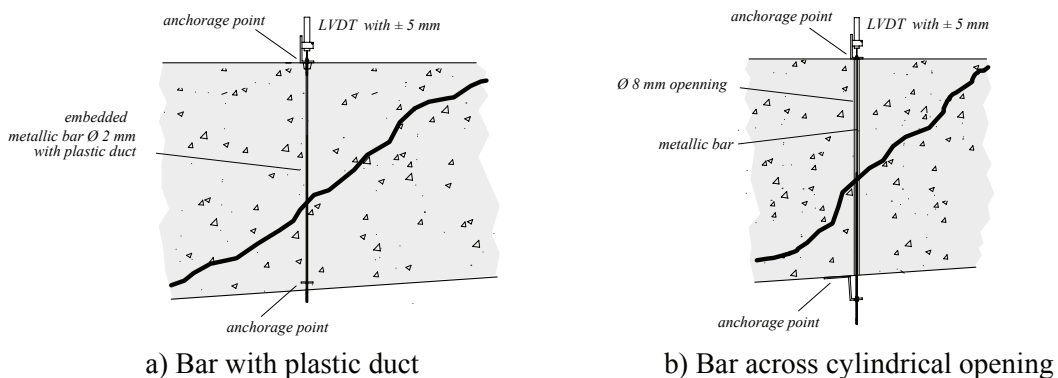


Figure A-3.12: Two systems for measuring the variation of the thickness of the slab

The rotations were measured using inclinometers. The rotation vector is indicated in figs. A-3.8, A-3.9 and A-3.11 at each inclinometer. For the tests on cantilevers, inclinometers were placed between the concentrated loads and the fixed end (figs. A-3.8 and A-3.9). For slab PR1, inclinometers were placed along the perimeter of a circle with diameter of 1380 mm (fig. A-3.11).

For test PR1, the water pressure in the flat jack was measured at each load step (fig. A-3.6).

### A-3.4 Demountable deformer measurements

Figure A-3.13 shows the measuring grids used to determine the in-plane deformations of both top and bottom surfaces of the cantilevers. The measurements with demountable deformers were only made for tests DR1-a, DR2-a, DR2-b and DR2-c. Each line in the grid drawings represents a measurement. The measuring grid represents a highly redundant truss. The redundancy allows the random measuring errors to be distributed, as explained in chapter 4. Three measuring lengths were used ( $500 \pm 5$  mm,  $300 \pm 5$  and

100 ± 5 mm) and two demountable deformeters with accuracy of 5 µm. Measurements of an invar standard were taken approximately every twenty measurements. These measurements were used to account for the temperature changes and drift in the demountable deformeter.

### A-3.5 Test procedure

The operations related to demountable deformeter readings are only applicable to tests DR1-a, DR2-a, DR2-b and DR2-c.

The measuring grid was measured two times at undeformed position. These measurements correspond to load stage 0 and load stage 1.

During the test the sequence of the procedures is controlled using a check-list. Any unexpected event is registered in the lab journal. For each load stage the order of the procedures is the following:

- The frequency of continuous measurements is increased prior to increasing the load.
- At the end of the loading of the structure the pressure is locked-off in the hydraulic cylinders.
- The cracks are drawn and numbered using a heavy marker.
- The openings of the cracks are measured using a magnifying glass.
- Photographs are taken of the crack pattern and of other interesting aspects.
- A complete set of demountable deformeter readings is taken, recorded and controlled in the computer. At this point of load stage the deflections of the slab were stable.

For test DR1-a, the cantilever was subjected to one hundred load cycles at a load level of about 410 kN. The cantilever was afterwards taken to failure.

After failure the slabs were cut into two or more parts and the geometry of the critical shear crack was mapped. For tests DR1-b, DR1-c, DR2-a, DR2-b and DR2-c the geometry of the critical shear crack was three dimensionally mapped. This was performed by isolating the upper part of the slab (separated from the lower part by the surface defined by the shear crack). The distances from the ground to the failure surface were then measured using an optical laser and a measuring grid with about six hundred measuring positions.

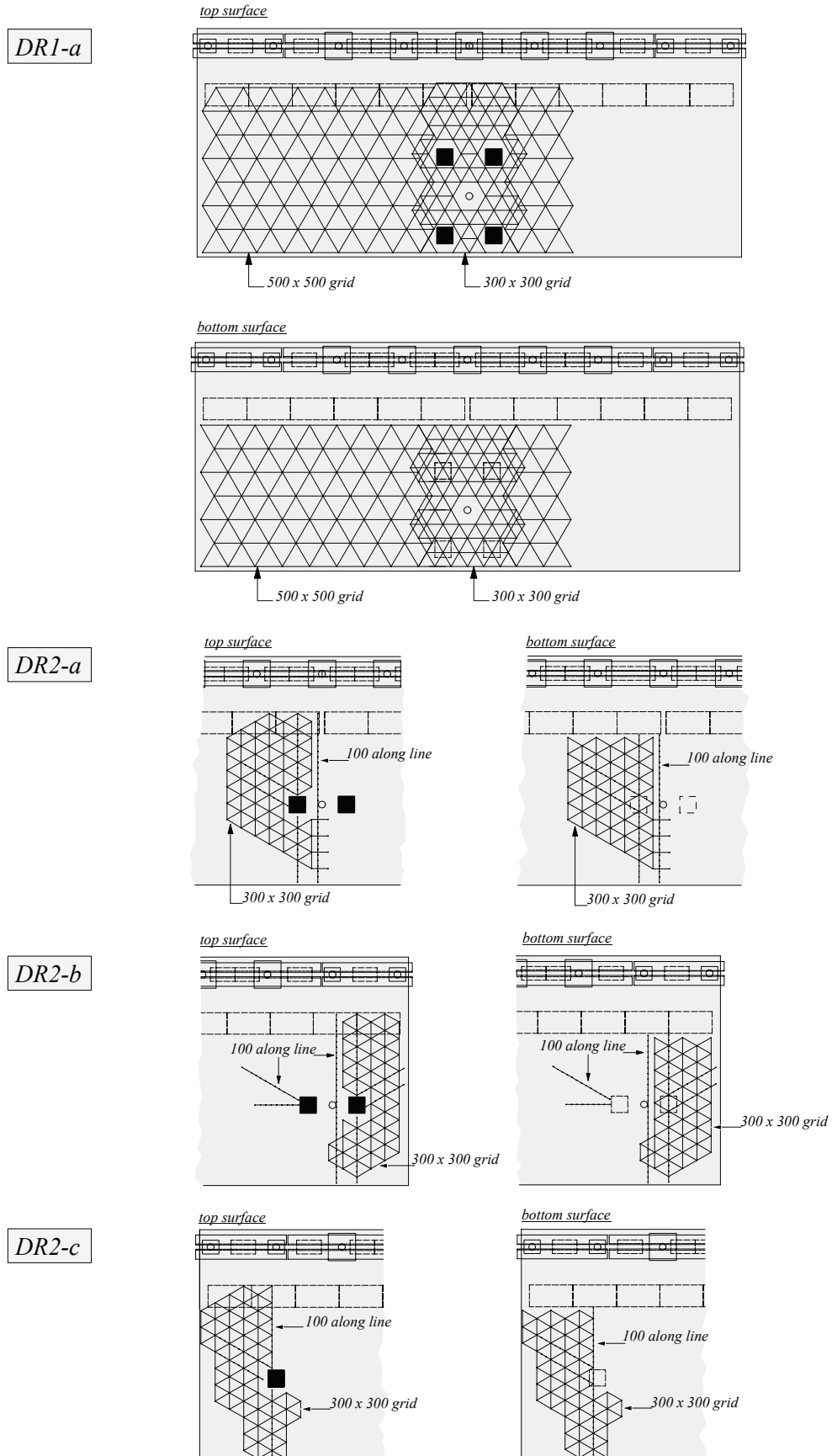


Figure A-3.13: Measuring grids for demountable deformaters (bottom surface as seen from above) [mm]



## A-4 Results

### A-4.1 Analysis and presentation of data

The values of the applied forces were measured simultaneously at load introduction plates and at the  $\varnothing$  75 mm steel bar for tests DR1-a (fig. A-3.2), DR1-b (fig. A-3.4), DR2-a (fig. A-3.3) and DR2-b (fig. A-3.3). The same force value should be obtained for the sum of the measured forces at the load introduction plates and for the measured force at the  $\varnothing$  75 mm steel bar. Very small differences are obtained. For slab DR1a the differences are less than 3%, for slab DR1b less than 1%, for slab DR2a less than 1.5% and for slab DR2b less than 1%. The measured forces at the load introduction plates are only used to calculate the distribution of the total force among the point loads.

The principal strains are calculated from the demountable deformer measurements of the measuring grid (fig. A-3.13). The highly redundant measuring grid allows the measured values to be corrected. The calculations of the corrections and principal strains are described in (Vaz Rodrigues, Muttoni 2004). These procedures were adapted to the grid dimensions used in the present experiments. The stiffness of the truss bars with gross errors was reduced to zero. The correct value of the measurement was determined from the truss analysis. Very few gross errors were found. Tables A-4.1 and A-4.2 show the standard deviation of the corrections for each test and for each load stage. The standard deviation is calculated without consideration of the gross errors.

Table A-4.1: Standard deviation of corrections for demountable deformer readings, for load stages of test DR1-a

Grid	# 0	# 1	# 2	# 3	# 4	# 5	# 6	# 8	# 10	# 11	# 12	# 13	# 14	# 15	# 16	Average
	[ $\mu\text{m}$ ]	[ $\mu\text{m}$ ]	[ $\mu\text{m}$ ]	[ $\mu\text{m}$ ]	[ $\mu\text{m}$ ]	[ $\mu\text{m}$ ]	[ $\mu\text{m}$ ]	[ $\mu\text{m}$ ]	[ $\mu\text{m}$ ]	[ $\mu\text{m}$ ]	[ $\mu\text{m}$ ]	[ $\mu\text{m}$ ]	[ $\mu\text{m}$ ]	[ $\mu\text{m}$ ]	[ $\mu\text{m}$ ]	[ $\mu\text{m}$ ]
300 bottom	4.0	4.9	5.0	2.9	2.6	3.0	5.7	3.5	3.5	3.3	3.7	3.1	3.6	4.7	3.7	3.8
300 top	3.0	2.7	2.5	2.3	2.7	2.5	2.8	2.3	2.5	3.1	2.8	3.7	2.6	6.3	4.6	3.1
500 bottom	13.3	3.1	3.9	5.4	7.1		2.7	3.7	3.4	5.8	3.2	5.5	3.3	7.3	3.3	5.0
500 top	7.1	7.1	7.1	7.6	7.3	10.9	7.9	8.2	7.2	8.4	8.3	7.5	6.6	8.3	7.6	7.8
Average of all grids																4.9

Table A-4.2: Standard deviation of corrections for demountable deformer readings, for load stages of tests DR2-a, DR2-b and DR2-c

Grid	# 0	# 1	# 2	# 3	# 4	# 5	# 6	Average	
	[ $\mu\text{m}$ ]	[ $\mu\text{m}$ ]	[ $\mu\text{m}$ ]	[ $\mu\text{m}$ ]	[ $\mu\text{m}$ ]	[ $\mu\text{m}$ ]	[ $\mu\text{m}$ ]	[ $\mu\text{m}$ ]	
DR2-a 300 bottom	7.4	2.5	1.8	6.8	2.0			4.1	
DR2-a 300 top	1.7	1.3	0.9	1.2	4.6			1.9	
DR2-b 300 bottom	5.4	5.7	2.5	2.9	2.6	3.6	2.8	3.7	
DR2-b 300 top	2.1	2.6	1.4	1.4	1.5	1.3	1.4	1.7	
DR2-c 300 bottom	4.4	4.1	2.2	5.5	3.4			3.9	
DR2-c 300 top	1.7	1.2	1.2	1.5	1.6			1.4	
Average of all grids									2.8

For test DR1-a the standard deviation of the corrections applied to the 300 mm measuring grid are smaller than those applied to the 500 mm measuring grid (table A-4.1). For the other measuring grids (table A-4.2), the standard deviation of measurements made from the bottom side is always larger than the standard deviation from the top side. This can be explained because of the uncomfortable measuring position (upside-down). Figure A-4.1 shows the dispersion of the corrections for two

extreme cases. The normal distribution is represented using the average and standard deviation of the corresponding load stage. The average standard deviation of the corrections is  $4.2 \mu\text{m}$  (0.01 ‰) for all grids and tests.

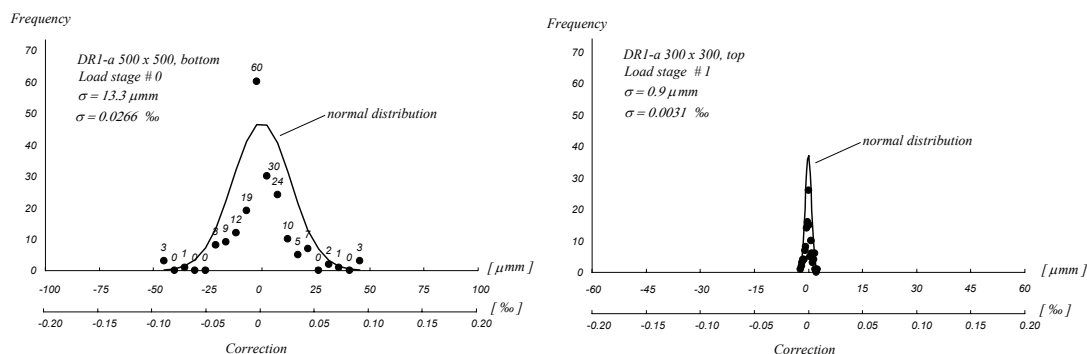


Figure A-4.1: Two load stages with large and small dispersion of corrections

The following results are presented for the tests:

- Force-deflection curves and force-time curves. The force  $Q$  is the measured on the  $\varnothing 75$  mm steel bar that applied the total load, above the hollow hydraulic jack. The self weight of the slab and test rig is not included in the diagrams.
- Tables with force values and deflection values at key locations, at the beginning of the load stage, at the end of the demountable deformer measurements and at the end of the load stage.
- The principal strains on top and bottom surfaces, with the cracks on background, for three representative chosen load stages (only for tests DR1-a, DR2-a, DR2-b and DR2-c).
- A photo of the failure.
- A sectional view of the cantilever showing the position of the shear cracks. The evolution of the surface strains measured on the concrete surface with the omega-shaped extensometers is also represented. The evolution of the rotations is represented from the measurements of the inclinometers.
- Level curves of the shear failure surface (only for tests DR1-b, DR1-c, DR2-a, DR2-b and DR2-c).
- Plots showing the variation of thickness of slab until failure (only for tests DR2-a, DR2-b and DR2-c).

The behavior under service loads was investigated in test DR1-a, under a total load of approximately 410 kN and at a low number of cycles (one hundred cycles). Magnified photos of the crack openings under and without load are shown. A diagram is provided with the evolution of the residual and under load crack openings and deflection under increasing cycles.



A-4.2 Test DR1-a

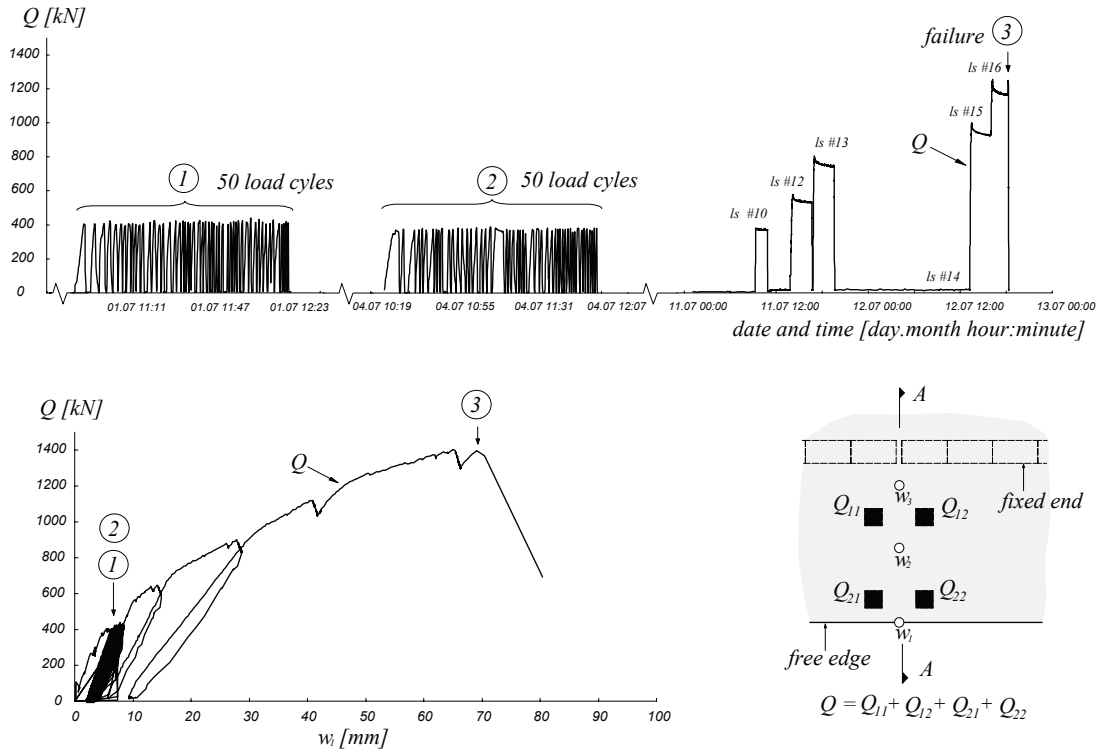


Figure A-4.2: Test DR1-a: Load history and load-deflection curve

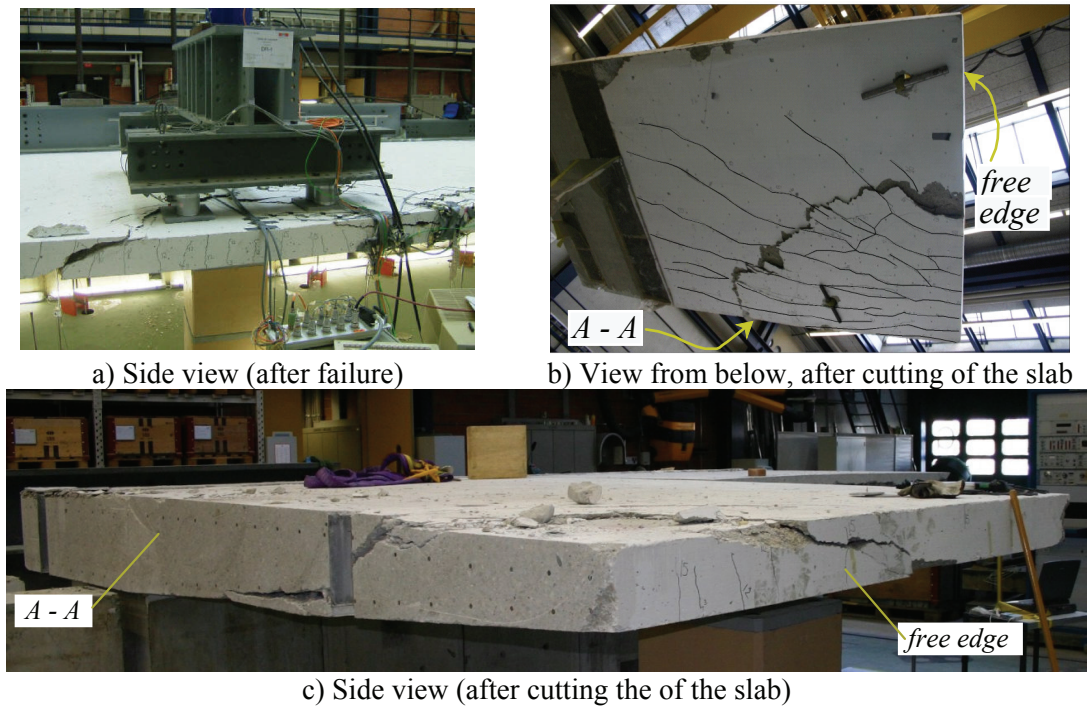


Figure A-4.3: Test DR1-a: Shear failure

Table A-4.3: Test DR1-a: Evolution of some measured values

Load stage	$Q$	$Q_{11}/Q$	$Q_{12}/Q$	$Q_{21}/Q$	$Q_{22}/Q$	$w_1$	$w_2$	$w_3$	$Q/Q_{FL}$	Remark
	[kN]	-	-	-	-	[mm]	[mm]	[mm]	%	
#0	4.1	15.3%	40.0%	20.0%	24.8%	0.1	0.0	0.0		
#1	10.8	15.8%	37.4%	17.8%	29.0%	0.1	0.1	0.0		
#2	278.7	17.1%	34.3%	32.0%	16.6%	3.5	1.8	0.5	20%	B
	265.3	17.0%	34.6%	32.1%	16.4%	3.5	1.8	0.5	19%	M
	258.7	16.8%	34.7%	32.2%	16.2%	3.5	1.7	0.5	19%	E
#3	399.6	18.7%	32.6%	30.6%	18.1%	5.9	2.9	0.8	29%	B
	383.8	18.5%	32.8%	30.7%	18.0%	6.0	2.9	0.8	27%	M
	373.5	18.4%	32.9%	30.8%	17.9%	6.1	2.9	0.8	27%	E
#4	1.0					2.1	1.5	0.2	0%	B
	0.2					2.1	1.5	0.2	0%	M
	1.1					2.0	7.1	0.2	0%	E
#5	413.0	19.0%	31.7%	30.4%	18.9%	8.0	5.0	1.0	30%	B
	411.7	19.0%	31.7%	30.4%	18.9%	8.0	5.0	1.0	29%	M
	406.0	18.9%	31.8%	30.5%	18.8%	8.0	5.0	1.0	29%	E
#6	5.4					3.0	1.7	0.3	0%	B
	3.8					3.0	1.7	0.4	0%	M
	2.7					3.0	1.6	0.4	0%	E
#7	406.1	19.0%	31.7%	30.5%	18.9%	8.2	4.1	1.0	29%	B
	402.2	18.9%	31.7%	30.5%	18.9%	8.2	4.1	1.0	29%	M
	386.9	18.8%	31.9%	30.6%	18.7%	8.1	4.1	1.0	28%	E
#8	413.0	19.1%	31.5%	30.4%	19.1%	8.5	4.4	1.0	30%	B
	412.0	19.0%	31.5%	30.4%	19.1%	8.5	4.4	1.0	29%	M
	399.7	18.9%	31.7%	30.5%	18.9%	8.4	4.4	1.0	29%	E
#9	6.2					3.4	2.0	0.4	0%	B
	4.0					3.4	2.0	0.3	0%	M
	6.6					3.3	1.9	0.3	0%	E
#10	422.0	19.0%	31.6%	30.2%	19.1%	8.4	4.5	0.9	30%	B
	420.9	19.0%	31.7%	30.2%	19.1%	8.4	4.4	0.9	30%	M
	411.2	18.9%	31.7%	30.4%	19.0%	8.4	4.7	1.0	29%	E
#11	14.3					3.5	2.4	0.4	1%	B
	19.0					3.4	2.4	0.4	1%	M
	20.2					3.4	2.7	0.4	1%	E
#12	629.0	20.9%	30.1%	28.4%	20.6%	14.5	7.5	1.5	45%	B
	616.4	20.9%	30.2%	28.4%	20.6%	14.6	7.5	1.5	44%	M
	597.7	20.9%	30.1%	28.2%	20.7%	14.8	6.9	1.6	43%	E
#13	871.5	22.2%	28.6%	27.3%	21.9%	28.2	12.2	2.7	62%	B
	862.7	22.2%	28.7%	27.3%	21.8%	28.3	12.2	2.7	62%	M
	841.9	22.1%	28.7%	27.3%	21.8%	28.6	12.3	2.8	60%	E
#14	19.5					9.4	4.2	0.8	1%	B
	17.1					9.4	4.2	0.9	1%	M
	17.5					9.4	4.2	0.9	1%	E
#15	1084.2	22.7%	27.8%	26.9%	22.6%	41.3	17.7	4.0	78%	B
	1073.2	22.7%	27.9%	26.9%	22.5%	41.4	17.6	4.0	77%	M
	1047.4	22.7%	27.9%	26.9%	22.5%	41.6	17.4	4.0	75%	E
#16	1361.9	24.1%	26.1%	25.6%	24.3%	65.7	27.2	6.7	97%	B
	1328.7	24.2%	26.0%	25.5%	24.4%	66.0	27.2	6.8	95%	M
	1303.5	24.2%	26.0%	25.4%	24.3%	66.3	27.1	6.8	93%	E
ML	1397.2	24.4%	25.7%	25.3%	24.6%	69.1	28.1	7.1	100%	ML
FL	1397.2	24.4%	25.7%	25.3%	24.6%	69.1	28.1	7.1	100%	FL

B : Beginning of load stage ; M : End of demountable deformer measurements ; E : End of load stage ; ML : Maximum load ; FL : Failure Load

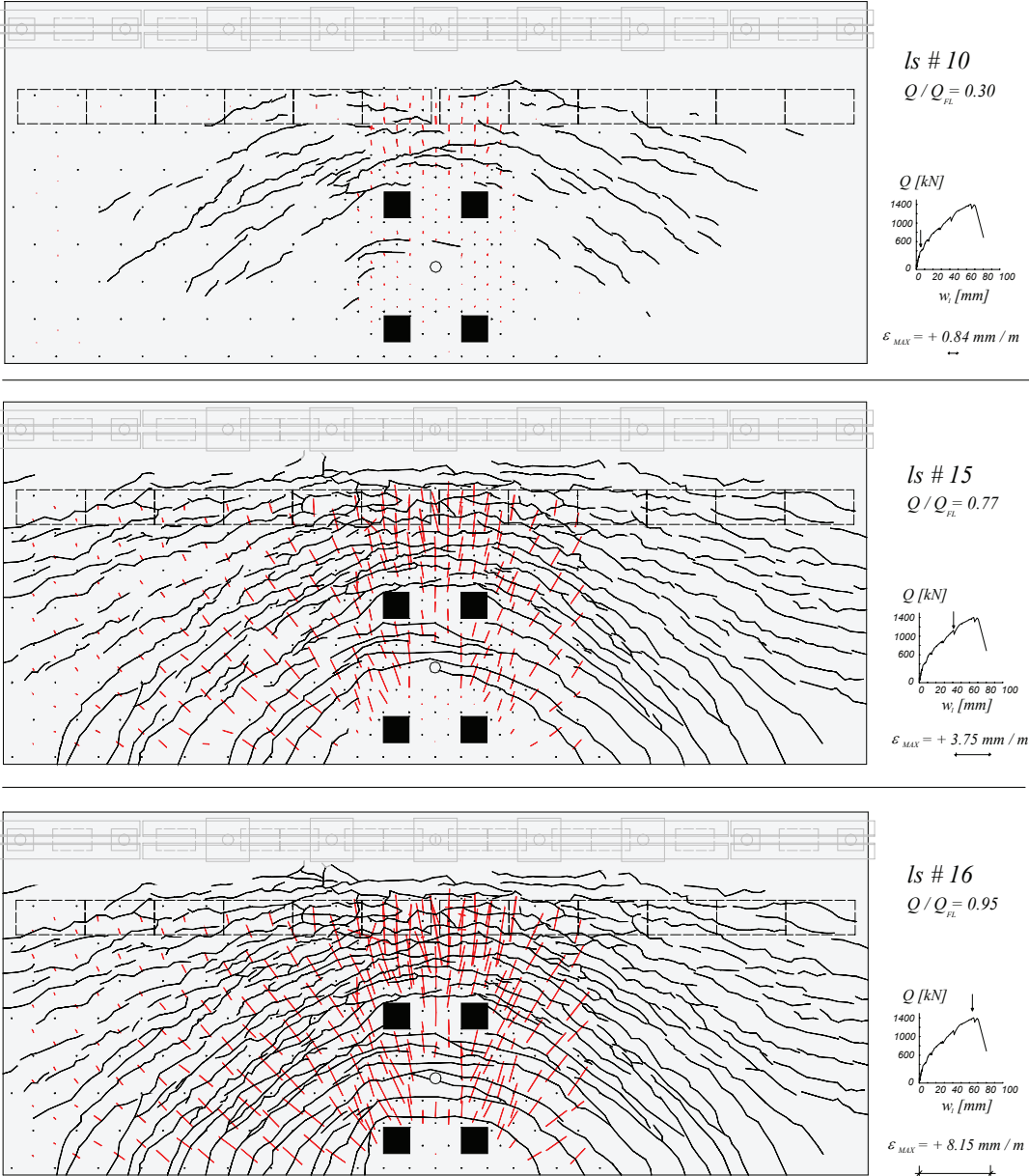


Figure A-4.4: Test DR1-a: Crack pattern and tensile principal strains on the top surface

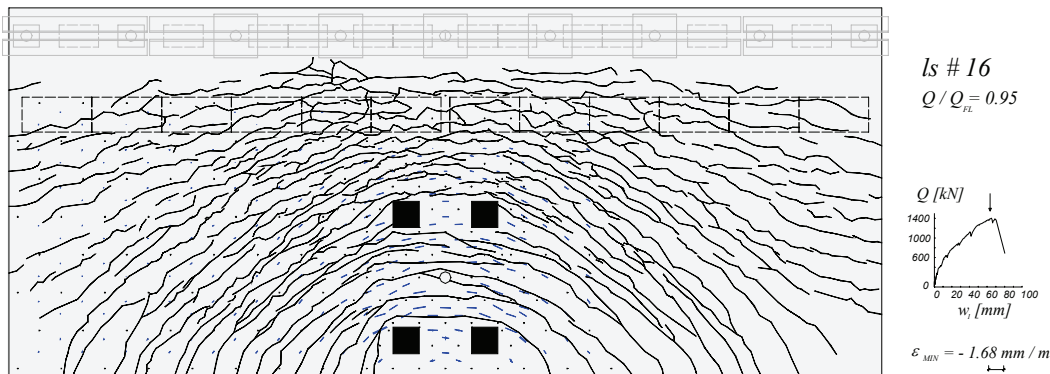
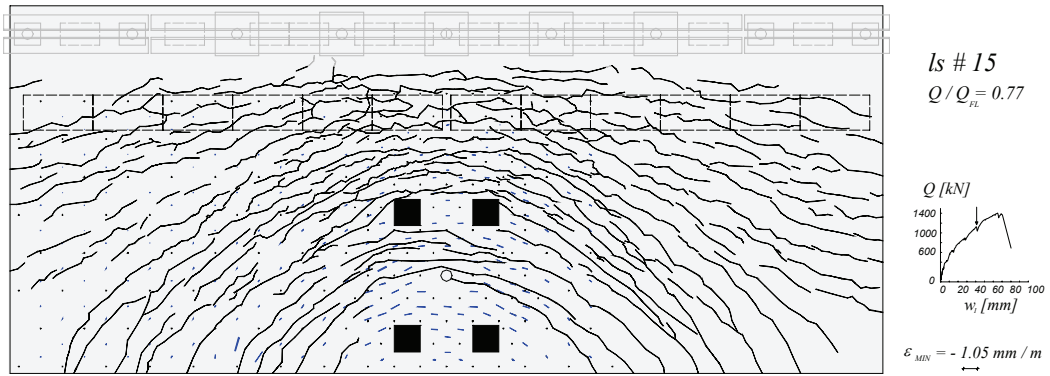
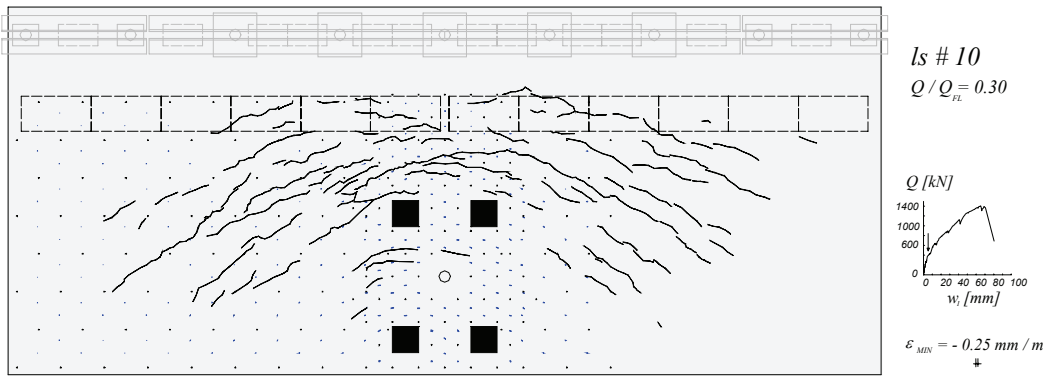


Figure A-4.5: Test DR1-a: Crack pattern and compressive principal strains on the top surface

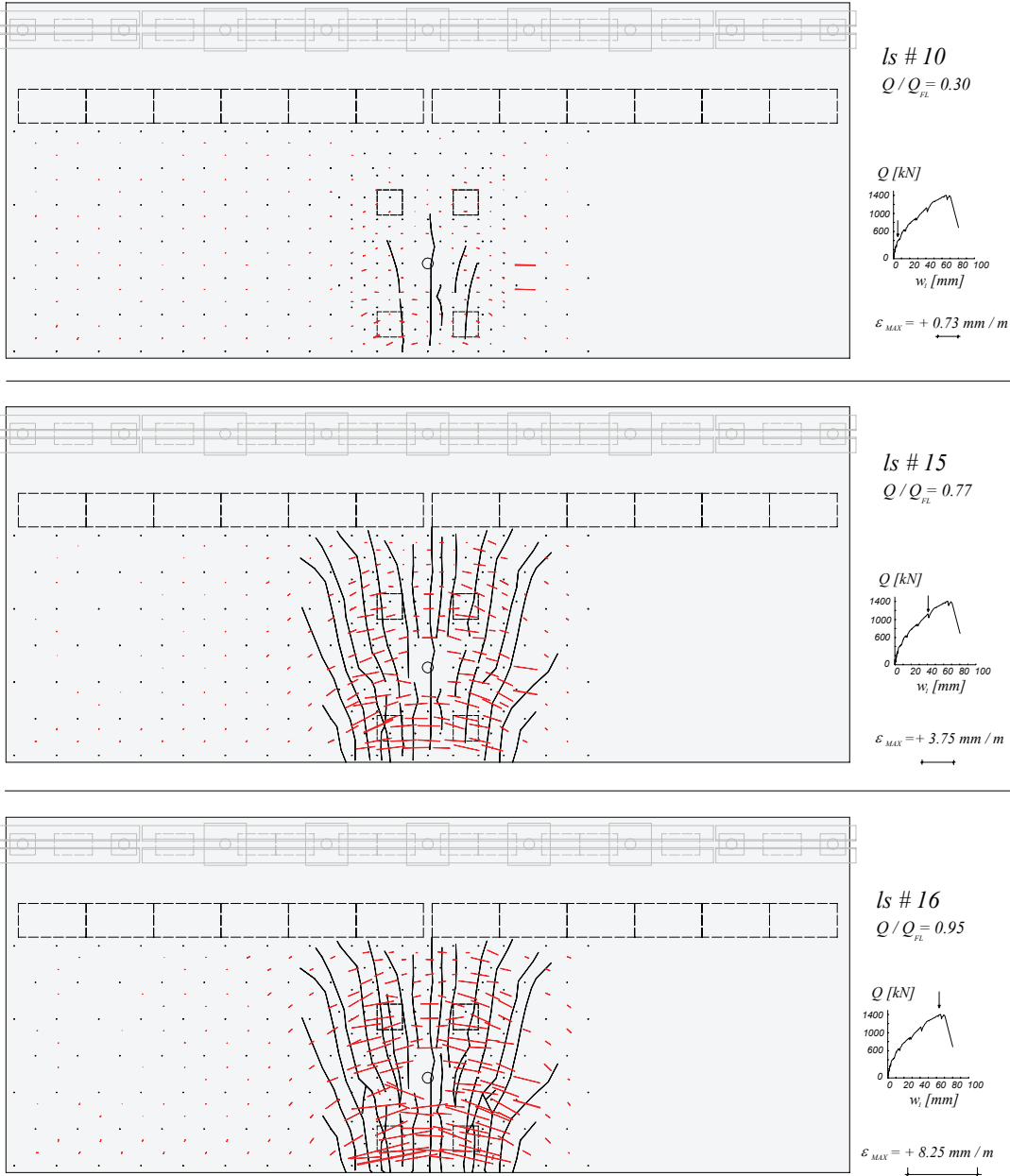


Figure A-4.6: Test DR1-a: Crack pattern and tensile principal strains on the bottom surface (as seen from above)

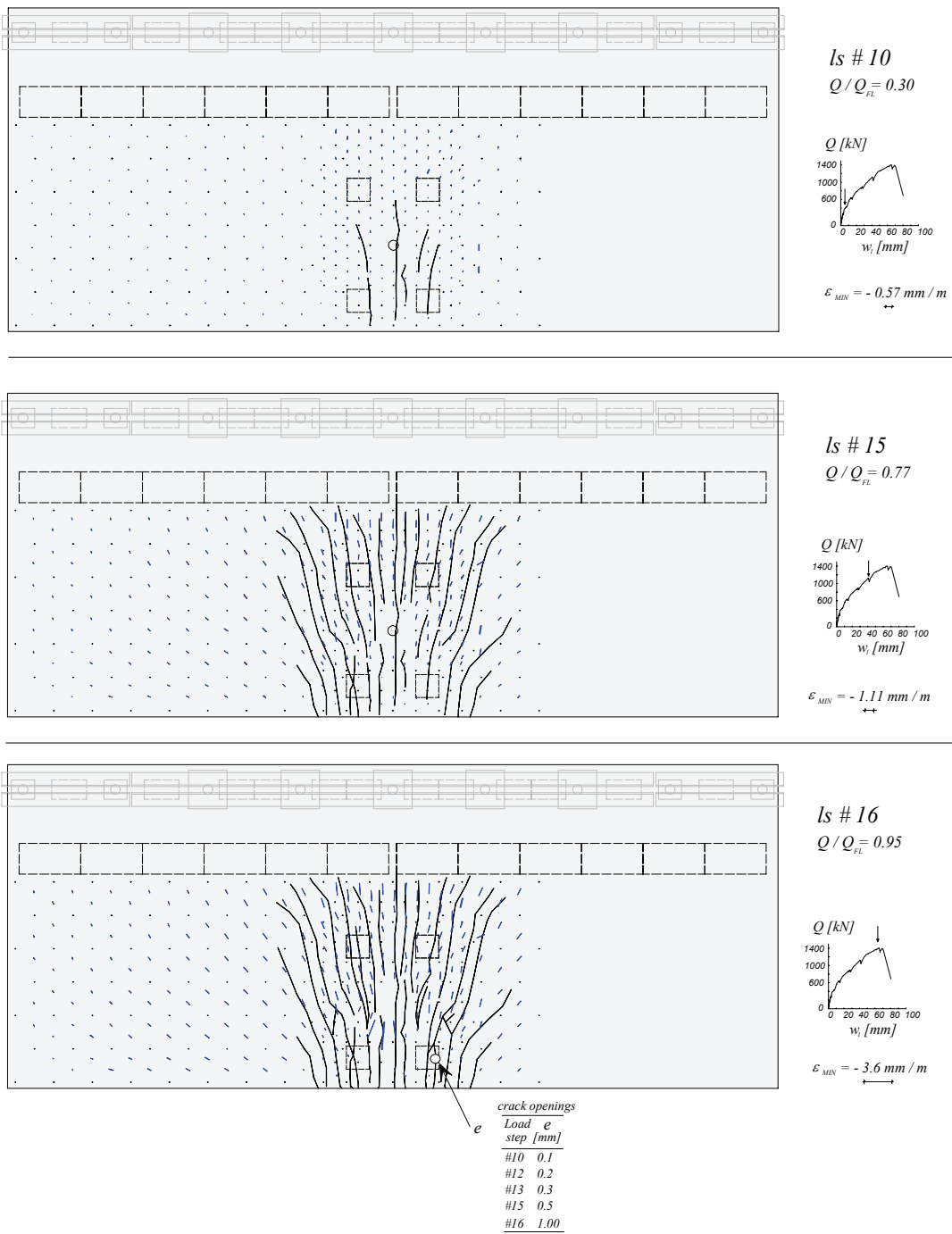


Figure A-4.7: Test DRI-a: Crack pattern and compressive principal strains on the bottom surface (as seen from above)

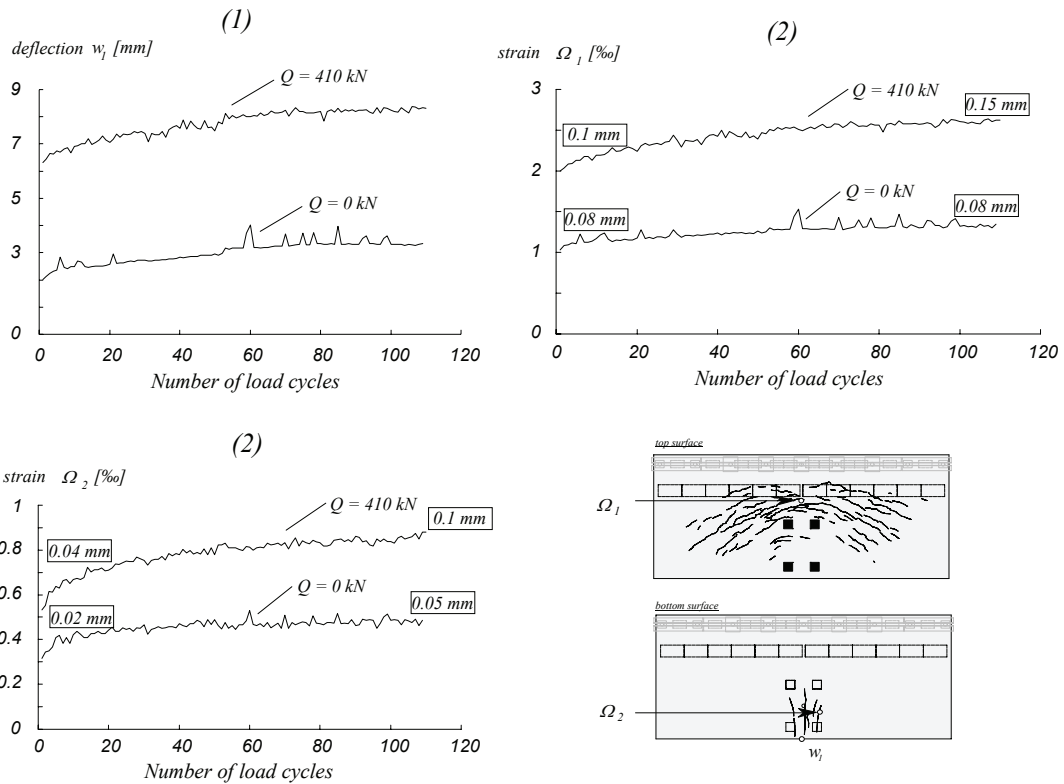
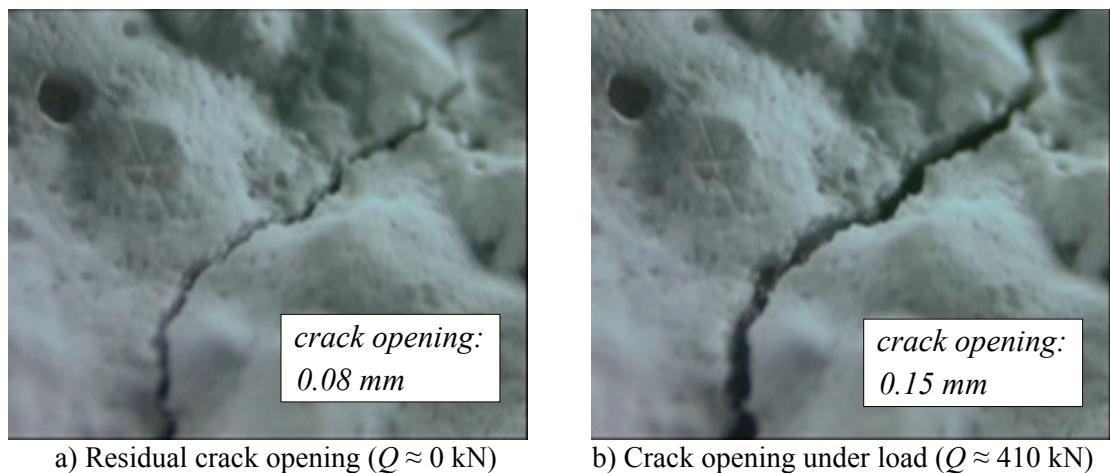


Figure A-4.8: Test DRI-a: (1) Evolution of the deflection with number of load cycles; (2) Evolution of maximal strains measured with omega-shaped extensometers on the concrete surface (length of measurement: 100 mm). The associated crack openings are indicated



a) Residual crack opening ( $Q \approx 0 \text{ kN}$ )

b) Crack opening under load ( $Q \approx 410 \text{ kN}$ )

Figure A-4.9: Test DRI-a: Maximal crack openings at the top surface of the cantilever after the load cycles

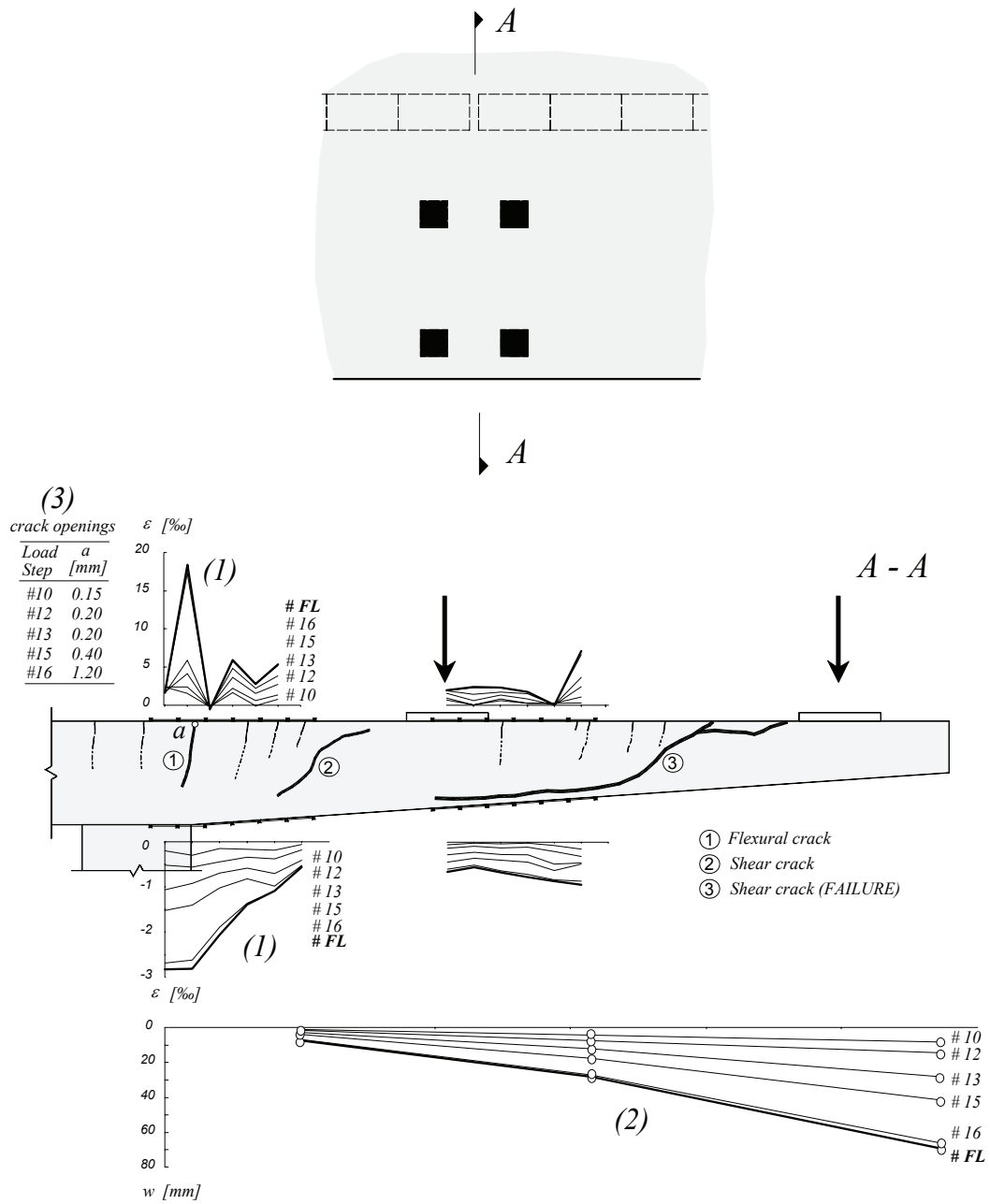


Figure A-4.10: Test DR1-a: (1) Strains measured on the surface of the slab with omega-shaped extensometers (100 mm length) ; (2) Deflections measured with LVDTs; (3) Crack openings measured with magnifying glass



A-4.3 Test DR1-b

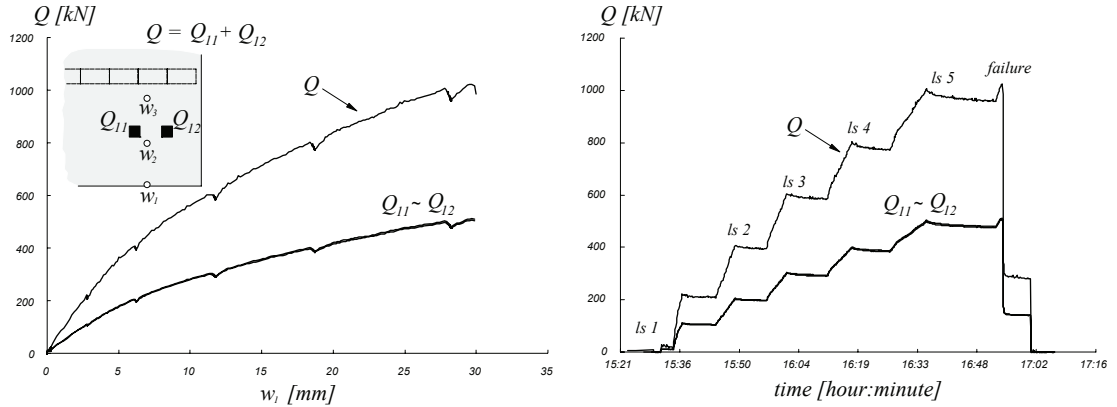


Figure A-4.11: Test DR1-b: Load history and load-deflection curve

Table A-4.4: Test DR1-b: Evolution of some measured values

Load stage	Q [kN]	Q <sub>11</sub> / Q	Q <sub>12</sub> / Q	w <sub>1</sub> [mm]	w <sub>2</sub> [mm]	w <sub>3</sub> [mm]	Q / Q <sub>FL</sub> [%]	Remark
#1	6.5	39.0%	61.0%	0.0	0.0	0.0		
#2	403.0	50.3%	49.7%	6.2	3.8	1.0	39%	
#3	595.9	50.3%	49.7%	11.7	7.0	1.7	58%	
#4	790.1	50.3%	49.7%	18.6	11.2	2.6	77%	
#5	984.4	50.3%	49.7%	28.1	17.0	3.7	96%	
ML	1030.0	50.2%	49.8%	29.7	18.0	3.9	101%	ML
FL	1024.5	50.2%	49.8%	29.9	18.1	3.9	100%	FL

ML : Maximum load ; FL : Failure Load

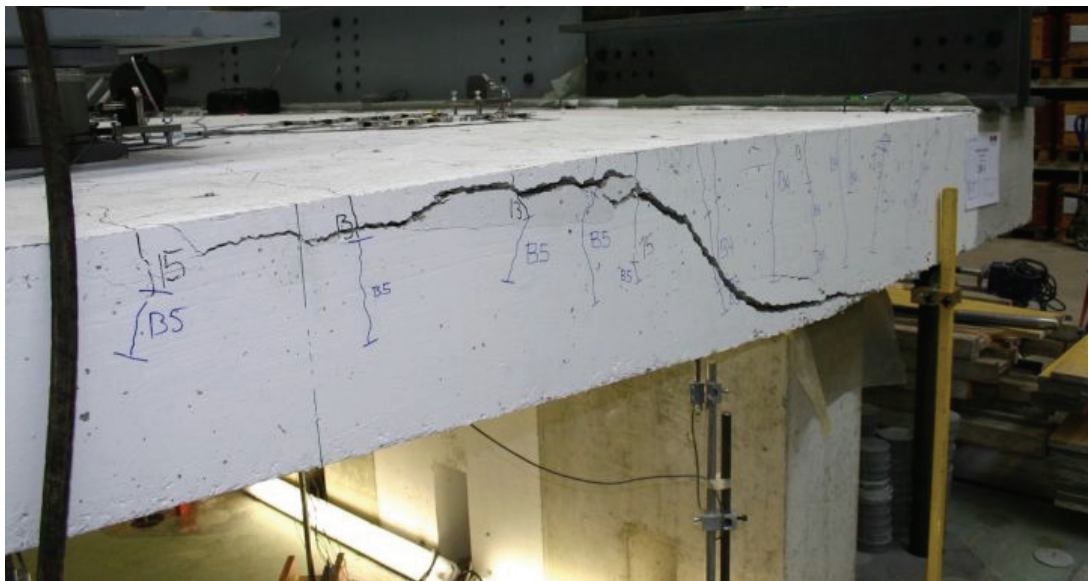


Figure A-4.12: Test DR1-b: Side view of the shear crack after failure

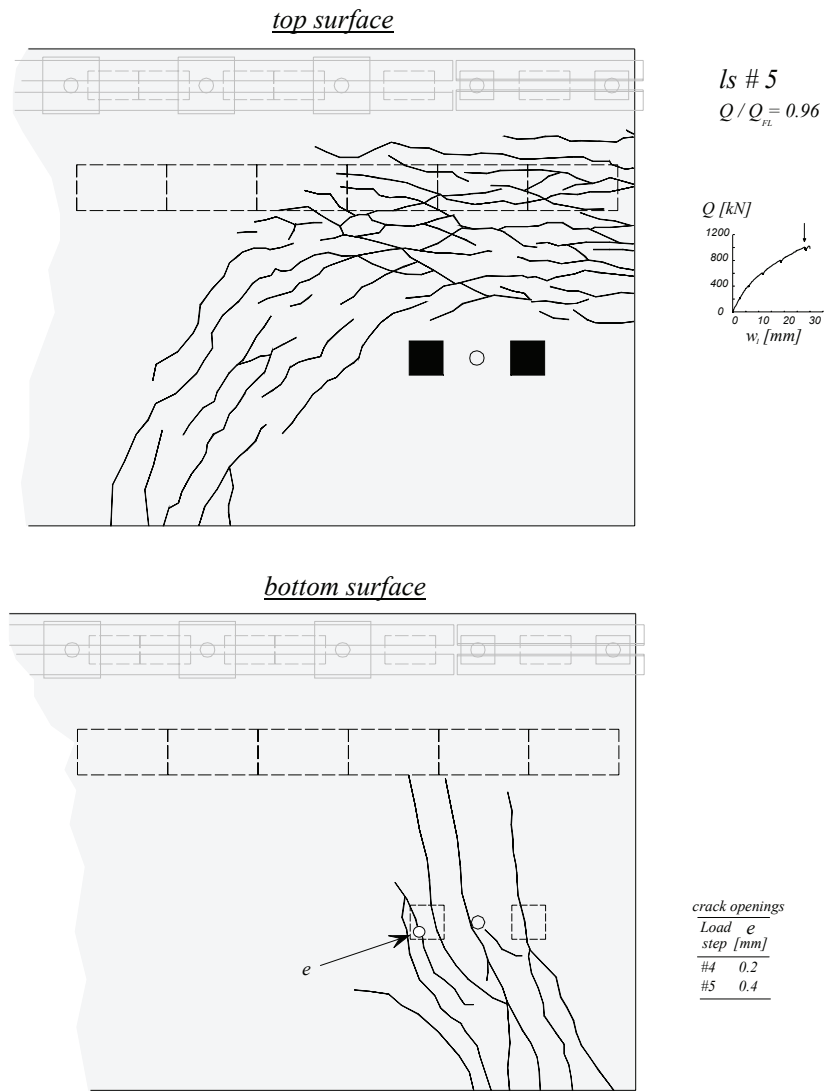


Figure A-4.13: Test DR1-b: Crack pattern

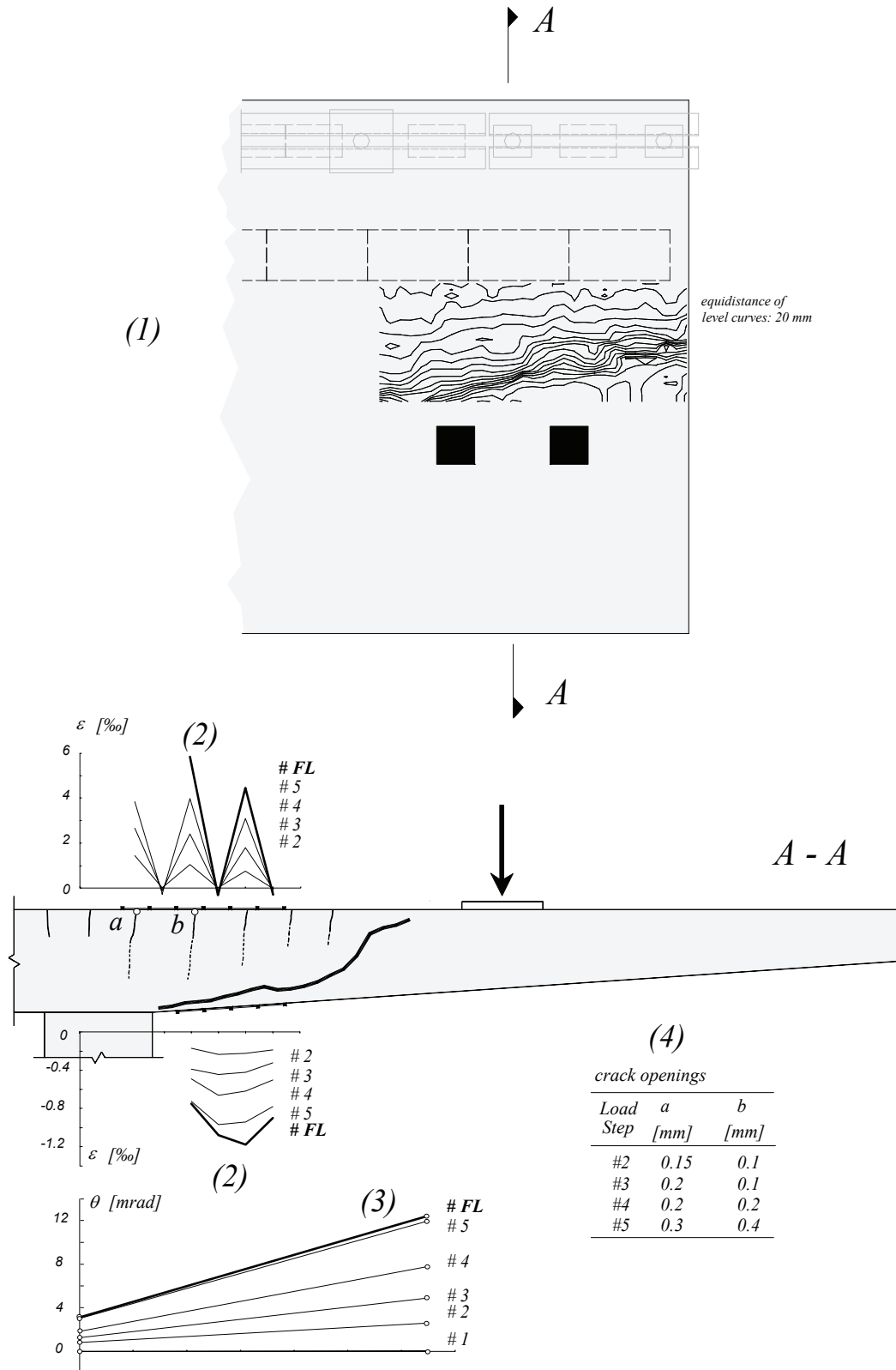


Figure A-4.14: Test DR1-b: (1) Level curves of the shear crack; (2) Strains measured on the surface of the slab with omega-shaped extensometers (100 mm length); (3) Rotations measured with inclinometers; (4) Crack openings measured with magnifying glass

A-4.4 Test DR1-c

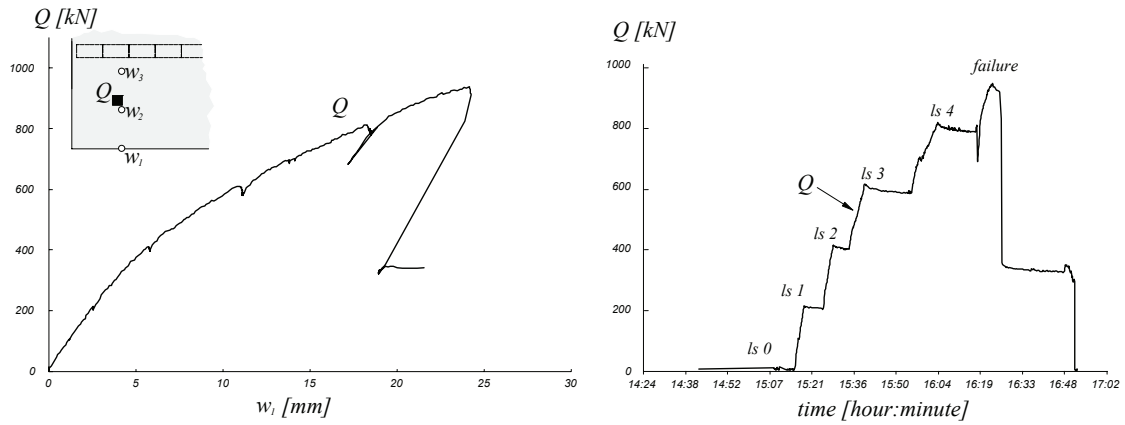


Figure A-4.15: Test DR1-c: Load history and load-deflection curve

Table A-4.5: Test DR1-c: Evolution of some measured values

Load stage	Q [kN]	w <sub>1</sub> [mm]	w <sub>2</sub> [mm]	w <sub>3</sub> [mm]	Q / Q <sub>FL</sub> [%]	Remark
#0	4.4	0.0	0.0	0.0		-
#1	208.3	2.5	1.6	0.4	23%	
#2	401.7	5.8	3.6	0.9	44%	
#3	586.7	11.1	6.9	1.7	64%	
#4	789.6	18.5	11.3	2.7	87%	
ML	938.0	24.2	14.3	3.4	103%	ML
FL	910.0	24.2	14.4	3.5	100%	FL

ML : Maximum load ; FL : Failure Load

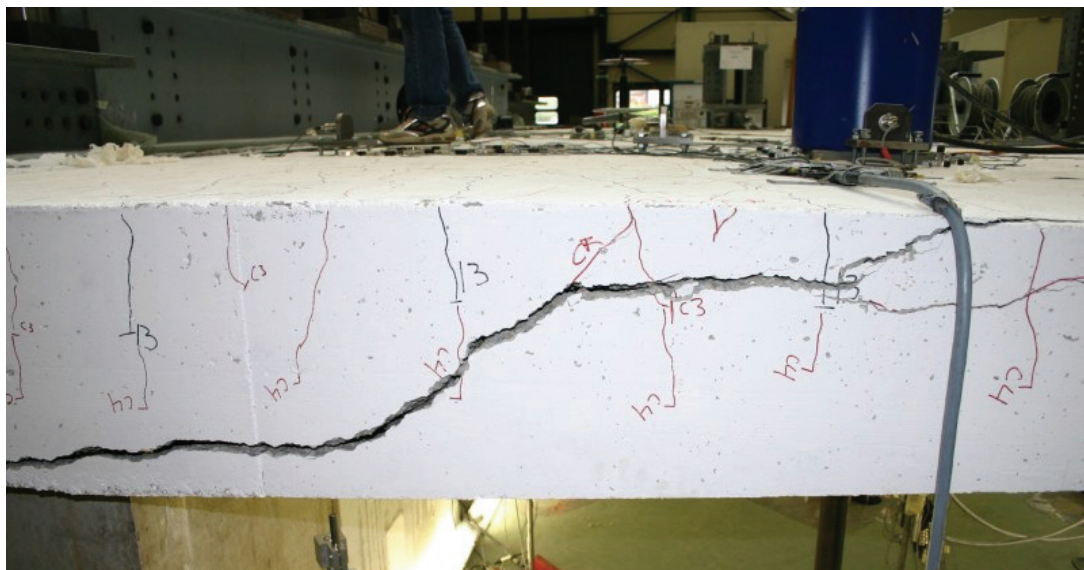


Figure A-4.16: Test DR1-c: Side view of the shear crack after failure

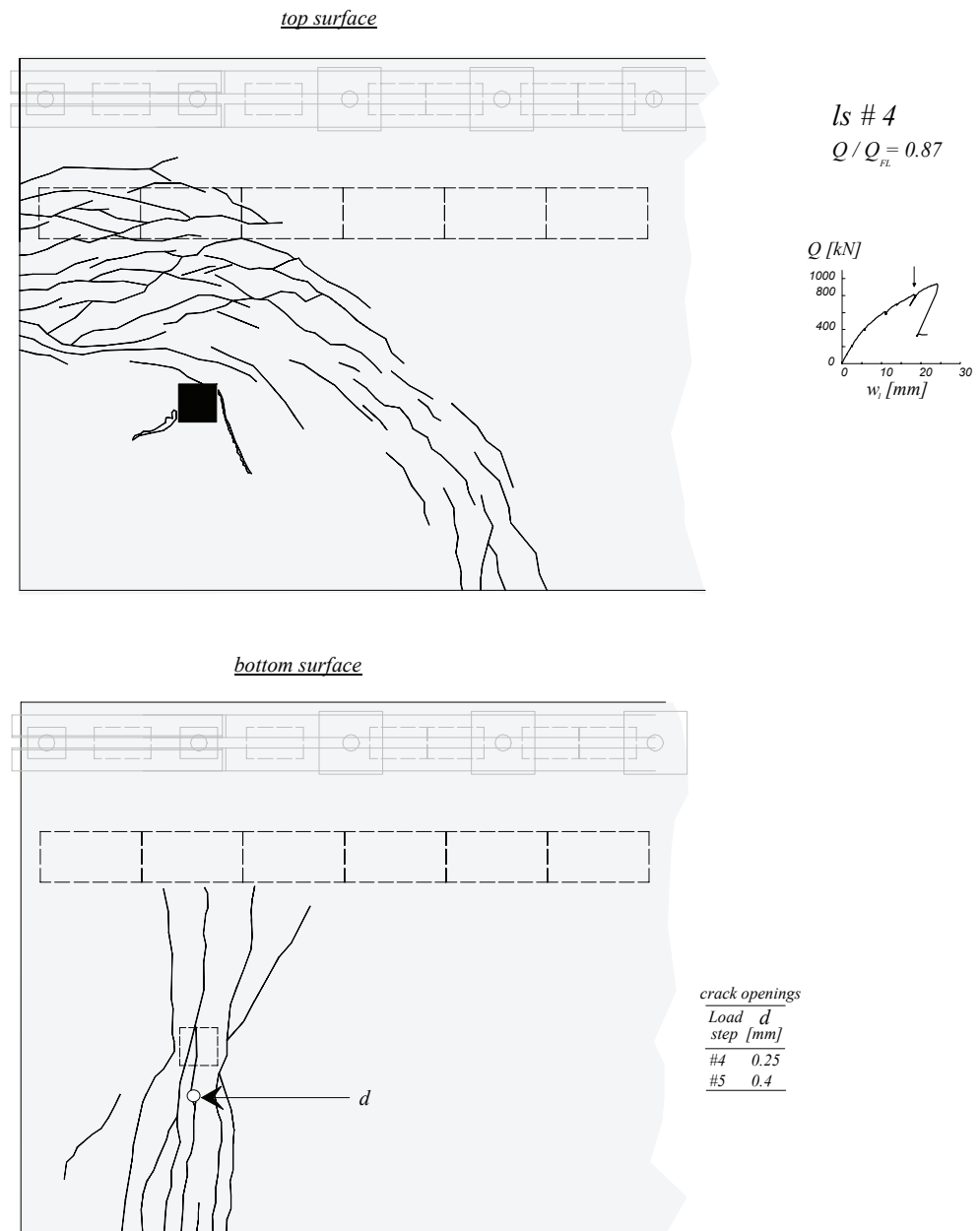


Figure A-4.17: Test DR1-c: Crack pattern

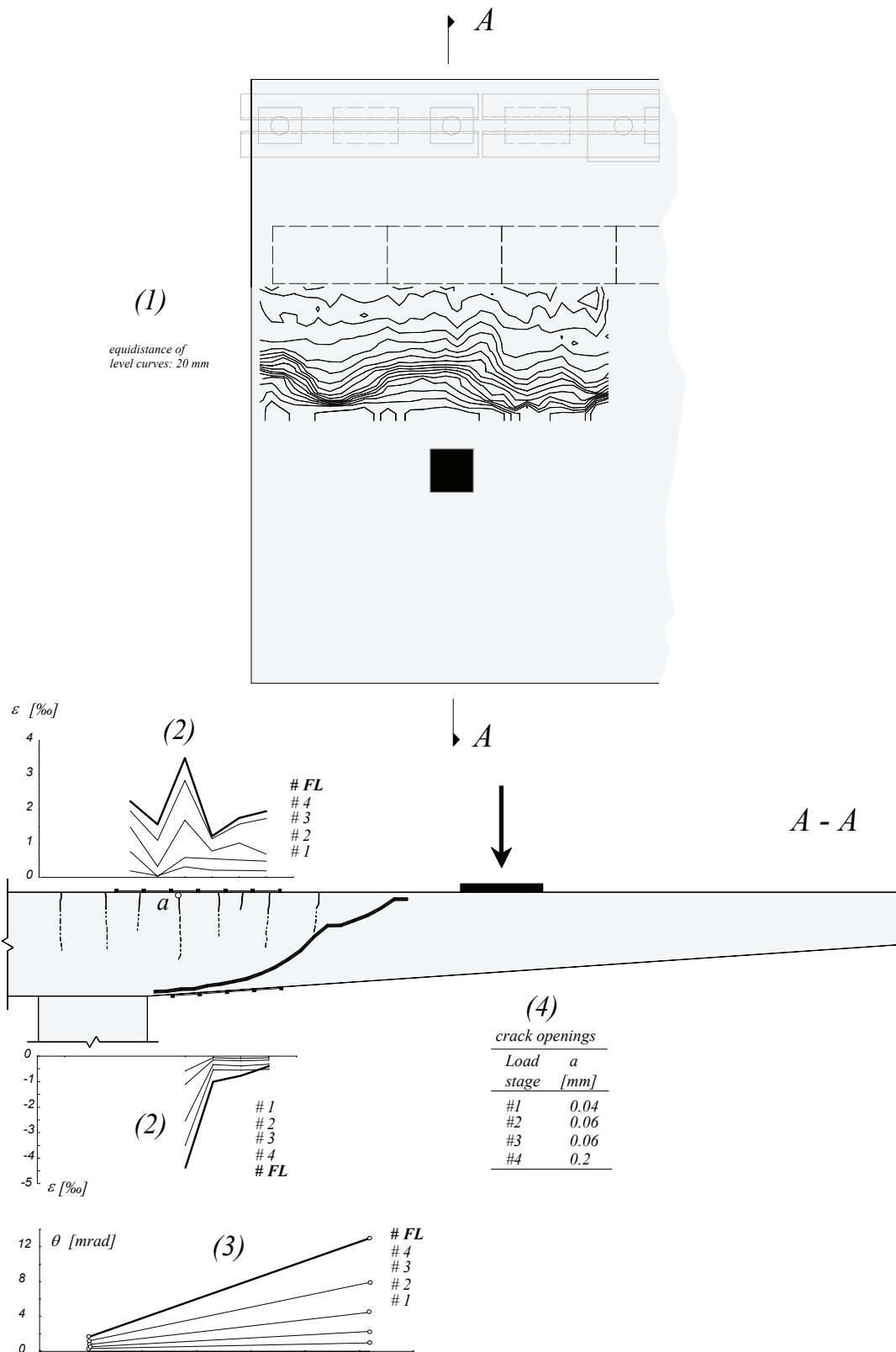


Figure A-4.18: Test DR1-c: (1) Level curves of the shear crack; (2) Strains measured on the surface of the slab with omega-shaped extensometers (100 mm length); (3) Rotations measured with inclinometers; (4) Crack openings measured with magnifying glass

A-4.5 Test DR2-a

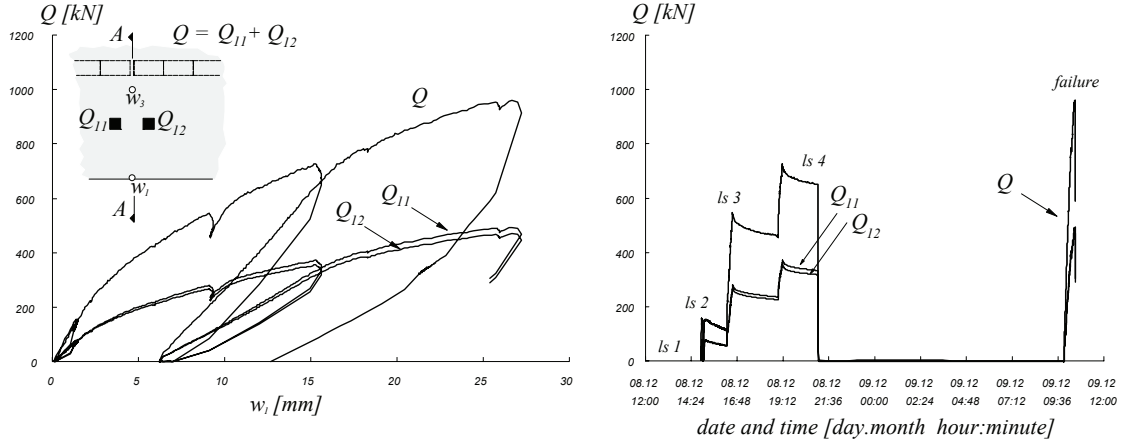


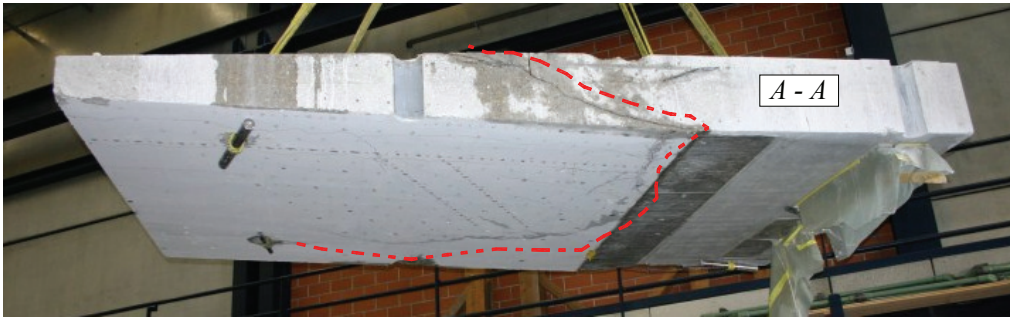
Figure A-4.19: Test DR2-a: Load history and load-deflection curve

Table A-4.6: Test DR2-a: Evolution of some measured values

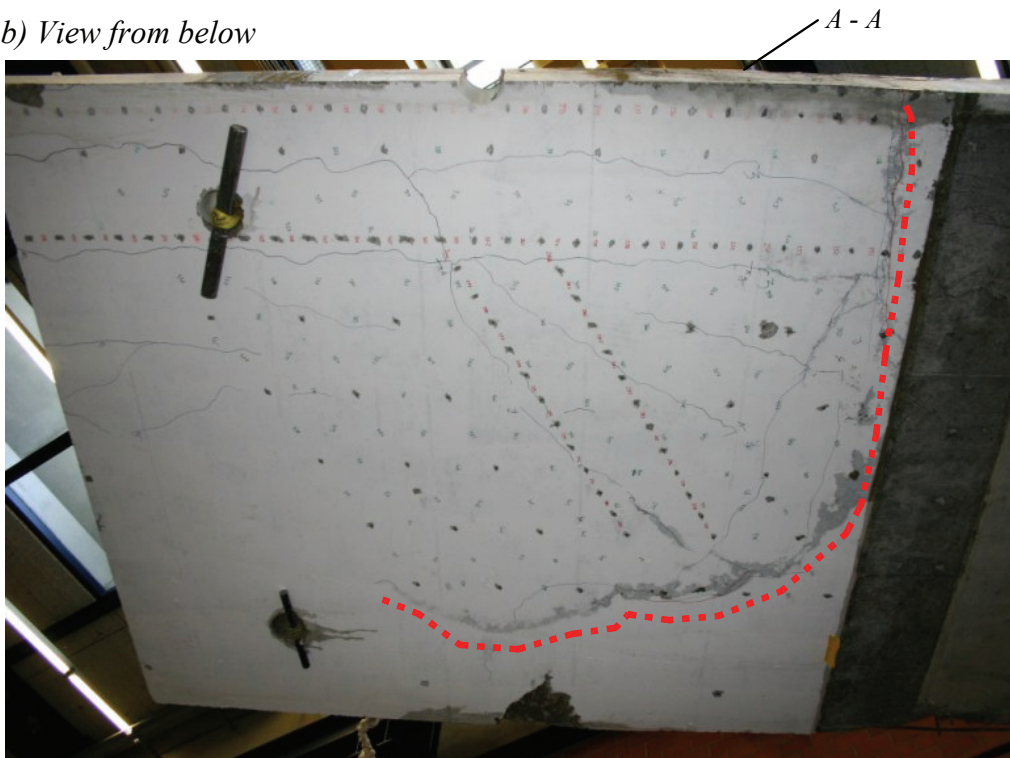
Load stage	$Q$ [kN]	$Q_{11}/Q$ -	$Q_{12}/Q$ -	$w_1$ [mm]	$w_3$ [mm]	$Q/Q_{FL}$ [%]	Remark -
#1	2.1			0.1	0.0	0%	
#2	153.5	50.7%	49.3%	1.5	0.2	16%	B
	153.0	50.7%	49.3%	1.5	0.2	16%	M
	117.9	50.7%	49.3%	1.3	0.2	12%	E
#3	535.8	51.1%	48.9%	9.2	1.3	56%	B
	474.5	51.1%	48.9%	9.2	1.3	49%	M
	462.7	51.1%	48.9%	9.2	1.3	48%	E
#4	698.6	51.2%	48.8%	15.5	2.2	73%	B
	664.1	51.2%	48.8%	15.6	2.2	69%	M
	650.8	51.2%	48.8%	15.6	2.2	68%	E
ML	961.4	51.2%	48.8%	26.7	3.5	100%	ML
FL	961.4	51.2%	48.8%	26.7	3.5	100%	FL
AFT	359.3	51.2%	48.8%	22.1	14.5	37%	AFT

B : Beginning of load stage ; M : End of demountable deformer measurements ; E : End of load stage ; ML : Maximum load ; FL : Failure Load; AFT: After Failure

a) Sectional view



b) View from below



c) View of the internal failure surface (upper lip of the shear crack)



Figure A-4.20: Test DR2-a: Views of the shear crack after cutting the slab



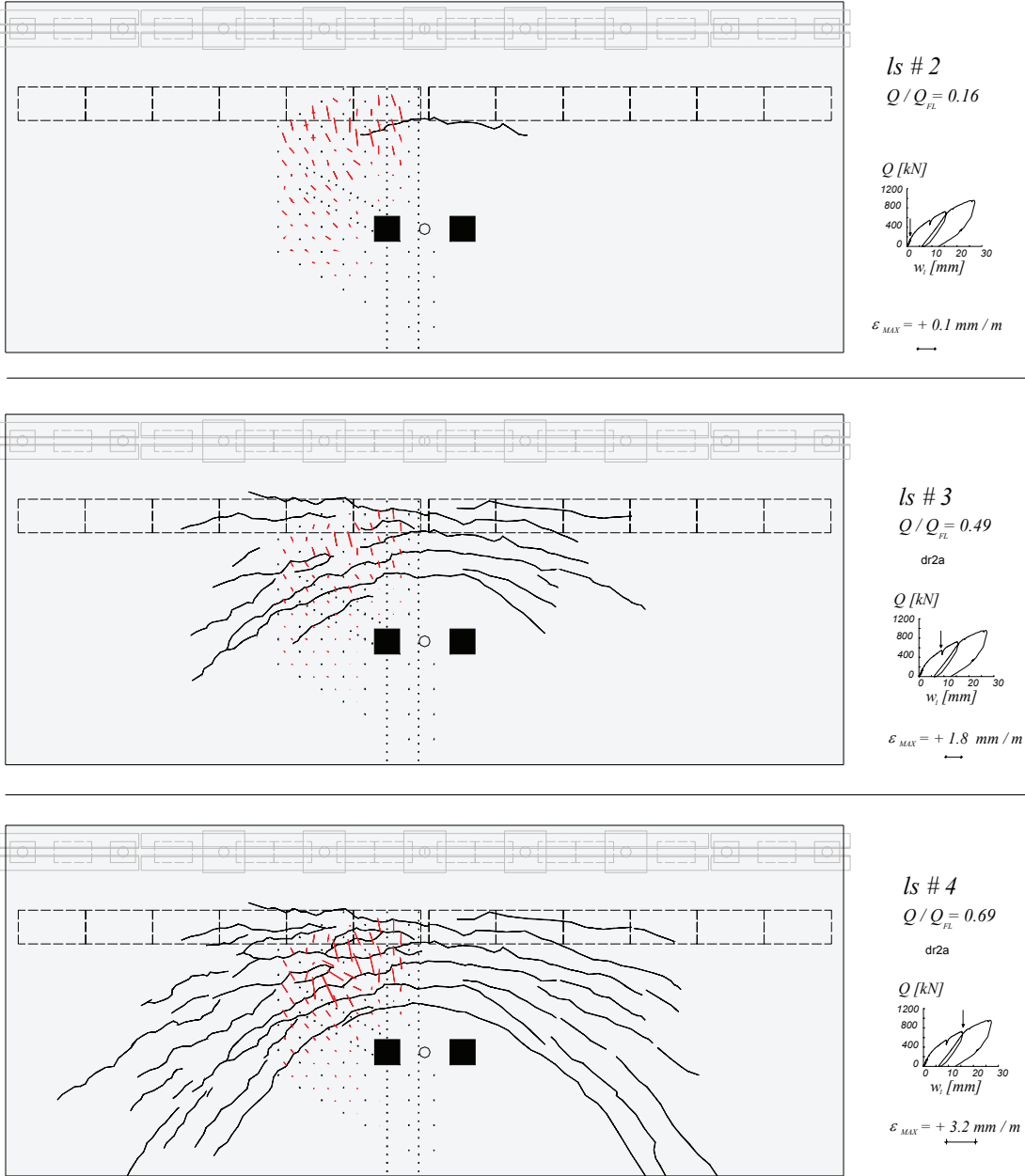


Figure A-4.21: Test DR2-a: Crack pattern and tensile principal strains on the top surface

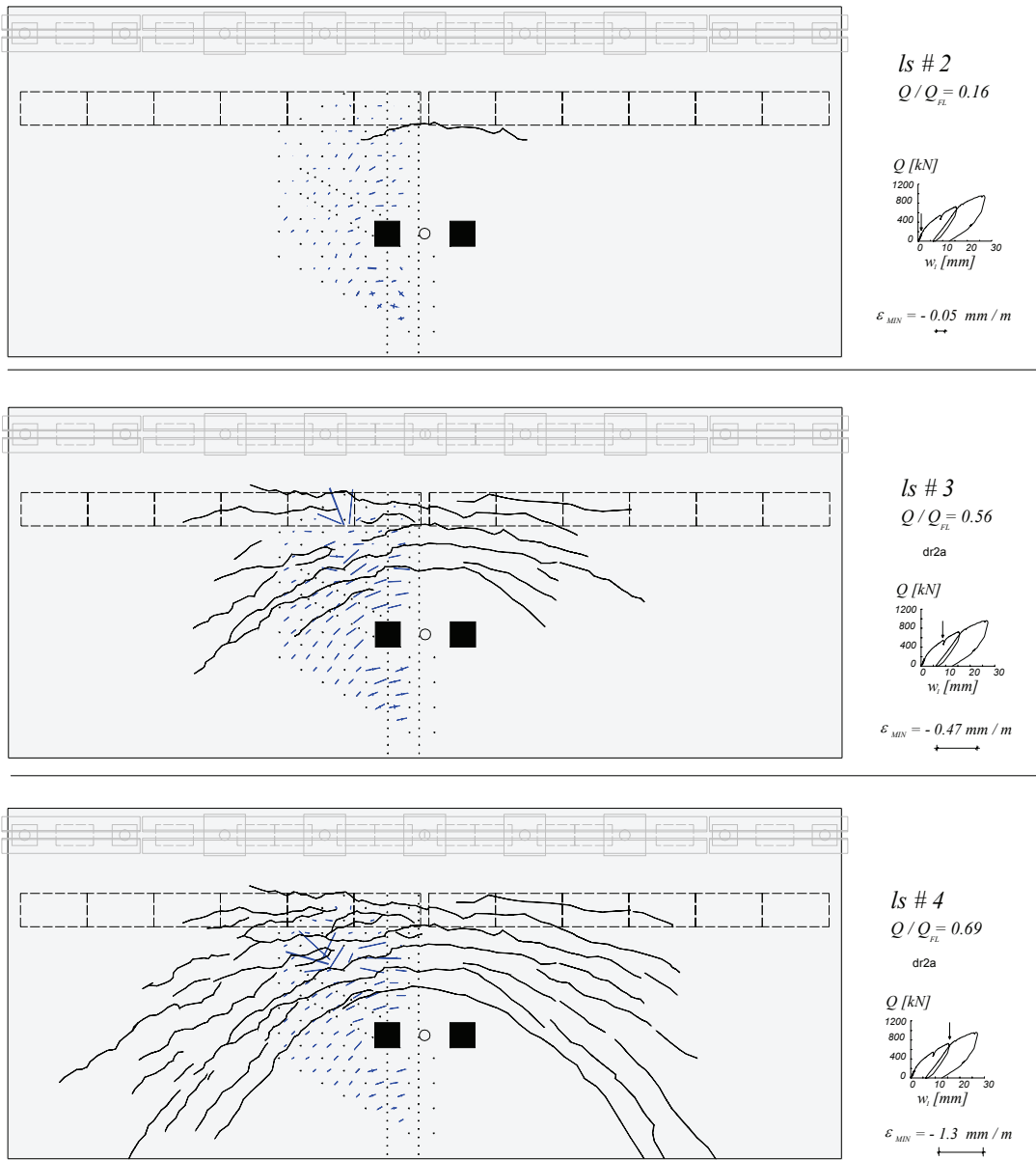


Figure A-4.22: Test DR2-a: Crack pattern and compressive principal strains on the top surface

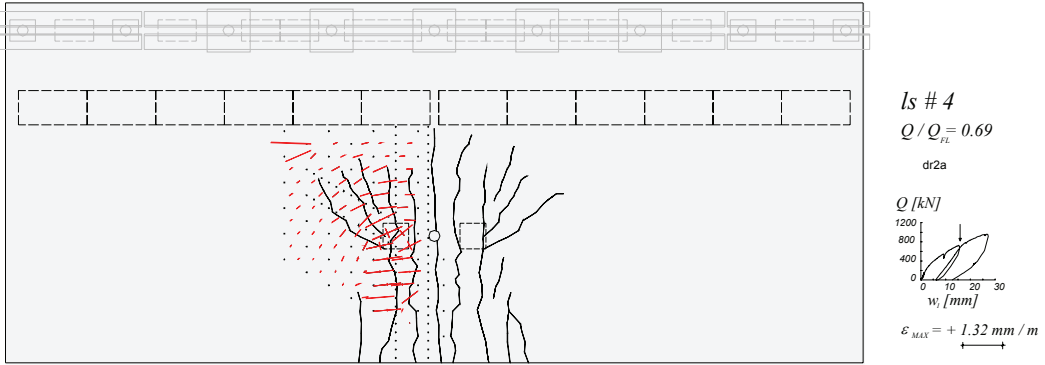
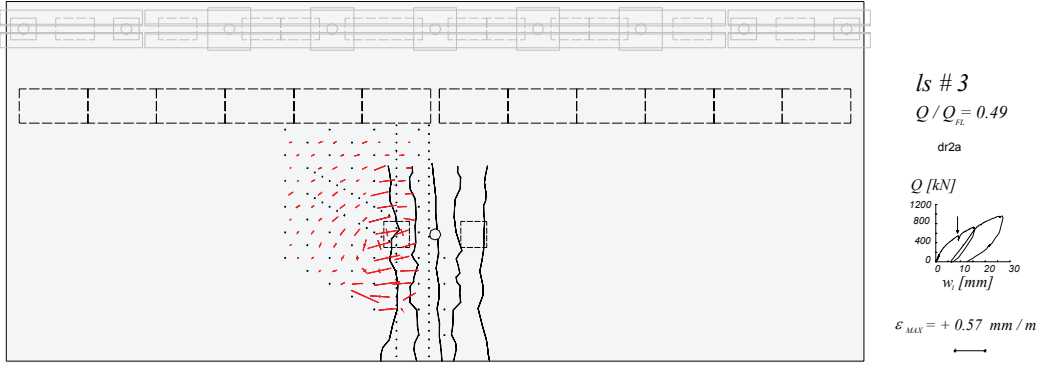
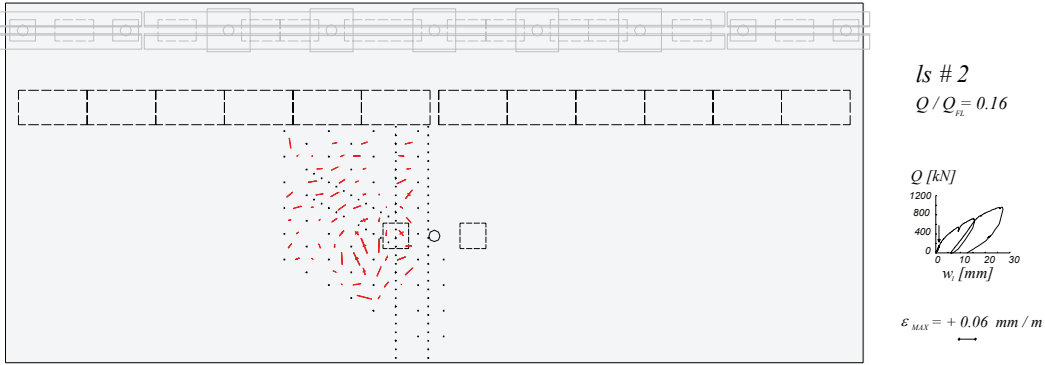


Figure A-4.23: Test DR2-a: Crack pattern and tensile principal strains on the bottom surface (as seen from above)

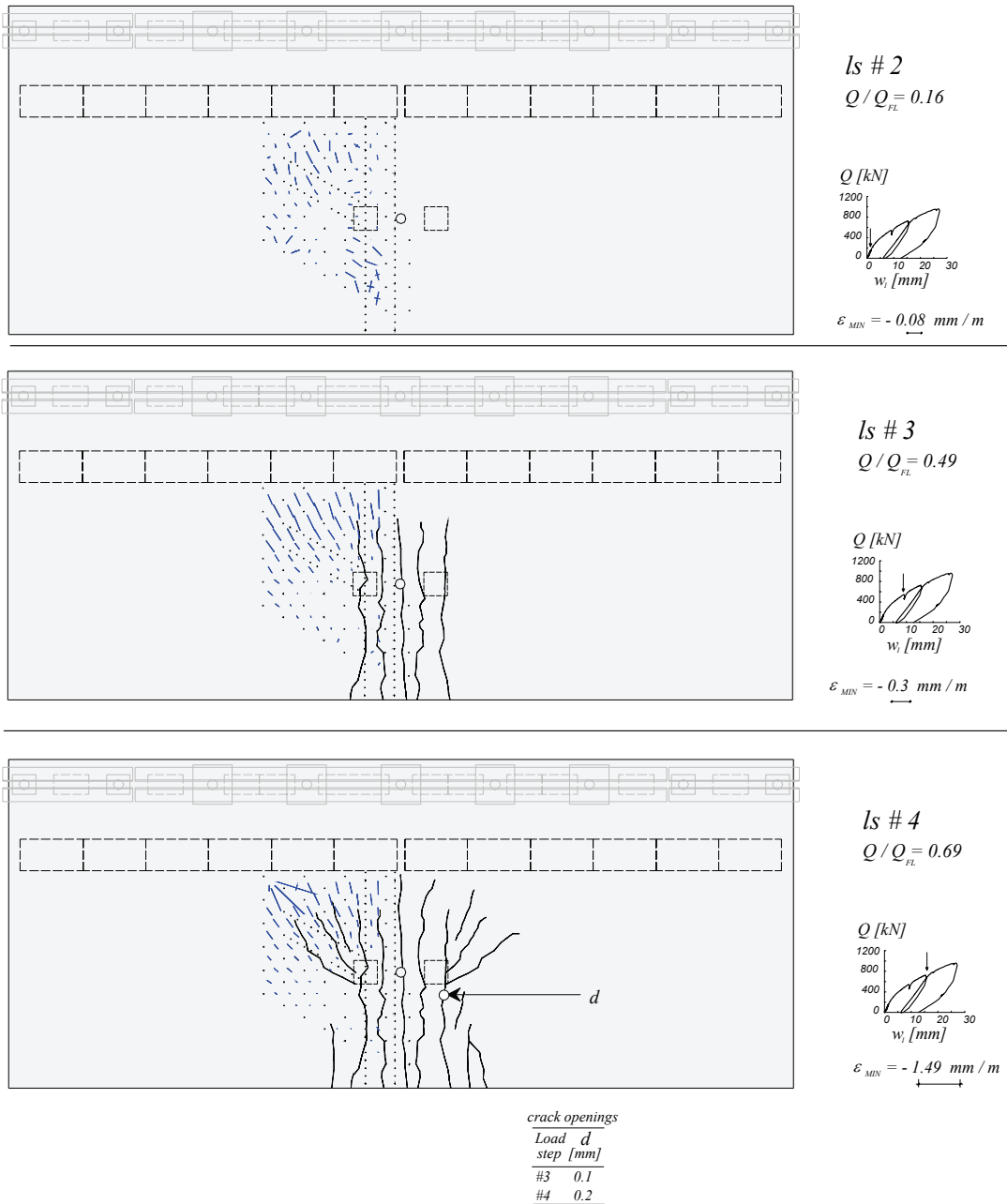


Figure A-4.24: Test DR2-a: Crack pattern and compressive principal strains on the bottom surface (as seen from above)

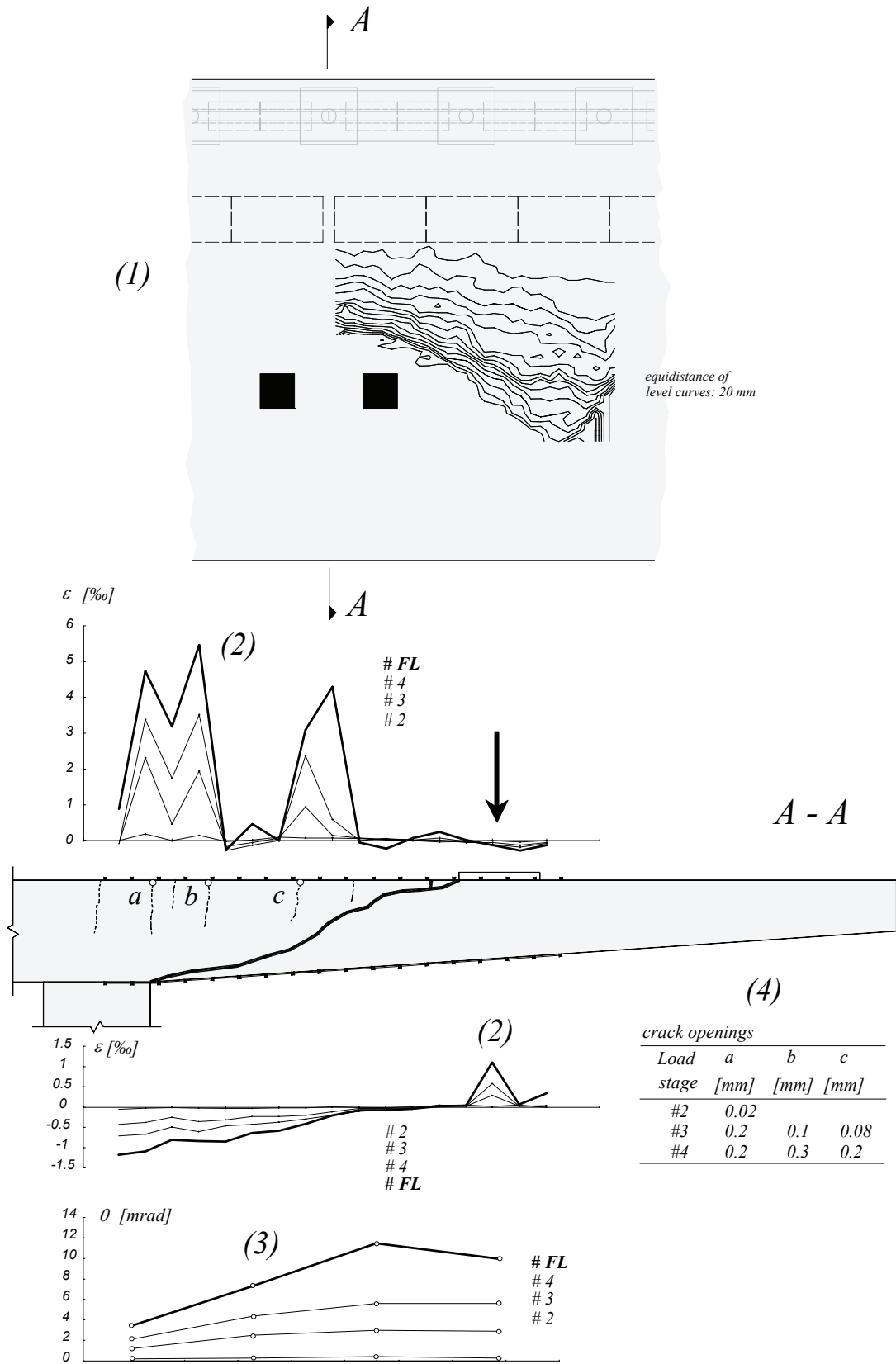


Figure A-4.25: Test DR2-a: (1) Level curves of the shear crack; (2) Strains measured on the surface of the slab with omega-shaped extensometers (100 mm length); (3) Rotations measured with inclinometers; (4) Crack openings measured with magnifying glass

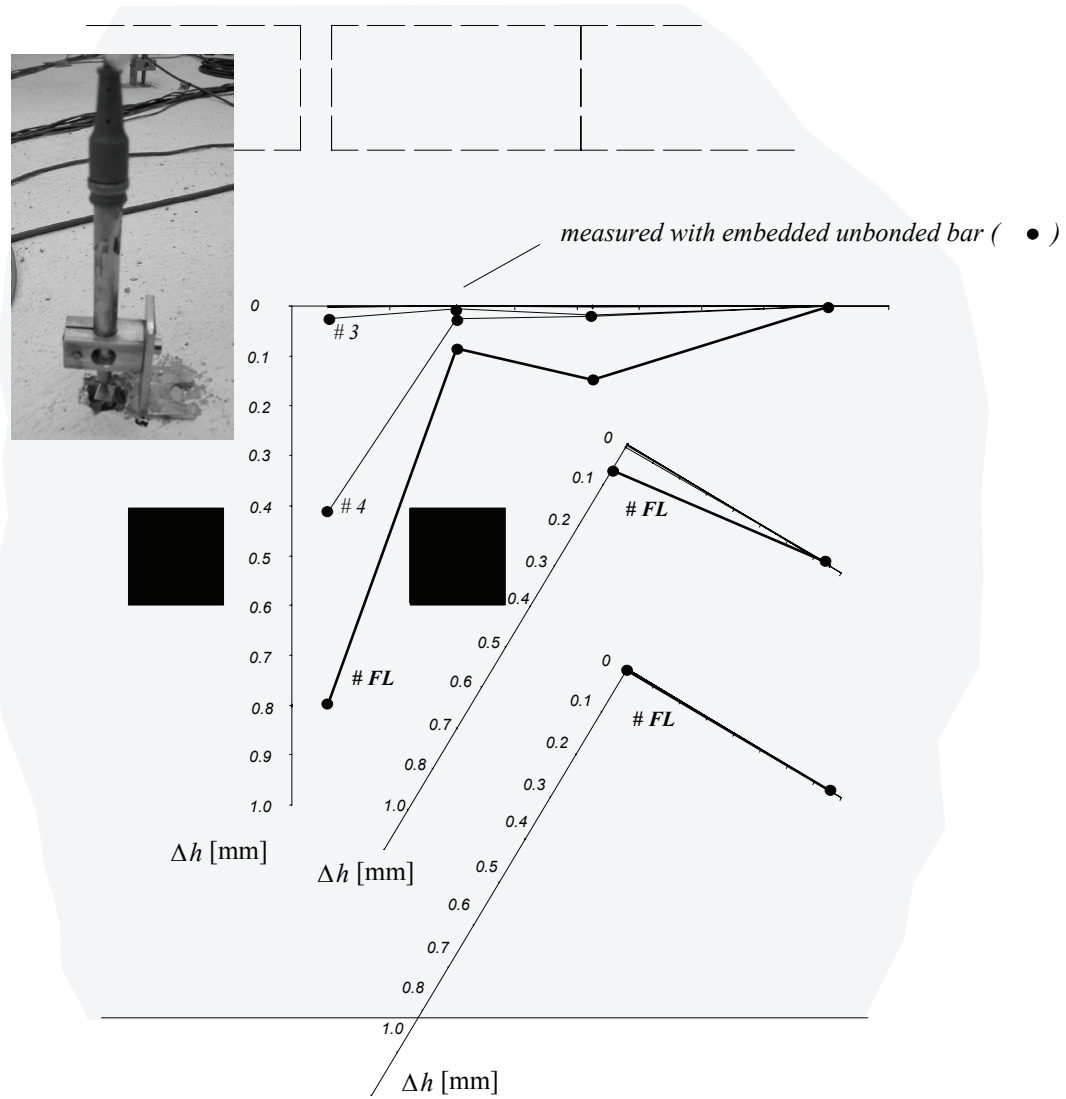


Figure A-4.26: Test DR2-a: Measurements of the variation of the thickness of the slab

A-4.6 Test DR2-b

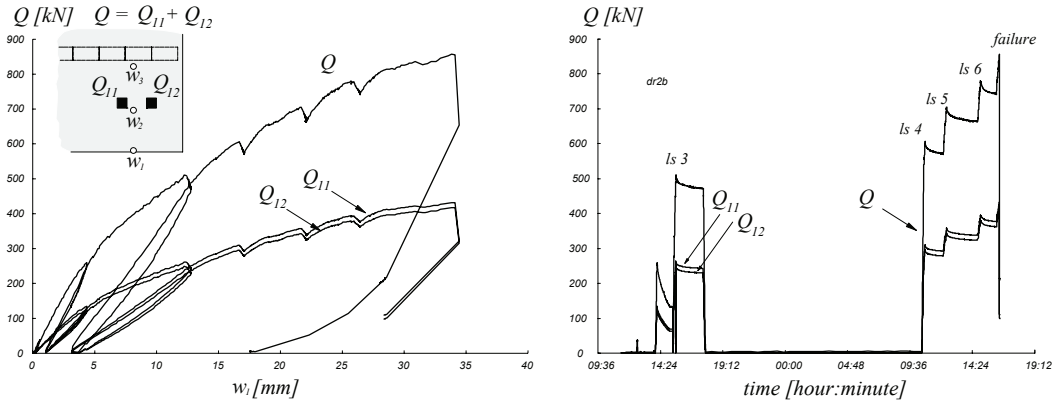


Figure A-4.27: Test DR2-b: Load history and load-deflection curve

Table A-4.7: Test DR2-b: Evolution of some measured values

Load Stage	Q [kN]	Q <sub>11</sub> /Q	Q <sub>12</sub> /Q	w <sub>1</sub> [mm]	w <sub>2</sub> [mm]	w <sub>3</sub> [mm]	Q/Q <sub>FL</sub> [%]	Remark
#1	1.4	-	-	0.0	0.0	0.0	0%	-
#2	247.6	52.0%	48.0%	4.3	2.6	0.8	29%	B
	226.6	52.0%	48.0%	4.1	2.5	0.7	26%	M
	141.2	52.4%	47.6%	3.1	1.9	0.6	16%	E
#3	495.1	51.3%	48.7%	12.6	7.5	1.9	58%	B
	476.4	51.4%	48.6%	12.7	7.6	1.9	56%	M
	471.3	51.4%	48.6%	12.8	7.6	1.9	55%	E
#4	603.2	51.2%	48.8%	16.7	10.0	2.5	70%	B
	581.5	51.2%	48.8%	17.0	10.1	2.5	68%	M
	570.8	51.2%	48.8%	17.1	10.2	2.5	67%	E
#5	696.7	51.1%	48.9%	21.8	13.0	3.1	81%	B
	667.3	51.1%	48.9%	22.1	13.2	3.1	78%	M
	665.4	51.1%	48.9%	22.1	13.2	3.1	78%	E
#6	773.8	51.0%	49.0%	26.0	15.6	3.6	90%	B
	752.2	51.0%	49.0%	26.3	15.8	3.7	88%	M
	743.0	51.0%	49.0%	26.4	15.8	3.7	87%	E
ML	856.6	50.9%	49.1%	33.8	20.3	4.6	100%	ML
FL	856.6	50.9%	49.1%	33.8	20.3	4.6	100%	FL

B : Beginning of load stage ; M : End of demountable deformer measurements ; E : End of load stage ; ML : Maximum load ; FL : Failure Load

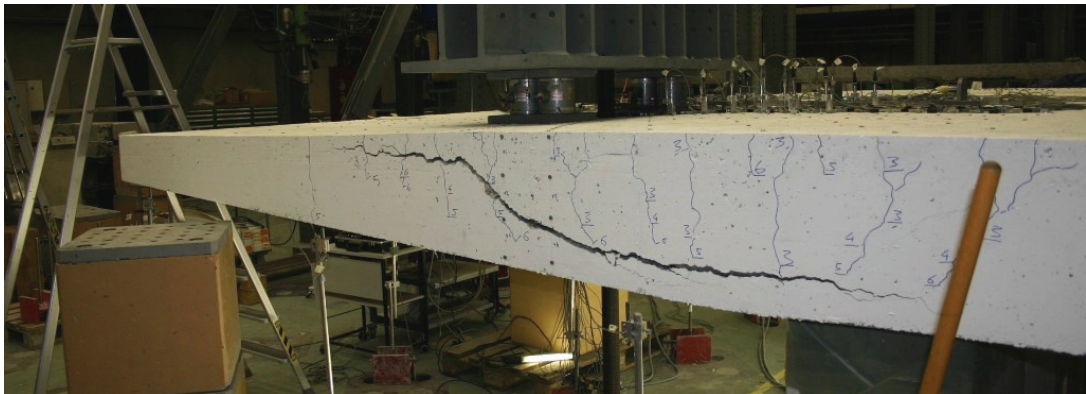


Figure A-4.28: Test DR2-b: Side view of the shear crack after failure

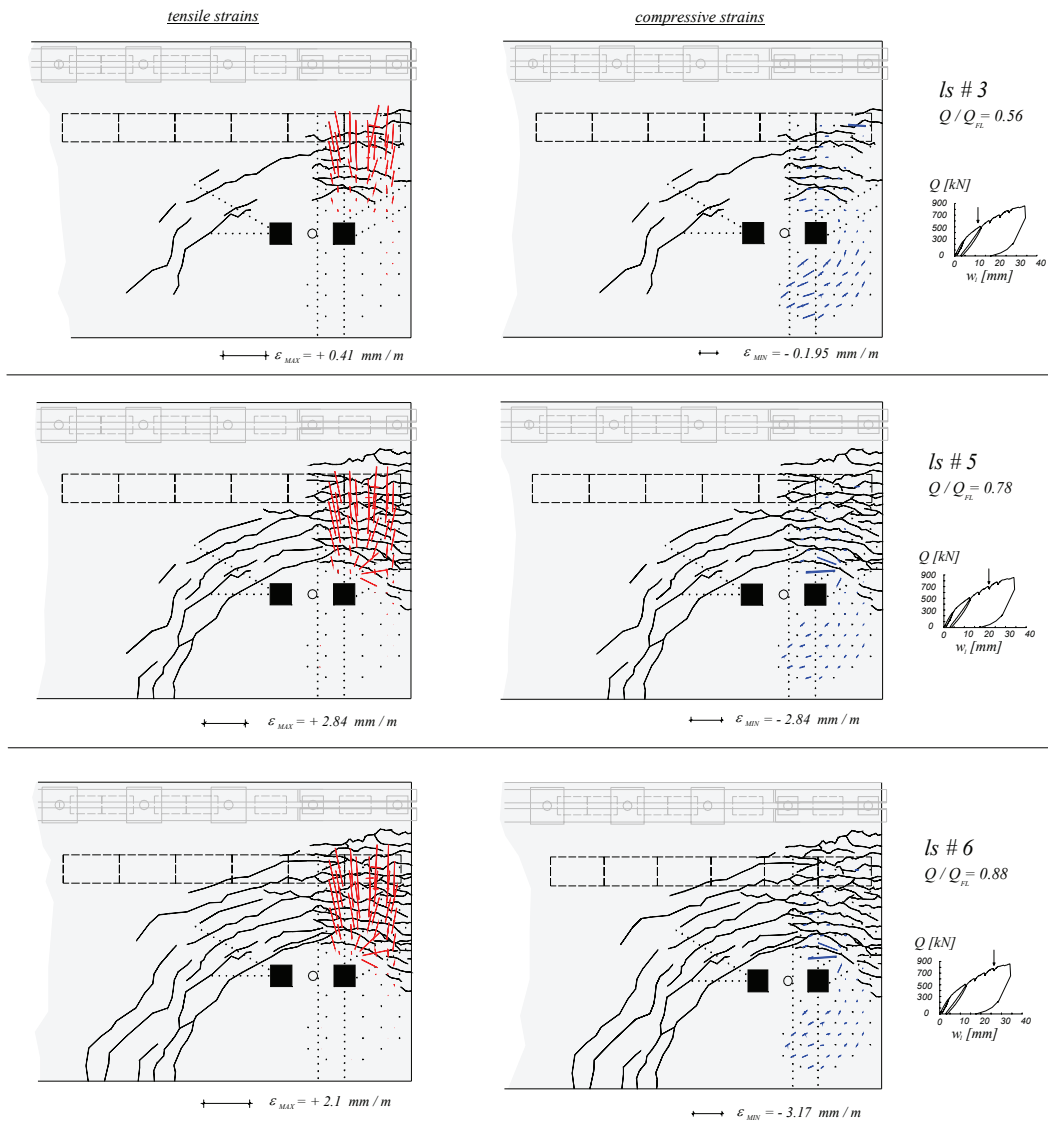


Figure A-4.29: Test DR2-b: Crack pattern and principal strains on the top surface



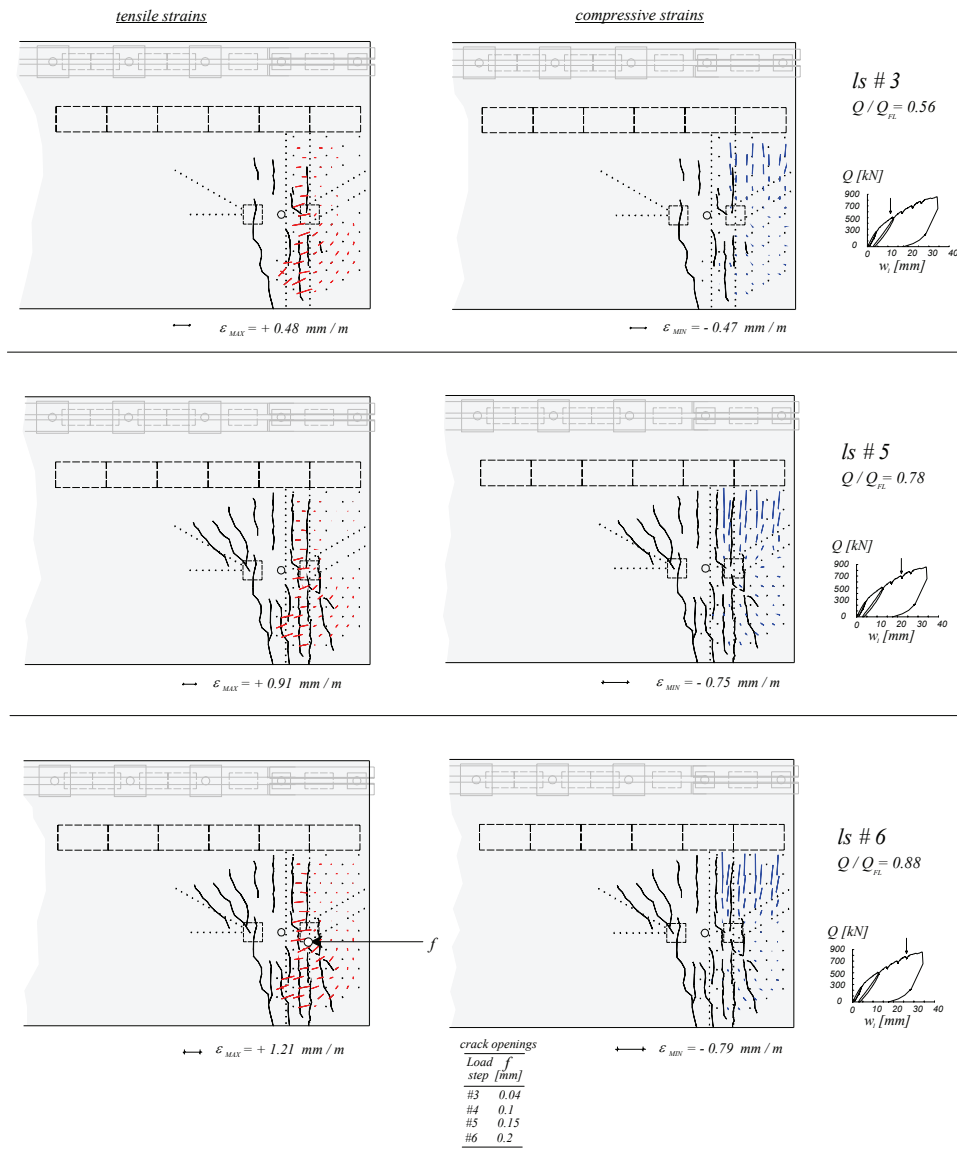


Figure A-4.30: Test DR2-b: Crack pattern and principal strains on the bottom surface (as seen from above)

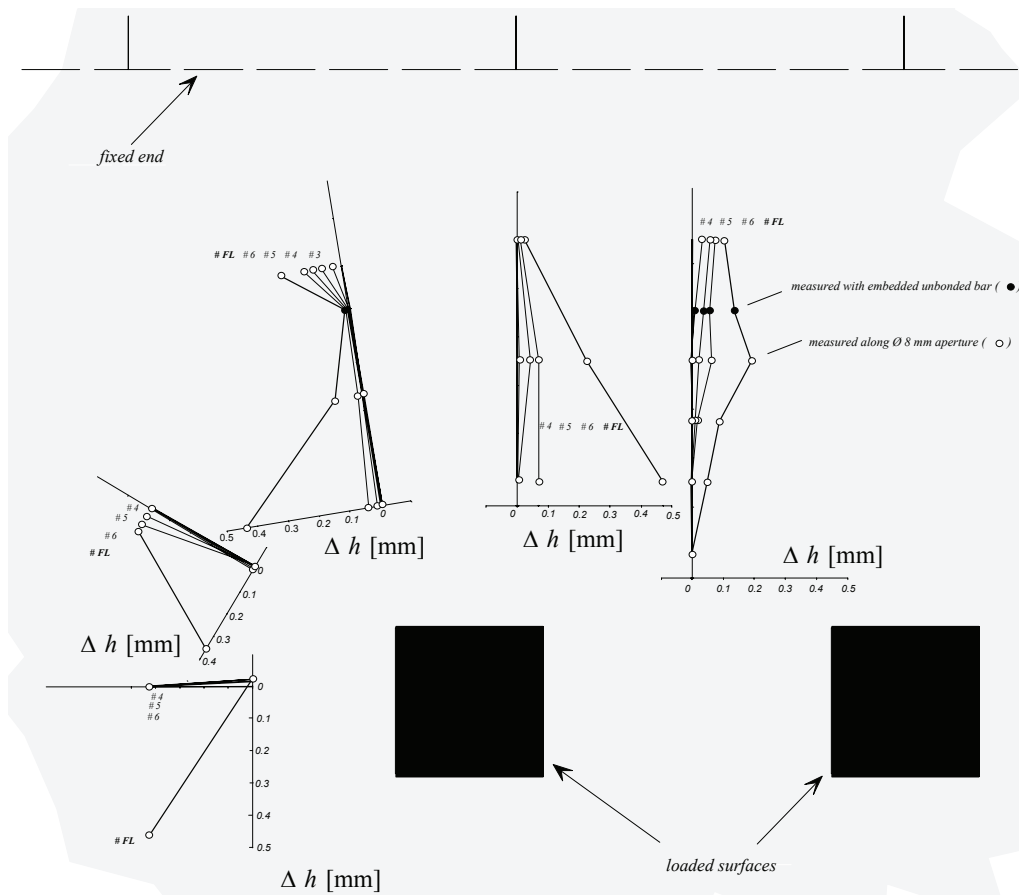


Figure A-4.31: Test DR2-b: Measurements of the variation of the thickness of the slab

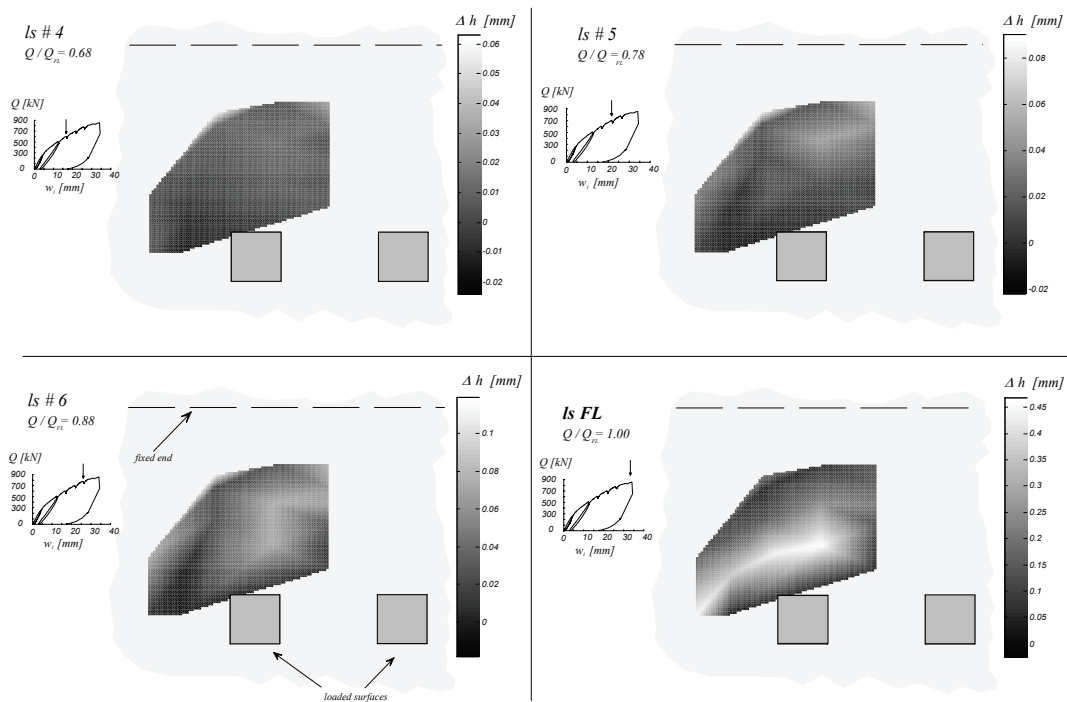


Figure A-4.32: Test DR2-b: Measurements of the variation of the thickness of the slab (interpolated values on all points inside the measurement zone)

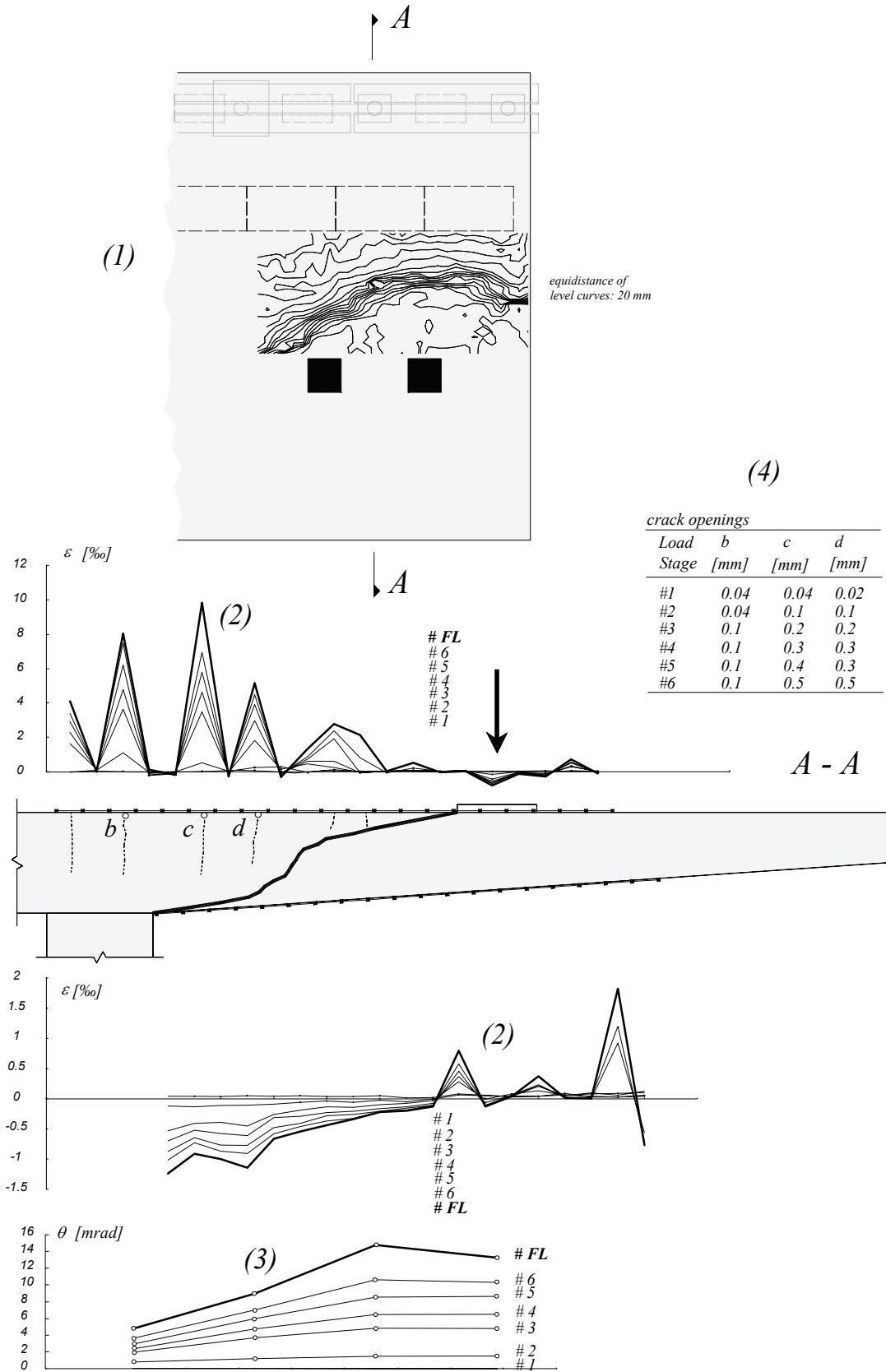


Figure A-4.33: Test DR2-b: (1) Level curves of the shear crack; (2) Strains measured on the surface of the slab with omega-shaped extensometers (100 mm length); (3) Rotations measured with inclinometers; (4) Crack openings measured with magnifying glass

A-4.7 Test DR2-c

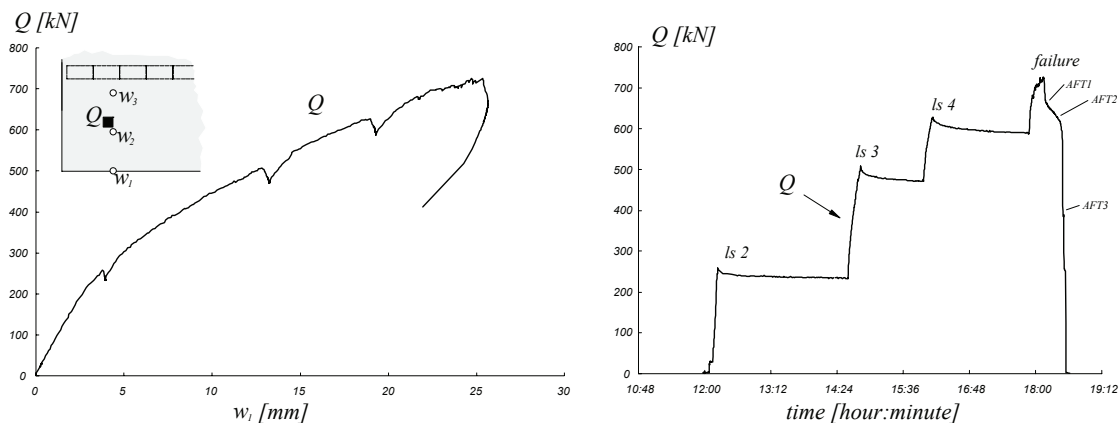


Figure A-4.34: Test DR2-c: Load history and load-deflection curve

Table A-4.8: Test DR2-c: Evolution of some measured values

Load stage	$Q$ [kN]	$w_1$ [mm]	$w_2$ [mm]	$w_3$ [mm]	$Q/Q_{FL}$ [%]	Remark -
#1	3.8	0.0	0.0	0.0	1%	
#2	254.4	3.8	2.4	0.7	35%	B
	240.2	3.9	2.5	0.7	33%	M
	237.1	3.9	2.5	0.7	33%	E
#3	498.9	13.0	8.1	2.0	69%	B
	480.3	13.2	8.2	2.0	67%	M
	471.3	13.2	8.3	2.0	66%	E
#4	620.5	19.0	12.1	2.8	86%	B
	594.3	19.3	12.2	2.8	83%	M
	589.8	19.3	12.3	2.8	82%	E
ML	726.1	25.4	16.1	3.5	101%	ML
FL	719.4	25.4	16.1	3.5	100%	FL
AFT1	664.4	25.7	16.4	3.4	92%	AFT1
AFT2	596.5	25.2	16.5	3.2	83%	AFT2
AFT3	384.6	21.3	16.5	34.6	53%	AFT3

B : Beginning of load stage ; M : End of demountable deformer measurements ; E : End of load stage ; ML : Maximum load ; FL : Failure Load ; AFT1, 2, 3 : After failure



Figure A-4.35: Test DR2-c: Side view of the shear crack after failure

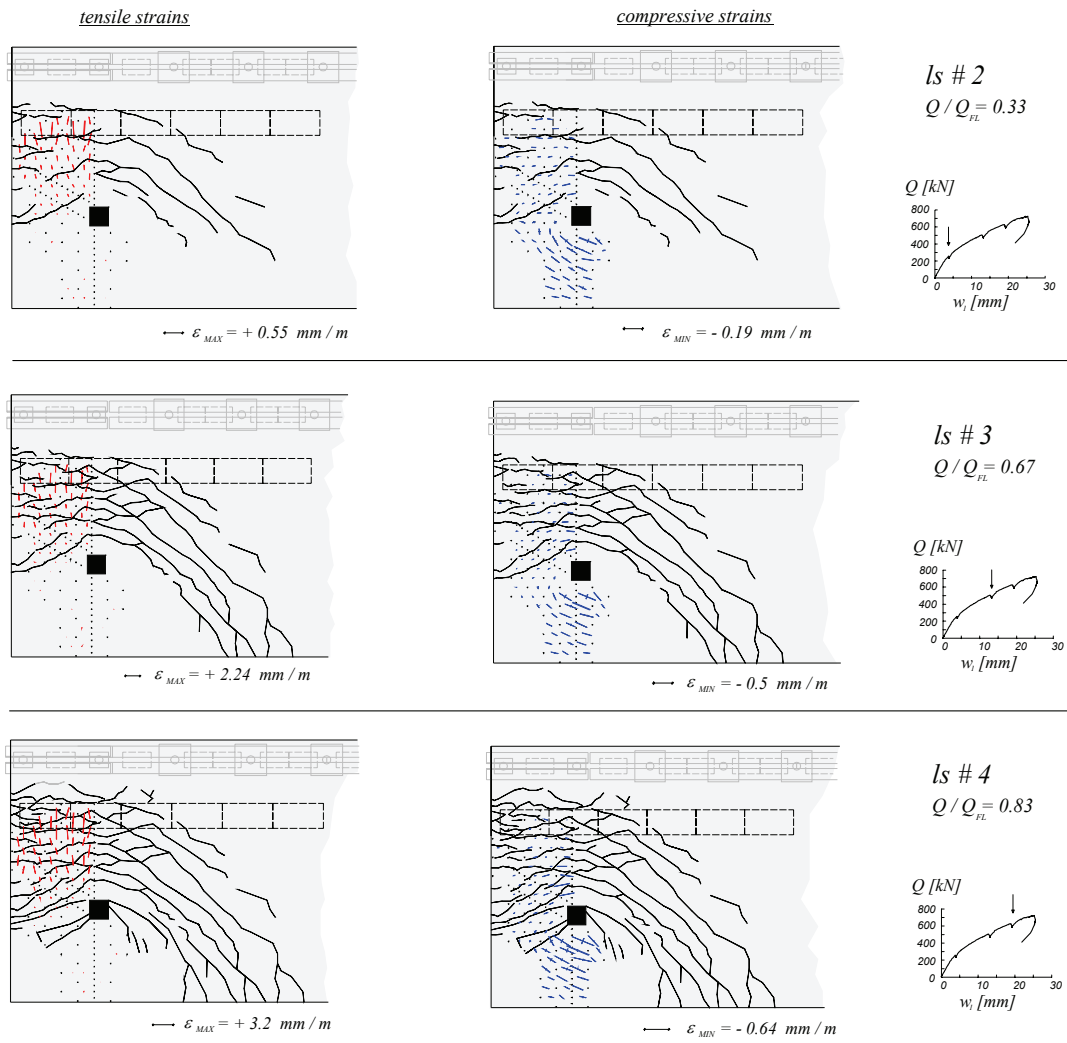


Figure A-4.36: Test DR2-c: Crack pattern and principal strains on the top surface

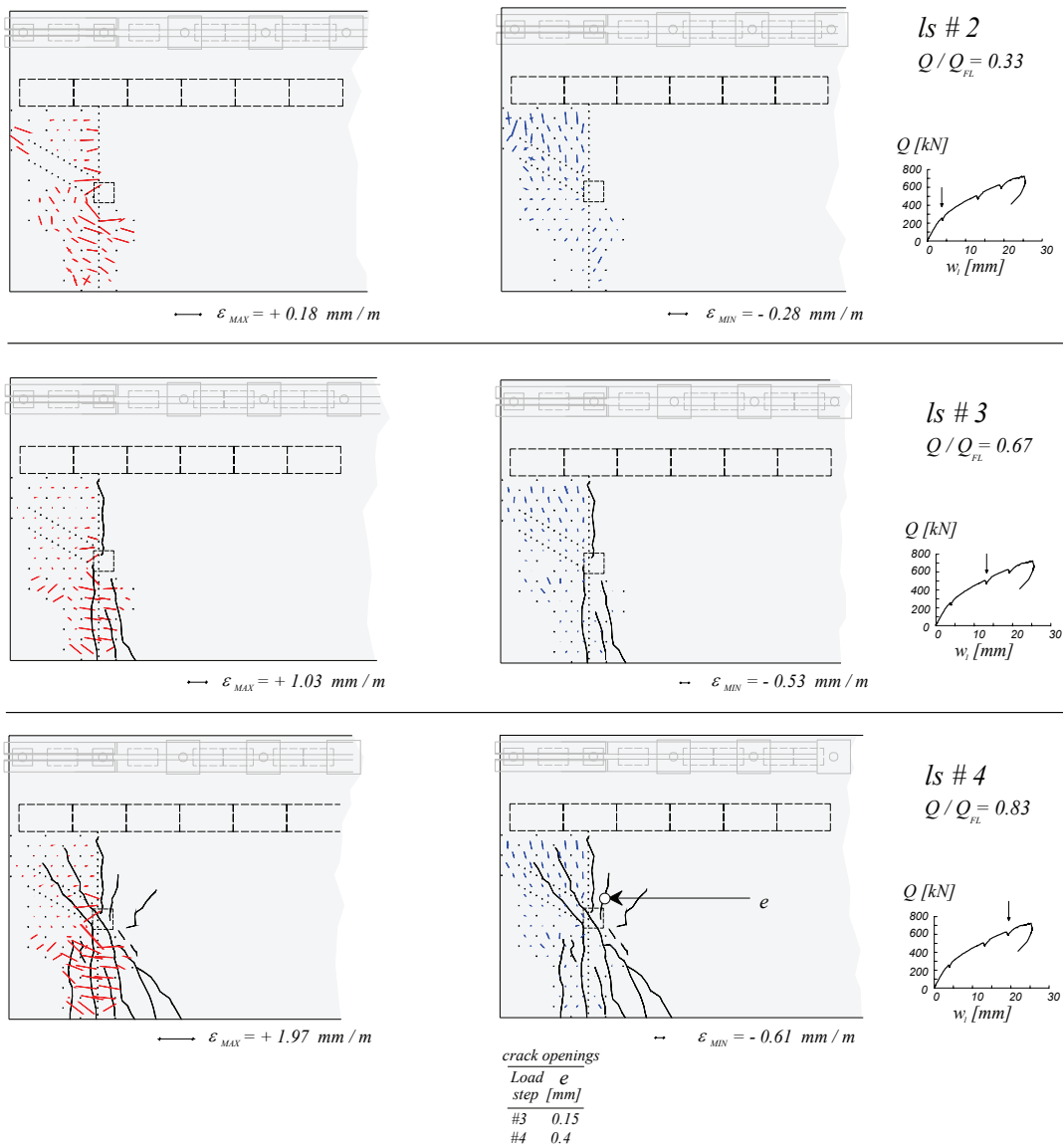


Figure A-4.37: Test DR2-c: Crack pattern and principal strains on the bottom surface (as seen from above)

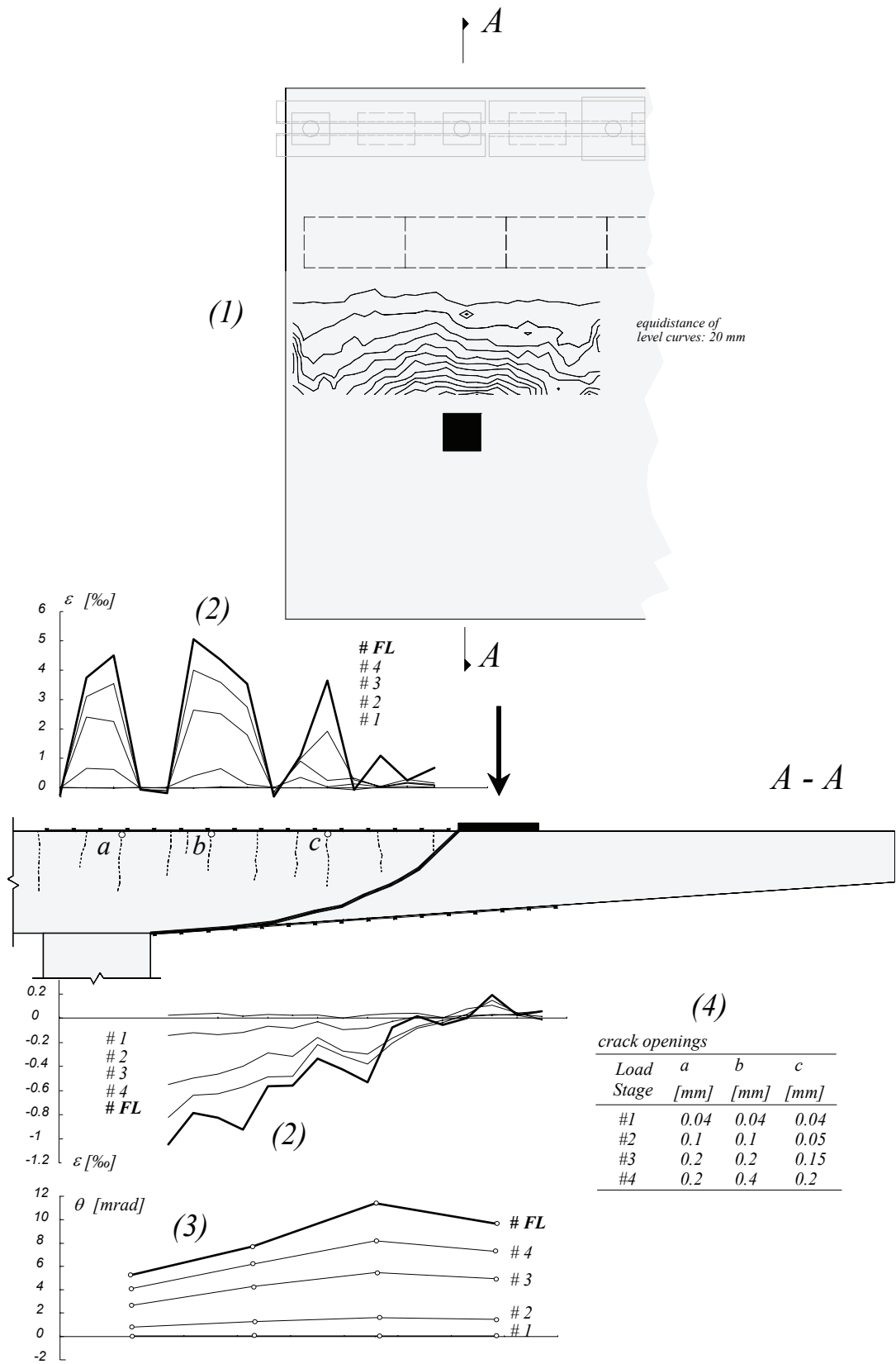


Figure A-4.38: Test DR2-c: (1) Level curves of the shear crack; (2) Strains measured on the surface of the slab with omega-shaped extensometers (100 mm length); (3) Rotations measured with inclinometers; (4) Crack openings measured with magnifying glass

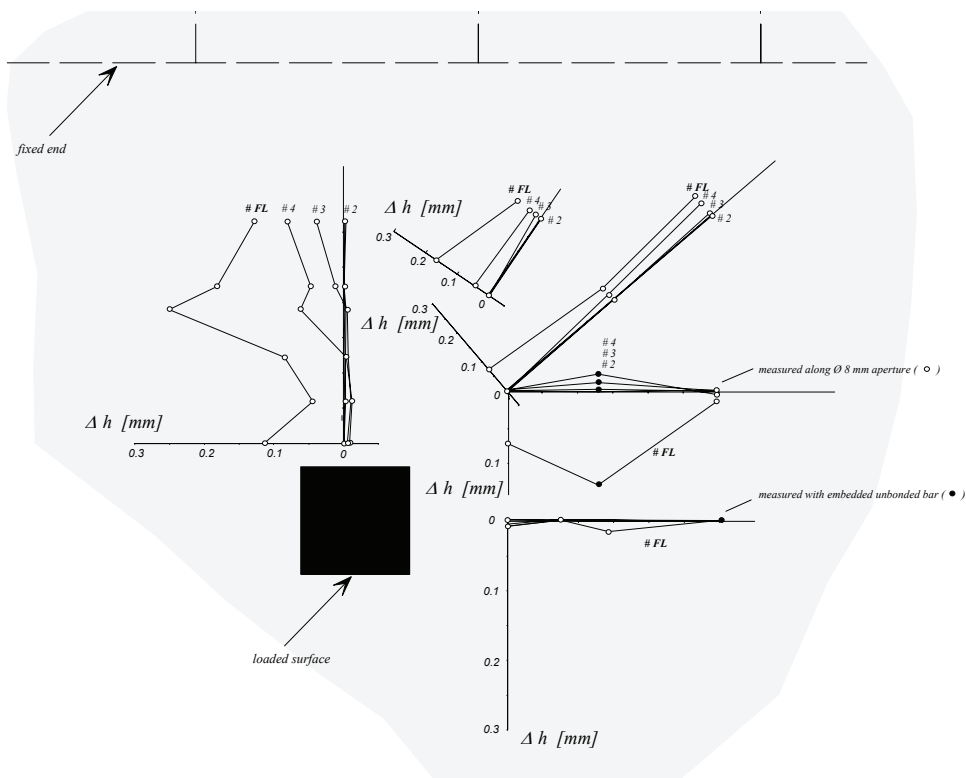


Figure A-4.39: Test DR2-c: Measurements of the variation of the thickness of the slab

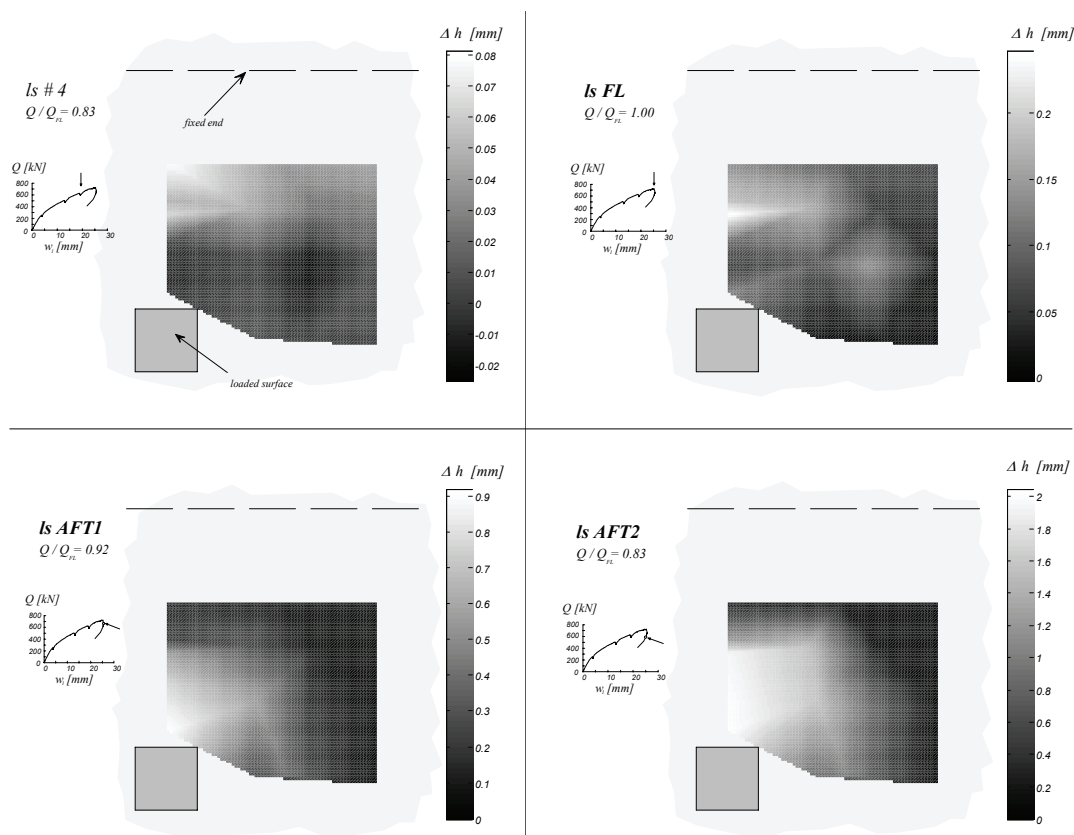


Figure A-4.40: Test DR2-c: Measurements of the variation of the thickness of the slab (interpolated values on all points inside the measurement zone)



A-4.8 Test PR1

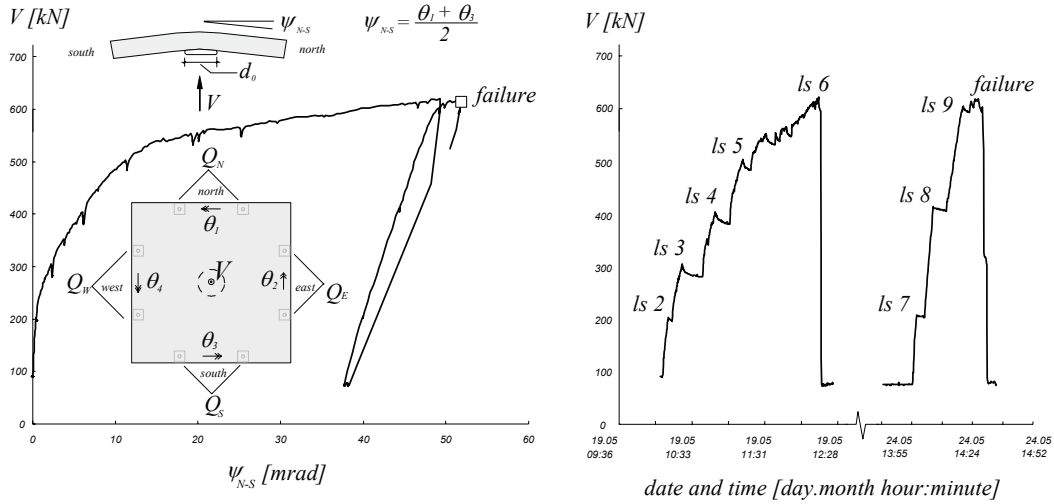


Figure A-4.41: Test PR1: Load history and load-deflection curve

The force on the central support is  $V$ .  $V$  is equal to the sum of the forces applied by the jacks ( $Q_N$ ,  $Q_S$ ,  $Q_W$  and  $Q_E$ ) with the self weight of the slab and test rig (about 73 kN). The rotations  $\theta_1$ ,  $\theta_2$ ,  $\theta_3$ ,  $\theta_4$  are measured with the inclinometers. The pressure  $p$  was measured at each load stage with a pressure gauge. The diameter  $d_0$  is calculated from the force  $V$  and the pressure  $p$  at each load stage:  $d_0 = \sqrt{4 \cdot V / (\pi \cdot p)}$ . The rotation  $\psi_{N-S}$  is the average of the rotations  $\theta_1$  and  $\theta_3$  and the rotation  $\psi_{E-W}$  is the average of the rotations  $\theta_2$  and  $\theta_4$ . Very large rotations were obtained near failure (fig. A-4.41).

Table A-4.9: Test PR1: Evolution of some measured values

Load stage	$Q$	$V$	$p$	$d_0$	$Q_N/Q$	$Q_S/Q$	$Q_W/Q$	$Q_E/Q$	$\theta_1$	$\theta_2$	$\theta_3$	$\theta_4$	$\psi_{NS}$	$\psi_{EW}$	$Q/Q_{FL}$	Rem.
	[kN]	[kN]	[bar]	[mm]	-	-	-	-	[mrad]	[mrad]	[mrad]	[mrad]	[mrad]	[mrad]	[%]	-
#0	15.8	88.8	5.7	445	19%	22%	30%	29%	0.0	0.0	0.0	0.0	0.0	0.0		
#1	126.3	199.3	13.7	430	24%	25%	26%	25%	0.1	2.0	0.7	-1.3	0.4	0.3	24%	
#2	226.4	299.4	20.0	437	25%	25%	26%	24%	3.5	6.2	1.0	-2.3	2.3	1.9	43%	
#3	319.9	392.9	25.3	445	24%	25%	26%	25%	8.9	13.5	3.1	-3.0	6.0	5.3	61%	
#4	420.9	493.9	31.1	450	25%	25%	26%	25%	13.3	23.0	9.4	-3.2	11.3	9.9	80%	
#5	469.1	542.1	33.7	453	24%	25%	26%	25%	21.1	30.0	17.4	-1.1	19.3	14.5	89%	
#6	547.0	620.0	35.0	475	25%	25%	26%	24%	49.3	42.9	49.1	31.7	49.2	37.3	104%	
#7	129.1	202.1	12.0	463	24%	25%	26%	25%	46.8	48.5	33.0	10.0	39.9	29.2	25%	
#8	331.1	404.1	23.6	467	25%	25%	25%	25%	53.6	56.3	35.1	10.1	44.3	33.2	63%	
#9	521.2	594.2	34.0	472	25%	25%	25%	25%	61.4	63.7	36.8	11.0	49.1	37.4	99%	
ML	541.5	614.5			25%	25%	25%	25%	64.1	64.7	39.0	12.9	51.6	38.8	103%	ML
FL	526.1	599.1			25%	25%	25%	25%	64.2	64.4	38.9	12.4	51.5	38.4	100%	FL

ML : Maximal load ; FL : Failure Load

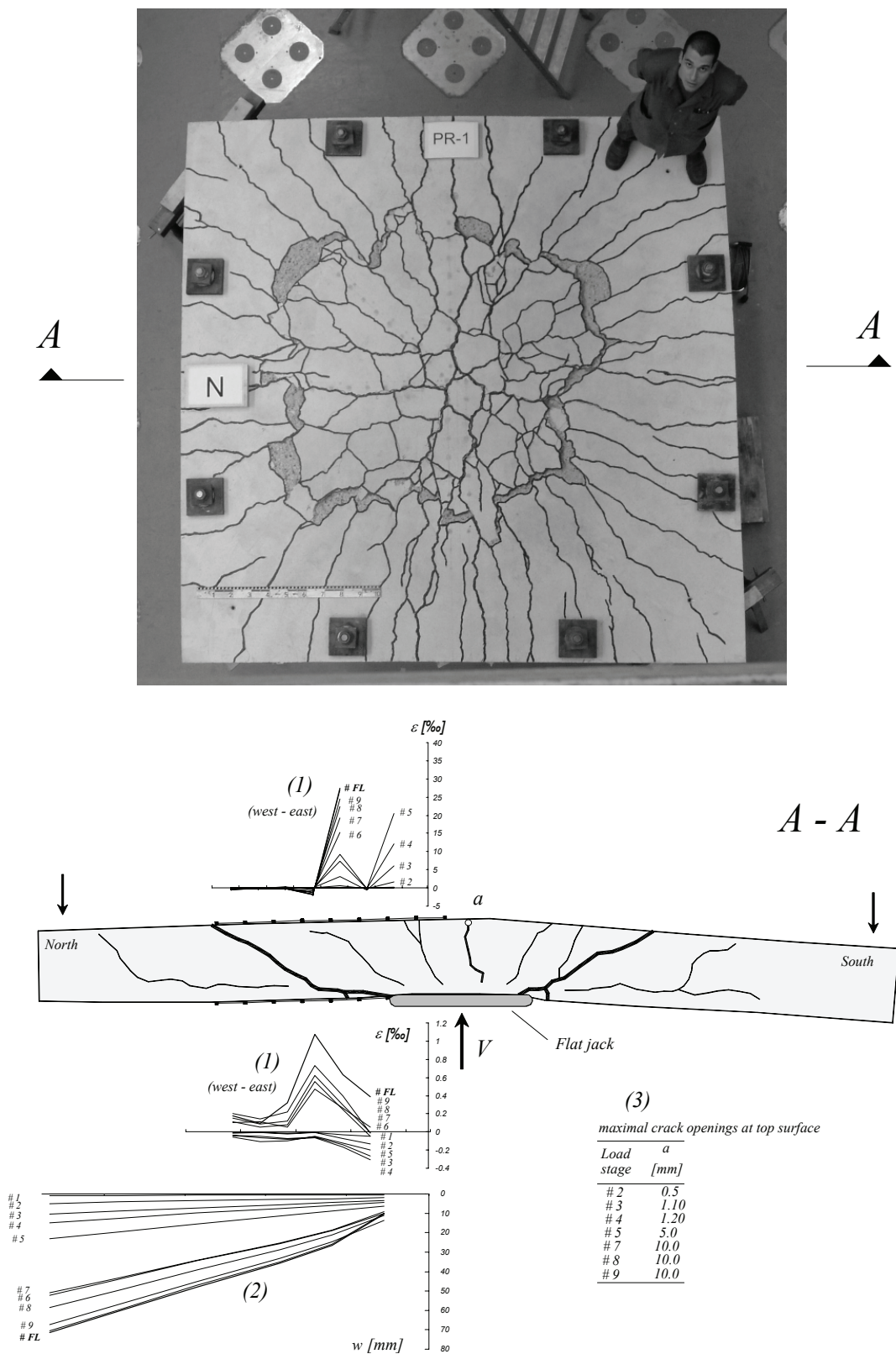


Figure A-4.42: Test PR1: Crack pattern on the top surface; (1) Strains measured on the surface of the slab with omega-shaped extensometers (100 mm length); (2) Deflections measured with LVDTs; (3) Crack openings measured with magnifying glass

## A-5 Conclusions

### A-5.1 Tests on bridge deck cantilevers

Table A-5.1 summarizes the obtained results on all tests on bridge deck cantilevers. Figure A-5.1 shows the load-deflection curves for all the six tests. Note that the self-weight of the test rig (table A-3.1) is not included in the force values. Test DR1-a had the highest failure load and the largest deflection  $w$ , measured at the tip of the cantilever. The measuring location of the deflection  $w$  is indicated in the same figure. The shape of the shear crack is indicated in figure A-5.2 for all tests on cantilevers, for the sectional view  $A - A$ , as explained in figure A-5.1. The strains on the concrete and the rotations are represented using the same scale for all tests. For test DR1-a, the rotations were not measured. The deflections are indicated instead.

Table A-5.1: Summary of the obtained results

Test	Reinforcement ratio <sup>*)</sup>	Location of loads (along $y$ )	Number of loads	Failure Load ( $Q_R$ ) [kN]	Failure location	Mode of failure
DR1-a	0.78 %	Centre	4	1397	Cantilever edge	Shear
DR1-b		North edge	2	1025	Fixed end	Shear
DR1-c		South edge	1	910	Fixed end	Shear
DR2-a	0.60%	Centre	2	961	Fixed end	Shear
DR2-b		North edge	2	857	Fixed end	Shear
DR2-c		South edge	1	719	Fixed end	Shear

<sup>\*)</sup> At the top transversal reinforcement (bars along  $y$ ) at the clamped edge

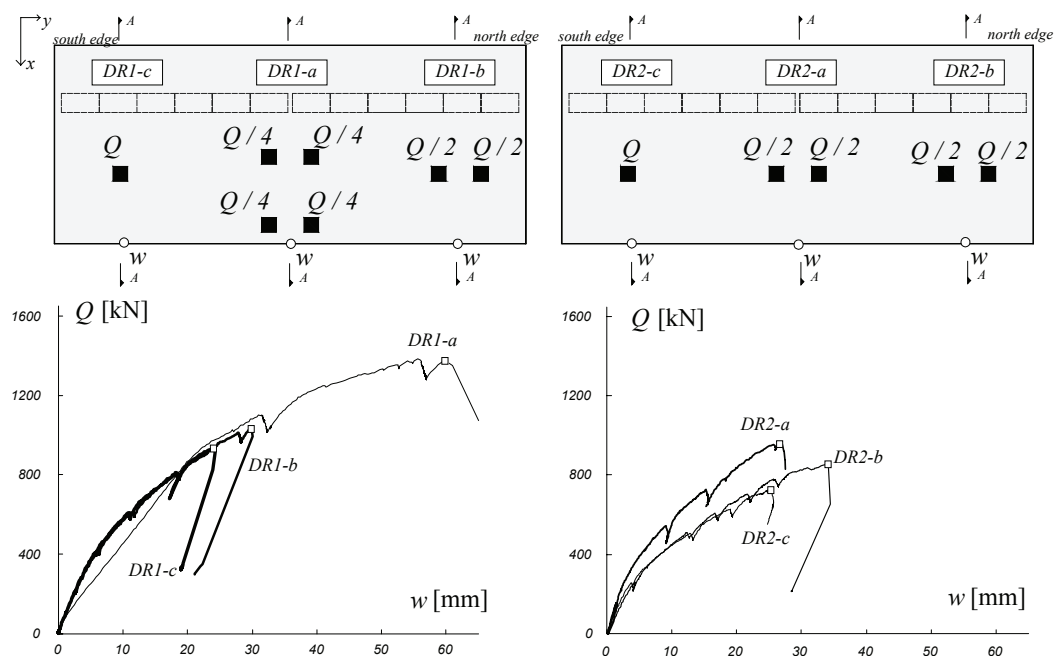


Figure A-5.1: Force-deflection curves for all tests on cantilevers

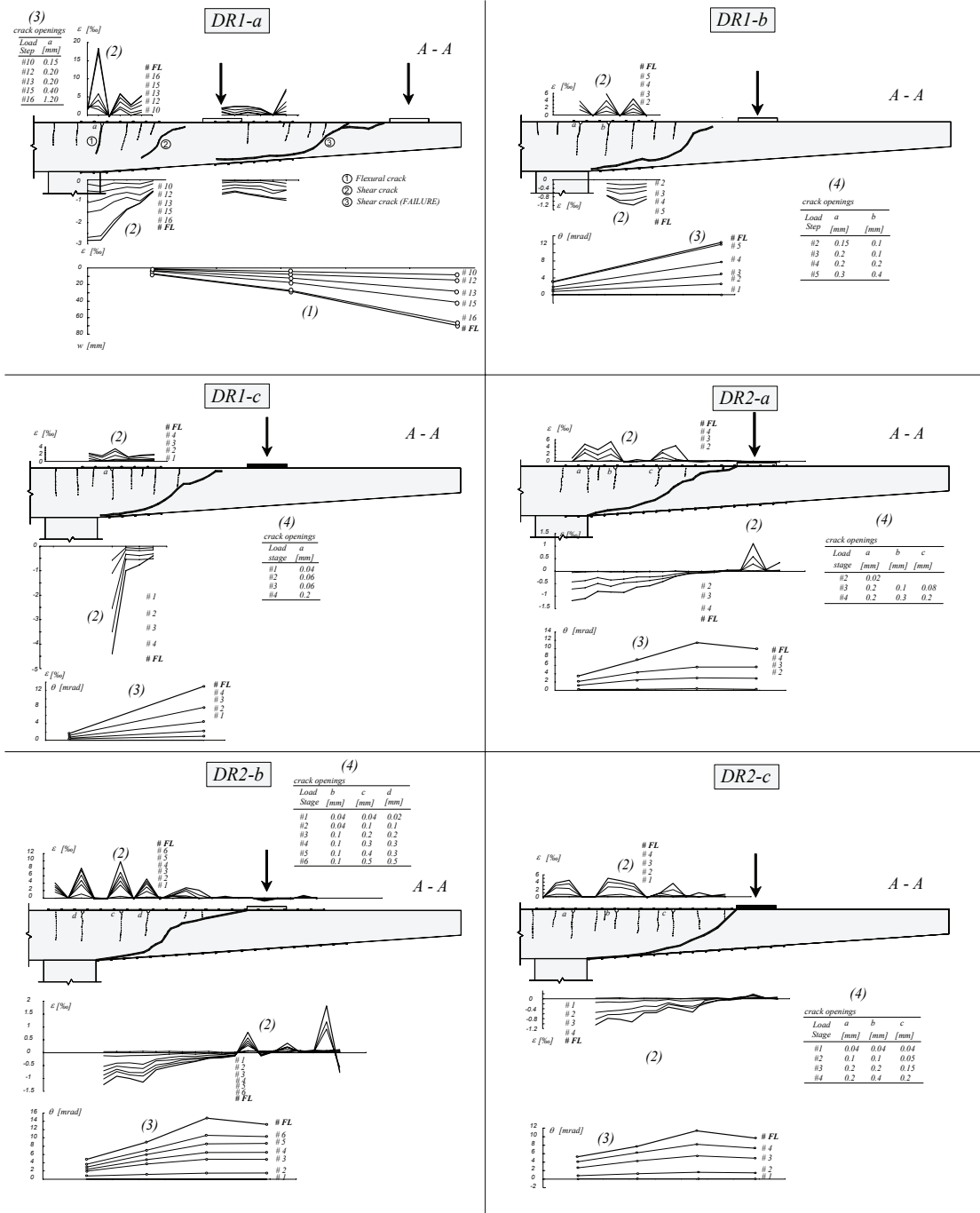


Figure A-5.2: Sectional views of all tests on bridge deck cantilevers: (1) Deflections measured with LVDTs; (2) Strains measured on the concrete surface with omega-shaped extensometers (100 mm length); (3) Rotations measured with inclinometers; (4) Crack openings measured with magnifying glass

The following conclusions can be drawn for the performed tests on cantilevers:

### 1. Behavior at failure

- The cantilevers always failed in shear, in a non ductile manner.
- The location of the shear failure was always in the region between the loads and the clamped edge. For test DR1-a the failure took place at the concentrated loads near the cantilever edge.
- For the tests performed on the same slab, the failure load increases with the number of applied loads (one, two or four).
- For tests performed with the same number of loads, the failure load decreases with the reinforcement ratio.
- For test DR1-a the shear crack that provoked the failure is indicated (DR1-a, ③ in fig. A-5.2). Besides from this crack, an important shear crack was found in the region between the clamped edge and the concentrated loads (DR1-a, ② in fig. A-5.2). It appears that a process of formation of the shear crack in this region was in progress, without leading to a shear failure.
- The critical shear cracks do not seem to form from the existing flexural cracks (fig. A-5.2).
- The surface defined by the failure crack resembles for all tests to a flat truncated conical surface.

### 2. Formation and openings of flexural cracks

- The first flexural crack has always appeared on the top surface at the clamped edge (cracks along  $y$ ).
- The maximal crack openings on the top surface, at failure, range from 0.3 mm for test DR1-c to 1.8 mm for test DR1-a. The cracks with maximal openings at the top surface are always located at the clamped edge (cracks along  $y$ ).
- The maximal crack openings measured on the bottom surface, at the load stage prior to failure, range from 0.2 mm for test DR2-b and DR2-a to 1.0 mm for test DR1-a. The cracks with maximal openings at the bottom surface are always located below the applied loads. These cracks are normally oriented along the cantilever span (cracks along  $x$ ).

### 3. Yielding of flexural reinforcement

Based on the analysis of the crack openings, omega-shaped extensometers and measurements with demountable deformer, it can be concluded that:

- For test DR1-a, significant yielding occurred in top and bottom reinforcement, namely over the clamped edge and under the applied loads. At failure, the crack openings at the clamped edge for top bars along  $x$  was of 1.8 mm. For bottom bars along  $y$  under the edge loads, the crack opening at failure was of 1.0 mm.
- No or very limited yielding occurred for the other tests, with crack openings at failure smaller than 0.6 mm at all locations and for all load levels.

#### 4. Variation of slab thickness and propagation of shear crack

- For test DR2-a, the thickness of the slab has increased after load stage # 3 ( $Q = 0.49 \cdot Q_{FL}$ ). At maximal load, the maximal variation of thickness was of about + 0.8 mm. The increase of thickness was more pronounced at the section A – A, between the load and the clamped edge.
- For test DR2-b the thickness of the slab has increased after load stage # 3 ( $Q = 0.56 \cdot Q_{FL}$ ). At maximal load, the maximal variation of thickness was of about + 0.5 mm. The increase of thickness concentrated in half-circular region around the concentrated load.
- For test DR2-c the thickness of the slab has increased after load stage # 3 ( $Q = 0.67 \cdot Q_{FL}$ ). At maximal load, the maximal variation of thickness was of about + 0.25 mm. The increase was more pronounced at section A – A, between the load and the clamped edge. After the maximal load was attained, the shear failure produced in a rather slow way. The variation of the slab thickness was recorded during the decrease of the load after failure. At load step AFT2 ( $Q = 0.83 \cdot Q_{FL}$ ) the maximal variation of the thickness was of about 2 mm. The increase of thickness was approximately distributed around the applied load, however with larger values at section A – A.

#### 5. Behavior under service load

A cyclical loading of the cantilever took place under the loading patterns of test DR1-a before going to failure. About one hundred cycles ranging from  $Q = 0$  to 410 kN were performed. The following conclusions can be drawn:

- The deflection at the tip of the cantilever increased from 6.3 mm to 8.3 mm (about 30%) after the cyclic loading.
- An increase due to load cycles was also observed in the maximal crack openings at the clamped edge, of 0.1 mm to 0.15 mm. At the bottom surface under the applied loads an increase was observed in the maximal and residual crack openings respectively of 0.04 to 0.1 and 0.02 to 0.05 mm.

### A-5.2 Punching shear test with simulation of vehicle wheel

The following conclusions can be drawn for the punching shear test PR1, with simulation of a vehicle wheel with pneumatic pressure:

- Slab PR1 failed in punching shear in presence of very large crack openings directly above the loaded surface (crack opening of 10.0 mm).
- A very large plateau is observed in the force-rotation diagram.
- Tensile stresses have appeared on the radial direction on the bottom side of the slab, near the central support. This was observed at very large rotations, near failure.
- The diameter of the contact surface between the flat jack and the concrete slab is calculated for each load step from the values of the force and pressure. The diameter sensibly increases along the load stages.

**Bibliography**

**Eurocode 1** , *Actions on structures – Part 2: Traffic loads on bridges*, EN 1991-2, September, **2003**.

**Fernández Ruiz M., Muttoni A.** , *Plain concrete behaviour under uniaxial compression*, IS-BETON, **2005**.

**Guandalini S.** , *Poinçonnement symétrique des dalles en béton armé*, Thèse de doctorat, N. 3380 (2005), 289 pp., Lausanne, Suisse, décembre, **2005**.

**Guandalini S., Muttoni A.** , *Essais de poinçonnement symétrique des dalles en béton armé sans armature à l'effort tranchant*, Rapport d'essai, Lausanne, Switzerland, **2004**.

**Muttoni A.** , *Schubfestigkeit und Durchstanzen von Platten ohne Querkarftbewehrung*, Beton- und Stahlbetonbau, Vol. 98, No 2, pp. 74-84, Berlin, Germany, Feb., **2003**.

**SIA** , *SIA 261 - Actions sur les structures porteuses*, 114p., Zurich, Suisse, **2003**.

**Vaz Rodrigues R.** , *Essai d'un porte-à-faux de pont sous charge concentrée*, EPFL - IS-BETON, Lausanne, **2002**.

**Vaz Rodrigues R.** , *Shear Strength of RC Bridge Deck Cantilevers*, 6th International PhD Symposium in Civil Engineering, IBK Publikation SP-015, pp. 160-161, August, **2006**.

**Vaz Rodrigues R.** , *Shear Strength of Reinforced Concrete Bridge Deck Slabs*, IS-BETON, PhD thesis, n° 3739, Lausanne, Switzerland, January, **2007**

**Vaz Rodrigues R., Muttoni A.** , *Influence des déformations plastiques de l'armature de flexion sur la résistance à l'effort tranchant des poutres sans étriers. Rapport d'essai*, IS-BETON, Lausanne, **2004**.

